

Summer 2017

## Computational Methods of Lattice Boltzmann Mhd

Christopher Robert Flint

College of William and Mary - Arts & Sciences, crflint@email.wm.edu

Follow this and additional works at: <https://scholarworks.wm.edu/etd>



Part of the [Physics Commons](#)

---

### Recommended Citation

Flint, Christopher Robert, "Computational Methods of Lattice Boltzmann Mhd" (2017). *Dissertations, Theses, and Masters Projects*. Paper 1530192360.

<http://dx.doi.org/10.21220/s2-2359-st76>

This Dissertation is brought to you for free and open access by the Theses, Dissertations, & Master Projects at W&M ScholarWorks. It has been accepted for inclusion in Dissertations, Theses, and Masters Projects by an authorized administrator of W&M ScholarWorks. For more information, please contact [scholarworks@wm.edu](mailto:scholarworks@wm.edu).

Computational Methods of Lattice Boltzmann MHD

Christopher Robert Flint

Orlando, Florida

Master of Science, College of William and Mary, 2013

Bachelor of Science, James Madison University, 2010

A Dissertation presented to the Graduate Faculty  
of The College of William & Mary in Candidacy for the Degree of  
Doctor of Philosophy

Department of Physics

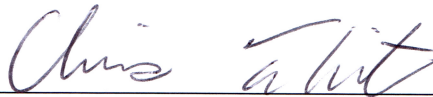
College of William & Mary  
January 2018

©2017  
Christopher Robert Flint  
All rights reserved.

## APPROVAL PAGE

This Dissertation is submitted in partial fulfillment of  
the requirements for the degree of

Doctor of Philosophy



---

Christopher Robert Flint

Approved by the Committee, November 2017



---

Committee Chair

Professor George Vahala, Physics  
College of William & Mary



---

Professor William Cooke, Physics  
College of William & Mary



---

Chancellor Professor Eugene Tracy, Physics  
College of William & Mary



---

Assistant Professor Saskia Mordijck, Applied Science  
College of William & Mary



---

Dr. Robert Rubinstein  
NASA Langley Research Center

## ABSTRACT

Lattice Boltzmann (LB) Methods are a somewhat novel approach to Computational Fluid Dynamics (CFD) simulations. These methods simulate Navier-Stokes and magnetohydrodynamics (MHD) equations on the mesoscopic (quasi-kinetic) scale by solving for a statistical distribution of particles rather than attempting to solve the nonlinear macroscopic equations directly. These LB methods allow for a highly parallelizable code since one replaces the difficult nonlinear convective derivatives of MHD by simple linear advection on a lattice. New developments in LB have significantly extended the numerical stability limits of its applicability. These developments include multiple relaxation times (MRT) in the collision operators, maximizing entropy to ensure positive definiteness in the distribution functions, as well as large eddy simulations of MHD turbulence. Improving the limits of this highly parallelizable simulation method allows it to become an ideal candidate for simulating various fluid and plasma problems; improving both the speed of the simulation and the spatial grid resolution of the LB algorithms on today's high performance supercomputers. Some of these LB extensions are discussed and tested against various problems in magnetized plasmas.

## TABLE OF CONTENTS

Acknowledgments . . . . .	iv
Dedication . . . . .	v
List of Tables . . . . .	vi
List of Figures . . . . .	vii
CHAPTER	
1 Introduction . . . . .	2
2 Derivation of Lattice Boltzmann . . . . .	7
2.1 Deriving Boltzmann . . . . .	7
2.2 $\mathcal{H}$ Theorem . . . . .	10
2.3 Boltzmann Equilibrium . . . . .	11
2.4 Discrete Boltzmann Distribution . . . . .	12
3 LB Procedure . . . . .	15
3.1 Stream and Collide . . . . .	15
3.2 Lattice Velocities . . . . .	17
3.3 Moment Basis Representation . . . . .	19
3.4 Derivation of the Navier-Stokes Equations . . . . .	21
4 Magnetohydrodynamics . . . . .	28
4.1 MHD Magnetic Equation . . . . .	30
4.2 MHD Fluid Equations . . . . .	32
4.2.1 Continuity Equation . . . . .	32
4.2.2 Momentum Equation . . . . .	33

4.3	Dellar’s lattice Boltzmann MHD model . . . . .	35
4.3.1	Lattice Velocities . . . . .	37
4.4	Return to MHD equations . . . . .	38
4.4.1	$\nabla \cdot \mathbf{B} = 0$ . . . . .	38
5	Characteristics of Simulations . . . . .	40
5.1	Energy Spectrum . . . . .	41
5.2	Kelvin-Helmholtz Instability . . . . .	43
5.2.1	Analytic Solution . . . . .	44
5.2.2	KH Simulation Results . . . . .	50
6	Partial Entropic MRT LB Model . . . . .	54
6.1	Multiple Relaxation Time (MRT) . . . . .	55
6.2	Entropic Method and its Partial Extension to MHD . . . . .	58
6.3	Partially Entropic LB-MHD Simulations . . . . .	62
6.3.1	Magnetized Kelvin-Hemholtz Jet Instability . . . . .	62
6.3.2	Chen <i>et. al.</i> Profile . . . . .	66
6.3.3	Biskamp-Welter Profile . . . . .	68
6.4	Conclusion . . . . .	69
7	Large Eddy Simulations . . . . .	71
7.1	Relative Scales . . . . .	71
7.2	Cost of DNS . . . . .	72
7.3	Filtering . . . . .	74
7.4	Early LES . . . . .	77
7.5	Advances in LES . . . . .	79
8	LES model for LB MHD . . . . .	81
8.1	Filters and Filter Widths . . . . .	84

8.2	Moment Basis Representation for LES LB-MHD . . . . .	85
8.3	Derivation of LES MHD Equations for LB MRT . . . . .	89
8.3.1	Filter expansion . . . . .	89
8.3.2	Knudsen expansion . . . . .	91
8.3.3	Final filtered LES-MHD equations . . . . .	93
8.4	Preparing LES for Simulation . . . . .	94
8.4.1	Filtering LB . . . . .	98
8.5	LES-LB-MHD Simulation . . . . .	99
8.6	Conclusion . . . . .	106
9	Conclusion . . . . .	108
APPENDIX A		
	MRT Chapman-Enskog Expansion in LES MHD . . . . .	109
APPENDIX B		
	Local Spatial Derivatives . . . . .	122
APPENDIX C		
	Entropic Derivation for LB . . . . .	125
	Bibliography . . . . .	129
	Vita . . . . .	134



## ACKNOWLEDGMENTS

I would like to first thank God for His provision and planning. I never expected to arrive at this point in life as blessed as I am. I would also like to thank my wife for her love, respect and patience as I finish my graduate studies. I would like to thank all of my family and friends for their continued support. And finally, I would like to thank my advisor George Vahala for his guidance and teachings in both physics and the Word.

I present this thesis in honor of my loving and supportive wife.

## LIST OF TABLES

3.1	Table of cubic lattice types. . . . .	19
-----	---------------------------------------	----

## LIST OF FIGURES

3.1	D2Q9 Lattice Representation . . . . .	20
5.1	A Model Energy Spectrum . . . . .	42
5.2	Concept Diagram of the KH Instability . . . . .	44
5.3	Initial profile of KH LB jet simulation . . . . .	50
5.4	KH LB simulation of a moderate velocity jet . . . . .	51
5.5	KH LB simulation of a high velocity jet . . . . .	52
6.1	Entropic MRT evolution in LB MHD of a weakly stabilized KH jet . . . . .	64
6.2	Spectral Plot of Entropic MRT KH Simulation . . . . .	65
6.3	Magnetic field line comparison in EMRT simulation against Chen Fig. 6a . . . . .	65
6.4	Magnetic field line comparison in EMRT simulation against Chen Fig. 4a . . . . .	66
6.5	Evolution of magnetic field lines in EMRT simulation of Chen Fig. 4a . . . . .	67
6.6	Comparison of current lines in Entropic MRT simulation of Biskamp . . . . .	68
6.7	Plot of $\gamma^*$ in Entropic MRT simulation of Biskamp . . . . .	69
6.8	Plot of energy dissipation over time for the Biskamp-Welter profile . . . . .	69
7.1	Relative Size of DNS Energy Scales . . . . .	75
7.2	1D Filtering Example . . . . .	76
7.3	2D Filtering Example . . . . .	76
8.1	Lattice vectors for D2Q5 . . . . .	87
8.2	Initial Vorticity Profile of LES-LB-MHD Simulation . . . . .	100
8.3	Comparison of Vorticity Evolution in the KH jet between DNS and LES . . . . .	101
8.4	A late time vorticity comparison between DNS and LES . . . . .	102
8.5	A late time spectral comparison between DNS and LES . . . . .	103
8.6	A late time current line comparison between DNS and LES . . . . .	104

COMPUTATIONAL METHODS OF LATTICE BOLTZMANN MHD

# CHAPTER 1

## Introduction

When considering the flow of liquids such as ocean currents, the flow of a gas over an airfoil, or the flow of plasma either on the sun or in a tokamak fusion reactor, it is important to be able to understand, predict and eventually control these flows.

The flow of liquids and gases can be described by the Navier-Stokes equations which appear as

$$\frac{\partial \rho}{\partial t} + \nabla \cdot (\rho \vec{u}) = 0 \quad (1.1a)$$

$$\frac{\partial \vec{u}}{\partial t} + (\vec{u} \cdot \nabla) \vec{u} = -\frac{1}{\rho} \nabla p + \nabla \cdot 2\nu \mathbf{S} . \quad (1.1b)$$

where  $\rho$  is the fluid density,  $\vec{u}$  is the fluid velocity,  $p$  is the pressure,  $\nu$  is the kinematic viscosity, and  $\mathbf{S}$  is the rate of strain tensor in which  $\mathbf{S} = \frac{1}{2} (\nabla \vec{u} + (\nabla \vec{u})^T)$ . The Navier-Stokes equations were discovered when Newton's second law was applied to fluid motion. Stress was brought in by assuming that it is related to the sum of a diffusing viscous term ( $\sim \nabla \vec{u}$ ) and a pressure term ( $p$ ).

Plasmas found in fusion reactors and on the sun are made up of ions and electrons.

These plasmas can be modeled using magnetohydrodynamics (MHD), a model similar to the Navier-Stokes equation which includes magnetic field influences. The MHD equations are defined as

$$\frac{\partial \rho}{\partial t} + \nabla \cdot (\rho \vec{u}) = 0 \quad (1.2a)$$

$$\frac{\partial \vec{u}}{\partial t} + (\vec{u} \cdot \nabla) \vec{u} = -\frac{1}{\rho} \nabla p - \vec{B} \times (\nabla \times \vec{B}) + \nabla \cdot 2\nu \mathbf{S} \quad (1.2b)$$

where  $\vec{B}$  is the magnetic field which evolves according to the MHD induction equation

$$\frac{\partial \vec{B}}{\partial t} = \nabla \times (\vec{u} \times \vec{B}) + \eta \nabla^2 \vec{B} \quad (1.3)$$

and  $\eta$  is the resistivity.

Both sets of equations can be solved analytically for only a few set of initial conditions due to existing nonlinearity. In order to solve the vast majority of relevant geometries which cannot be determined analytically, computation is required to determine solutions. This is known as computational fluid dynamics (CFD) and is typically done by modeling a fluid over a spatial lattice of discrete points and evolving the system over discrete units of time. This approach is successful in modeling the fluid, but the computational cost in CFD tends to scale poorly for turbulence simulations that require high accuracy.

Modern High Performance Computers (HPCs) are built around many processing cores (on the order of 10,000s to 100,000s). As new HPCs are produced, the number of processing cores in these machines continues to increase rapidly while the speed of each core has little, if any, improvement. HPCs require highly parallelized code in order to take advantage of the potential speedups from adding more cores to the newer HPC models. Communication between processing cores has a very high latency rate (on the order of microseconds) compared to the latency rate of simply reading values from memory (on the

order of nanoseconds). A highly parallelizable code will attempt to minimize interprocessor communication in order to decrease the total computation time.

Solving the set of MHD equations at a lattice site requires a solution to many spatial derivatives. The difficulty with CFD is that the convective nonlinear derivative is spatially dependent ( $\vec{u} \cdot \nabla \vec{u}$  is dependent on  $\vec{u}$  at the lattice sites). Thus one can not easily find a synchronization between processors performing this evaluation. However, the linear advection in lattice Boltzmann has perfect synchronization and hence excellent parallelization.

LB is a novel, alternative approach to CFD which models fluid on the mesoscopic scale as a distribution of particles wherein each distribution is delineated by a discrete position and momentum. The lattice Boltzmann procedure stems from the lattice Boltzmann equation

$$\partial_t f_i + \partial_\alpha e_{\alpha i} f_i = \frac{1}{\tau} (f_i - f_i^{\text{eq}}) \quad (1.4)$$

where  $\alpha$  follows Einstein summation and corresponds to each of the spatial dimensions,  $f_i^{\text{eq}}$  is the value of  $f_i$  at equilibrium where  $i$  denotes the velocity component,  $e_{\alpha i}$  represents a unit vector for each velocity  $i$ , and  $\tau$  is the relaxation rate related to viscosity by  $\nu = c_s^2 (\tau - \frac{1}{2})$  upon performing Chapman Enskog expansions on LB, and  $c_s$  is the sound speed.

The LB procedure follows two main procedural steps based on equation (1.4) at each timestep:

1. Stream each distribution along the spatial lattice according to each distribution's momentum. This corresponds to the advective term in the lattice Boltzmann equation ( $\partial_\alpha e_{\alpha i} f_i$ ) and can be simply described as a transfer/movement of data between nearest neighbors on the lattice.
2. Locally collide all distributions with the same spatial position on the lattice. This corresponds to the right-hand side of the lattice Boltzmann equation ( $\frac{1}{\tau} (f_i - f_i^{\text{eq}})$ ) where each distribution relaxes towards a locally prescribed equilibrium  $f_i^{\text{eq}}$  defined by



the moments at each lattice point (sec. 3.3).

The LB method features some great improvements over the classical CFD methods. Besides the great improvement in parallelizability due to the advective term and the simple two step process of LB, there is also the short code length of LB. A minimal LB code consists of about 1,000 lines making it very easy to write, debug, and edit.

Another notable feature is that simple LB is designed to run at lower fluid velocities (subsonic speeds) and requires more discrete distribution velocities to run at higher fluid velocities. This problem exists because a distribution of particles would have to move more than one lattice site per timestep without a collision in order to model the higher velocities. Increasing the number of discrete distribution velocities will require a greater computational cost and is typically undesirable. Therefore research [1, 2] has been pushing LB into the supersonic and transonic regime while attempting to minimize the computational cost.

A general downfall to LB is that it is designed as a positive definite system in order for the sum of the distributions to be equal to the fluid density. If any of the fluid distributions become negative due to a number of factors, the simulation will become unstable and break down. A new model of LB MHD partially developed by myself and based on work by Karlin *et. al.* [3] is introduced in order to improve the overall stability of a simulation. This stability improvement is introduced by separating the single relaxation time (SRT),  $\tau$ , into multiple relaxation times (MRT), one for each distribution  $f_i$ . In MRT, the relaxation rates are so chosen that they do not affect the viscosity of the fluid. In the case of this new model, the relaxation times are also then chosen as a function of maximum entropy. This model allows distributions prone to becoming negative to have a shorter relaxation rate without modifying the underlying MHD equations where a longer relaxation rate will slow the overall change of a distribution's value. This new model is a partial maximization of entropy; partial because it only maximizes the fluid's entropy, not

the magnetic field's entropy.

A second problem expected to occur in CFD and LB is the computational cost required of highly accurate simulations whose cost is calculated as the product of the total number of spatial grid points and timesteps. As a gridsize increases, so does the computational cost. Large eddy simulations (LES) are a technique designed to increase simulation accuracy without increasing the number of gridpoints which leads to a minimal increase in computational cost. The approach is to model the naturally generated subgrid scales of motion by some form of subgrid viscosity. While many LES models exist for CFD and some exist for LB, very few (if any) exist for LB MHD while taking advantage of its features. A new LES model for LB MHD, developed by myself and based on theory by Ansumali [4], is presented in chapter 8.

This paper begins by deriving the lattice Boltzmann equation from kinetic first principles in chapter 2. An explanation on how to use LB as a simulation method with variations of some of its features is presented in chapter 3. Then, chapter 4 will derive the MHD equations along with its application in LB. chapter 5 will cover some analytical theory on the turbulent energy spectrum and the Kelvin-Helmholtz instability. The new model on improving LB MHD stability by directly maximizing entropy in the fluid velocity is in chapter 6 along with corresponding simulation results. The concept behind the theory of large eddy simulations is explained in chapter 7. Finally, a new LES technique for LB-MHD is presented in chapter 8 along with simulation results.

# CHAPTER 2

## Derivation of Lattice Boltzmann

Gases are a statistical distribution of many ( $N \gg 1$ ) small particles, whose probability is given by the N-body distribution function. This can be broken down into a BBGKY hierarchy and which under certain conditions can be approximated by kinetic equations (and 1-particle distribution functions). A mathematical probability distribution function can be built to describe the probability that a particle exists in a phase space location at a specific time  $f_N(1, 2, \dots, N, t)$  where  $1, 2, \dots, N$  represents the coordinates  $\vec{x}_1, \vec{x}_2, \dots, \vec{x}_N, \vec{p}_1, \vec{p}_2, \dots, \vec{p}_N$ . This function allows the tracking of every particle in the system. Integrating the distribution function over a given phase space provides the normalized probability of all particles in all space such that

$$1 = \iint f_N(1, 2, \dots, N, t) dx^{3N} dp^{3N} . \quad (2.1)$$

### 2.1 Deriving Boltzmann

A change in the particle distribution function can occur due to external forces and particle collisions. The total change of a distribution,  $D_t f = \frac{df}{dt}$ , is broken into a set of

partial derivatives using the chain rule on each component of the distribution function. The Liouville equation defines the precise evolution of the distribution function which is defined as

$$\begin{aligned}
D_t f_N &= \left[ \partial_t + \sum_i^N \frac{\vec{p}_i}{m} \cdot \nabla_{\vec{x}_i} + \sum_i^N \frac{\vec{F}_i}{m} \cdot \nabla_{\vec{p}_i} \right] f_N(1, 2, \dots, N, t) \\
&= \left[ \partial_t + \sum_i^N \frac{\vec{p}_i}{m} \cdot \nabla_{\vec{x}_i} + \sum_i^N \left( \frac{\partial \Phi_i^{ext}}{\partial \vec{x}_i} + \sum_j^N \frac{\partial \Phi_{ij}^{col}}{\partial \vec{x}_i} \right) \cdot \nabla_{\vec{p}_i} \right] f_N = 0
\end{aligned} \tag{2.2}$$

where  $f_N$  is the distribution of the full system of particles  $N$ ,  $\vec{x}_i$  and  $\vec{p}_i$  are respectively the position and momentum of the  $i^{\text{th}}$  particle,  $\Phi_i^{ext}$  is the potential of the  $i^{\text{th}}$  particle due to an external force and  $\Phi_{ij}^{col}$  is the inter-particle potential between particles  $i$  and  $j$ . The Liouville equation tracks the position and momentum of every particle and evolves the distribution for the system [5]. The number of particles in an environment can add up to more than  $10^{23}$ . With such a large number of particles, it's impossible to track each one through time, even in a simulation.

An approach to tracking fewer particles in each distribution comes from the BBGKY hierarchy. Although, the BBGKY hierarchy describes the evolution of the system using distributions of fewer than  $N$  particles, the hierarchy is a precise equation equivalent to the Liouville equation. For a subset,  $s$  of the total number of particles  $N$ , the BBGKY equation becomes

$$\begin{aligned}
&\left[ \partial_t + \sum_i^s \frac{\vec{p}_i}{m} \cdot \nabla_{\vec{x}_i} + \sum_i^s \left( \frac{\partial \Phi_i^{ext}}{\partial \vec{x}_i} + \sum_j^s \frac{\partial \Phi_{ij}^{col}}{\partial \vec{x}_i} \right) \cdot \nabla_{\vec{p}_i} \right] f_s(1, 2, \dots, s, t) \\
&= (N - s) \sum_i^s \nabla_{\vec{p}_i} \int \frac{\partial \Phi_{i s+1}^{col}}{\partial \vec{x}_i} \cdot f_{s+1} d\vec{x}_{s+1} d\vec{p}_{s+1}
\end{aligned} \tag{2.3}$$

where  $f_s$  is the distribution function for a subset,  $s$ , of particles such that  $f_s(1, 2, \dots, s, t) = \iint f_N dx_{s+1}^3 dx_{s+2}^3 \dots dx_N^3 dp_{s+1}^3 dp_{s+2}^3 \dots dp_N^3$ . The BBGKY hierarchy tells us that the evo-

lution of just one particle requires the knowledge of a second. And the evolution of a second requires a third which continues until the entire system is required to be tracked.

Boltzmann introduced closure to the BBGKY hierarchy by assuming uncorrelated particles, except at their binary collision. This assumption is appropriate for a neutral rarefied gas with very short range but strong interaction potential. Collisions between more than two particles are considered to be far too rare to significantly effect the macroscopic state of the gas. Thus for a 2-particle distribution function, one can reduce it to a product of 1-particle distribution function together with the pair correlation term  $P$

$$f_2(1, 2, t) = f_1(1, t) f_1(2, t) + P(1, 2, t) \quad (2.4)$$

The 1<sup>st</sup> term on the right hand side is the result if particles 1 and 2 were totally uncorrelated [ideal gas] i.e., statistically independent of each other. The pair correlation  $P(1, 2, t)$  tells how particle 1 is correlated to particle 2. Under the molecular chaos assumption, Boltzmann then deduced that the evolution of the 1-particle distribution function can be given by

$$\left[ \partial_t + \frac{\vec{p}_1}{m} \cdot \nabla_{\vec{x}_1} + \frac{\partial \Phi_1^{ext}}{\partial \vec{x}_1} \cdot \nabla_{\vec{p}_1} \right] f_1(\vec{x}_1, \vec{p}_1, t) = (\partial_t f_1)_{col} \quad (2.5)$$

where  $(\partial_t f_1)_{col}$  is the rate of change in the 1-particle distribution function due to particle ‘1’ colliding with other particles in the gas at position  $\vec{x}_1$ . A precise definition of the particle collision term is

$$(\partial_t f_1)_{col} = \sum_j^N \int g_{1j} \sigma_{1j} \left( f_1'(\vec{p}_1) f_1'(\vec{p}_j) - f_1(\vec{p}_1) f_1(\vec{p}_j) \right) d\Omega d^3 \vec{p}_1' d^3 \vec{p}_j' \quad (2.6)$$

where primed values represent post-collision states,  $g_{1j} = |\vec{p}_1 - \vec{p}_j| = |\vec{p}_1' - \vec{p}_j'|$ ,  $\sigma$  is the

differential scattering cross-section and  $d\Omega$  is the solid angle of the collision. Although the evolution of the distribution is now greatly simplified, the collision term requires a pairwise comparison between every particle in the system to determine if any collision has occurred, making the collision integral nonlinear and difficult to use.

## 2.2 $\mathcal{H}$ Theorem

An approach to simplifying the collision term came about as a side effect Boltzmann's  $\mathcal{H}$ -Theorem. Boltzmann's  $\mathcal{H}$ -theorem is similar to a negative entropy of the system derived from the assumption of molecular chaos. For  $f_1 \rightarrow f_1 \ln f_1$  then integrating over phase space, the LHS of the Boltzmann equation (2.5) becomes

$$\iint d^3 \vec{x}_1 d^3 \vec{p}_1 \left[ \partial_t + \frac{\vec{p}_1}{m} \cdot \nabla_{\vec{x}_1} + \frac{\partial \Phi_1^{ext}}{\partial \vec{x}_1} \cdot \nabla_{\vec{p}_1} \right] f_1 \ln f_1 \quad (2.7)$$

The second and third terms can be transformed from volume integrals to surface integrals such that

$$\partial_t \mathcal{H} + \iint d^3 \vec{p}_1 d\Sigma_x \cdot \frac{\vec{p}_1}{m} f_1 \ln f_1 + \iint d^3 \vec{x}_1 d\Sigma_p \cdot \frac{\partial \Phi_1^{ext}}{\partial \vec{x}_1} f_1 \ln f_1 \quad (2.8)$$

$f_1 \rightarrow 0$  as  $\vec{p}_1 \rightarrow \infty$  and  $\vec{x}_1 \rightarrow \infty$  so the surface integrals in the second and third terms equal 0.  $\mathcal{H}$  is defined as

$$\mathcal{H} \equiv \iint f_1(\vec{x}, \vec{p}, t) \ln f_1(\vec{x}, \vec{p}, t) d\vec{x} d\vec{p} \quad (2.9)$$

Observing how  $\mathcal{H}$  changes over time,

$$d_t \mathcal{H} = \iint (1 + \ln f_1) \frac{\partial f_1}{\partial t} d\vec{x}_1 d\vec{p}_1 \quad (2.10)$$

It can be proved [5] that the RHS collision term of (2.5) is shown to be  $\leq 0$  forcing  $d_t \mathcal{H} \leq 0$ . This is significant because it shows that a statistical distribution of particles under molecular chaos will tend towards an equilibrium (when  $d_t \mathcal{H} = 0$ ) and can thus be considered irreversible since  $d_t \mathcal{H}$  cannot be positive. This corresponds with the irreversibility stated in the second law of thermodynamics. A bridge now exists between the microscopic and macroscopic scales of statistical mechanics/thermodynamics thanks to Boltzmann's  $\mathcal{H}$  theorem.

## 2.3 Boltzmann Equilibrium

The concept of an equilibrium, determined from the collision term of (2.5) when  $\frac{d}{dt} \mathcal{H} = 0$ , requires  $f_1(1)f_1(2) = f'_1(1)f'_1(2)$  for  $f_1(i)$  where  $i$  represents the coordinates of particle  $i$ . If the log is taken of this equation, we find the  $\ln f$  is a collisional invariant; meaning that  $\ln f_1(1) + \ln f_1(2) = \ln f'_1(1) + \ln f'_1(2)$  can be defined by conservation equations  $\vec{p}_1 + \vec{p}_2 = \vec{p}'_1 + \vec{p}'_2$  and  $\frac{p_1^2}{2m} + \frac{p_2^2}{2m} = \frac{p_1'^2}{2m} + \frac{p_2'^2}{2m}$ . If  $[\ln f = A(\vec{v} - \vec{B})^2 + \ln C]$  or equivalently  $[f = C \exp(-A(\vec{v} - \vec{B})^2)]$ , then  $f$  can be replaced with the Maxwell Boltzmann distribution

$$f = f^{\text{eq}} = \left(\frac{n}{2\pi RT}\right)^{3/2} \exp\left(-\frac{(\vec{v} - \vec{u})^2}{2RT}\right) \quad (2.11)$$

with  $n$  as number density,  $\vec{u}$  as macroscopic velocity,  $R = \frac{k}{m}$  is the ratio of Boltzmann constant  $k$  over mass  $m$ , and temperature is  $T$ . The choice of these variables is made by choosing the lowest order moments of the distributions to reflect the conserved hydrody-

dynamic quantities. This corresponds to

$$\int f(\vec{x}, \vec{v}, t) dv^3 = \rho \quad (2.12a)$$

$$\int \vec{v} f(\vec{x}, \vec{v}, t) dv^3 = \rho \vec{u} \quad (2.12b)$$

$$\int \frac{(\vec{v} - \vec{u})^2}{2} f(\vec{x}, \vec{v}, t) dv^3 = \frac{\rho DRT}{2} . \quad (2.12c)$$

For an isothermal model,  $T$  has no significance. The collision term may now be approximated by the Maxwell Boltzmann distribution when the system is close to equilibrium.

Bhatnagar, Gross and Krook (BGK) discovered a short-hand, linear way of relating a particle collision to the equilibrium state. The BGK operator appears as

$$(\partial_t f_1)_{col} = -\tau^{-1} (f_1 - f_1^{eq}) \quad (2.13)$$

where  $\tau$  is a relaxation time related to the viscosity. Rather than making pairwise comparisons with every distribution to determine the collisional state, one simply compares the current distribution against its equilibrium. The BGK collision operator greatly simplifies the kinetics and shows up at the fluid level in the effect on the viscosity through  $\tau$ . If one is interested in kinetic properties of the gas, then these are butchered by the BGK collision operator. The Boltzmann equation becomes

$$\left[ \partial_t + \frac{\vec{p}_1}{m} \cdot \nabla_{\vec{x}_1} + \frac{\partial \Phi_1^{ext}}{\partial \vec{x}_1} \cdot \nabla_{\vec{p}_1} \right] f_1(\vec{x}, \vec{p}, t) = -\tau^{-1} (f_1 - f_1^{eq}) \quad (2.14)$$

## 2.4 Discrete Boltzmann Distribution

In many applications, including here, there is no need to introduce external forces simplifying  $\Phi^{ext} = 0$  in (2.14). At this point, It is instructive to integrate (2.14) along



particle trajectories. In this Lagrangian picture

$$D_t f(\vec{x}(t), \vec{p}(t), t) = [\partial_t + \vec{v} \cdot \nabla_{\vec{x}}] f(\vec{x}, \vec{p}, t) = -\frac{1}{\tau} (f - f^{\text{eq}}) \quad (2.15)$$

The Lagrangian derivative following the particle trajectory is simply the free-streaming trajectory

$$\frac{d\vec{x}(t')}{dt'} = \vec{v}(t') \quad , \quad \frac{d\vec{v}(t')}{dt'} = 0 \quad (2.16)$$

with trajectory parametrization to the Eulerian description at:  $t = t'$ ,  $\vec{x}(t) = \vec{x}$ , and  $\vec{v}(t) = \vec{v}$ . Thus, on integrating (2.15) along Lagrangian trajectories,

$$\int_t^{t+\Delta t} ds D_t f(\vec{x}(s), \vec{p}(s), s) = -\frac{1}{\tau} \int_t^{t+\Delta t} dt (f - f^{\text{eq}}) \quad (2.17)$$

yields

$$f_i(\vec{x} + \vec{c}_i \Delta t, t + \Delta t) - f_i(\vec{x}, t) = -\frac{1}{\tau} \int_t^{t+\Delta t} ds [f(\vec{x}(s), s) - f^{\text{eq}}(\vec{x}(s), s)] \quad (2.18)$$

The notation has been simplified since the kinetic velocity is constant along trajectories of (2.16) and hence is not explicitly shown in the distribution functions. Instead a change in notation for simplicity has occurred for the remainder of this paper. The distribution  $f_i$  is now denoted as the distribution with discrete velocity  $\vec{c}_i$ . In a lattice representation, the nodes at  $\vec{x}$  will be connected to their neighbors  $\vec{x} + \vec{c}_i \Delta t$ , where  $\vec{c}_i$  are the discrete velocities on the specifically chosen lattice (and which now replace the continuous independent variable  $\vec{v}$ ).

While there are various approximations one can make on the collision term in (2.18), the simplest, under the assumption that  $\Delta t \ll t$ , is to treat the integrand as slowly varying

and evaluating it at the lower terminal

$$f_i(\vec{x} + \vec{c}_i \Delta t, t + \Delta t) - f_i(\vec{x}, t) = -\frac{\Delta t}{\tau} [f(\vec{x}, t) - f^{\text{eq}}(\vec{x}, t)] \quad (2.19)$$

By evaluating at the lower terminal, a simple explicit finite difference scheme is available to solve. 5 The final lattice Boltzmann equation is acquired by relabeling  $\tau$  in non-dimensional units.

$$f_i(\vec{x} + \vec{c}_i \Delta t, t + \Delta t) = f_i(\vec{x}, t) - \frac{1}{\tau} (f_i - f_i^{\text{eq}}) \quad (2.20)$$

The procedure of converting the lattice Boltzmann equation (2.20) into a useful simulation will now be discussed.

# CHAPTER 3

## LB Procedure

We now have an equation for lattice Boltzmann derived from kinetic theory. How do we implement this equation in a simple way to produce a meaningful simulation? In this chapter, the basic LB simulation procedure will be explained. And the accuracy of LB will be shown as the Chapman-Enskog procedure is used to derive the well-known Navier-Stokes equations which govern basic fluid dynamics.

### 3.1 Stream and Collide

Implementing the lattice Boltzmann equation (LBE) in a simulation is rather simple. The LBE

$$f_i(\vec{x} + \vec{c}_i \Delta t, t + \Delta t) = f_i(\vec{x}, t) - \frac{1}{\tau} (f_i - f_i^{\text{eq}}) \quad (3.1)$$

will evolve fluid particle distributions across a spatial grid at each timestep ( $\Delta t$ ). In modeling this behavior, we can perform operator splitting, separating the equation according

to the dimensions of change.

$$f_i^t(\vec{x}, t + \Delta t) = f_i(\vec{x}, t) - \frac{1}{\tau} (f_i(\vec{x}, t) - f_i^{\text{eq}}(\rho, \vec{u})) \quad (3.2a)$$

$$f_i(\vec{x} + \vec{c}_i \Delta t, t + \Delta t) = f_i^t(\vec{x}, t + \Delta t) \quad (3.2b)$$

where  $\rho$  and  $\vec{u}$  are respectively the density and macroscopic velocity of the fluid at position  $\vec{x}$ . (3.2a) represents a change in the time dimension and (3.2b) represents a change in the spatial dimension. From the perspective of the particle distributions, these are described as the collide and stream equations respectively for (3.2a) and (3.2b).

These two steps would be taken consecutively for every timestep in the simulation with (3.2a) relaxing a group of distributions at a single spatial point and (3.2b) simply moving (streaming) particle distribution data from one spatial point to the next. As these steps are taken, it can be seen that this model is extremely parallelizable [6, 7] given that the collision equation only requires local data at a single lattice site and the stream equation is simply an advective movement of said local data across the lattice. On HPCs, the spatial domain is decomposed allowing each process to hand a spatial subdomain of the simulation. MPI is needed to pass the streaming information to neighboring processes. As this interprocess streaming is performed simultaneously for all processes, the algorithm is well parallelized.

The LB procedure is in essence inverse statistical mechanics. The nonlinear problem is being embedded into a higher dimension kinetic space, while minimizing the number of phase velocities needed. The gain is that the nonlinear convective derivatives in Navier-Stokes and MHD are replaced by linear advection in kinetic space. The nonlinear terms are then introduced into LB as simple quadratic algebraic nonlinearities in  $f^{\text{eq}}$ .

Given the evolution of a LB fluid, we can extract useful information at the end of each timestep (just after streaming or before collision) by a process of taking moments.

The conserved moments  $(\rho, \rho\vec{u})$  of the lattice Boltzmann distribution ( $f$ ) are necessary to evaluate the equilibrium function ( $f^{\text{eq}}$ ) at every timestep and so the process of taking conserved moments becomes an unofficial third step in the lattice Boltzmann procedure. The conserved moments for any lattice are defined similar to (2.12) as

$$\rho = M_0 = \sum_i f_i \quad , \quad \rho\vec{u} = M_1 = \sum_i \vec{c}_i f_i \quad (3.3)$$

and only requires spatially local distributions (same as the collision equation). This means the lattice Boltzmann method (LBM) remains extremely parallelizable even when taking moments.

The procedure to take an  $i^{\text{th}}$  moment  $M_i$  is

$$M_i = \sum_{j=0}^8 T_{ij} f_j \quad (3.4)$$

for some transformation matrix  $T$  whose size is determined by the total number of discrete distribution velocities. The transformation matrix  $T$  will be discussed shortly.

## 3.2 Lattice Velocities

A lattice can take any isotropic geometric shape [2, 8]. The tendency has been to push the geometries to be as simple as possible while remaining isotropic and using space-filling lattices to prevent interpolation (which can cause numerical errors). In two dimensions, this has resulted in square and hexagonal lattices to be most commonly used in research.

In one dimension (1D), only three moments are required to properly reproduce the physical evolution equations (1 density, 1 velocity dimension, 1 element of the stress tensor). This 1D lattice can be easily represented in the D1Q3 lattice as shown in table

### 3.1.

On a square lattice, as used throughout this thesis, we can discretize the fluid distribution velocity  $\vec{v}$  in the four cardinal directions to maintain isotropy. In this most simple case, we find that a change of basis to hydrodynamic moments only produces four independent moments (velocity and shear stress in the  $x$  and  $y$  directions). Although we have four distribution velocities for the fluid, they equate to only one speed and prevent the fluid from reaching a Maxwellian equilibrium distribution.

Adding one resting velocity to the square lattice allows a better approximation for the equilibrium to approach a Maxwellian distribution, thus making the simulation more stable, but still only provides five independent moments in a moment transformation (velocity and shear stress in the  $x$  and  $y$  directions and density). According to Chapman-Enskog, we need at least six moments (1 density, 2 velocity dimensions, 3 elements of symmetric stress tensor) for 2D modeling. Without all six moments being stored, the Chapman-Enskog expansion for the lattice will not match the proper macroscopic fluid evolution equations. In order to maintain isotropy for a lattice, four more discrete distribution velocities must be added to the four corners of the square. This velocity discretization on a square lattice now meets all requirements for accurate modeling and resembles Fig. 3.1. In the D2Q9 lattice (2 dimensions, 9 distribution velocities), there are a total of 3 distribution speeds as can be found in table 3.1.

With an hexagonal 2D lattice, we instantly meet the minimum number of lattice velocities and maintain isotropy. In order to improve stability by ensuring more than one distribution speed, a seventh rest velocity may be added. At the cost of a more complex hexagonal lattice (compared to a square lattice), the number of velocities can be reduced from 9 to 7 for a given fluid.

In 3D, the minimum number of moments is 10 (1 density, 3 velocity dimension, 6 elements of symmetric stress tensor), allowing for a large number of 3D cubic lattice

Lattice Name	Lattice Velocities	Speeds (Quantity)
D1Q3	(0), ( $\pm 1$ )	0 (1), 1 (2)
D2Q9	(0, 0), ( $\pm 1, 0$ ), ( $\pm 1, \pm 1$ )	0 (1), 1 (4), $\sqrt{2}$ (4)
D3Q15	(0, 0, 0), ( $\pm 1, 0, 0$ ), ( $\pm 1, \pm 1, \pm 1$ )	0 (1), 1 (6), $\sqrt{3}$ (8)
D3Q19	(0, 0, 0), ( $\pm 1, 0, 0$ ), ( $\pm 1, \pm 1, 0$ )	0 (1), 1 (6), $\sqrt{2}$ (12)
D3Q27	(0, 0, 0), ( $\pm 1, 0, 0$ ), ( $\pm 1, \pm 1, 0$ ), ( $\pm 1, \pm 1, \pm 1$ )	0 (1), 1 (6), $\sqrt{2}$ (12), $\sqrt{3}$ (8)

TABLE 3.1: Table of cubic lattice types.

options.

### 3.3 Moment Basis Representation

The bulk of work in this thesis uses the 2 dimensional 9-bit (D2Q9) phase space velocities  $\vec{c}_i$  for the density distribution, (Fig. 3.1). The D2Q9 lattice naturally uses a given equilibrium function along with a corresponding set of weights  $w_i$  and lattice speed of sound  $c_i$  calculated using Hermite polynomials. The choice of  $f_i^{\text{eq}}$  is made as a truncated small velocity (low Mach number) expansion of the Maxwell-Boltzmann distribution whose factors before each term are determined by the lattice weights and speed of sound [9]. The LB  $f_i^{\text{eq}}$  for the D2Q9 lattice is

$$f_i^{\text{eq}} = w_i \rho \left[ 1 + 3 (\vec{c}_i \cdot \vec{u}) + \frac{9}{2} (\vec{c}_i \cdot \vec{u})^2 - \frac{3}{2} \vec{u}^2 \right], i = 0, \dots, 8 \quad (3.5)$$

with lattice speed of sound  $c_s = \frac{1}{\sqrt{3}}$  and lattice weights:  $w_0 = \frac{4}{9}$ ,  $w_{1\dots 4} = \frac{1}{9}$ , and  $w_{5\dots 8} = \frac{1}{36}$ .

To construct the moment space, it is natural to first choose the conservation moments (the zeroth and first moments of  $f_i$ ) [10, 11]. One then chooses the remaining higher moments to form an independent basis. The 1-1 mapping between the distribution space ( $f_i$ ) and the moment space ( $M_i$ ), as stated in (3.4), is given by a constant T matrix. For the simplest choice of moments used throughout this thesis, the specific form of this  $9 \times 9$

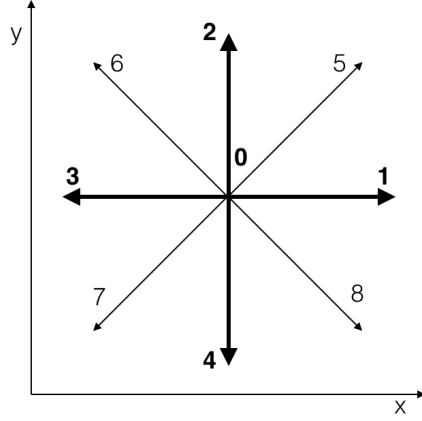


FIG. 3.1: **D2Q9 Lattice Representation.** The kinetic lattice vectors for 2D LB-MHD are, in our  $D2Q9$  model,  $\vec{c}_i = (0, 0), (0, \pm 1), (\pm 1, 0), (\pm 1, \pm 1)$ .  $w_i$  are appropriate weight factors dependent on the choice of lattice: for speed 0,  $w_0 = \frac{4}{9}$ ; for speed 1,  $w_i = \frac{1}{9}$ ; and for speed  $\sqrt{2}$ ,  $w_i = \frac{1}{36}$ .

T-matrix is

$$\mathbb{T} = \begin{pmatrix} \mathbf{1} \\ c_x \\ c_y \\ c_x c_y \\ c_x^2 \\ c_y^2 \\ c_x^2 c_y \\ c_x c_y^2 \\ c_x^2 c_y^2 \end{pmatrix} = \begin{pmatrix} 1 & 1 & 1 & 1 & 1 & 1 & 1 & 1 & 1 \\ 0 & 1 & 0 & -1 & 0 & 1 & -1 & -1 & 1 \\ 0 & 0 & 1 & 0 & -1 & 1 & 1 & -1 & -1 \\ 0 & 0 & 0 & 0 & 0 & 1 & -1 & 1 & -1 \\ 0 & 1 & 0 & 1 & 0 & 1 & 1 & 1 & 1 \\ 0 & 0 & 1 & 0 & 1 & 1 & 1 & 1 & 1 \\ 0 & 0 & 0 & 0 & 0 & 1 & 1 & -1 & -1 \\ 0 & 0 & 0 & 0 & 0 & 1 & -1 & -1 & 1 \\ 0 & 0 & 0 & 0 & 0 & 1 & 1 & 1 & 1 \end{pmatrix} \quad (3.6)$$

where the  $x$  and  $y$  components of the corresponding 9-dimensional lattice vectors are just

$$c_x = \{0, 1, 0, -1, 0, 1, -1, -1, 1\} \quad , \quad c_y = \{0, 0, 1, 0, -1, 1, 1, -1, -1\} \quad . \quad (3.7)$$



The first three fluid moments are simply the collisional invariants - being nothing but the conservation of density (the 1<sup>st</sup> row of the T-matrix) and momentum (the 2<sup>nd</sup> and 3<sup>rd</sup> rows of T). In particular, the moments can be written in terms of the conserved moments:

$$\begin{aligned}
M_0^{\text{eq}} &= M_0 = \rho & M_1^{\text{eq}} &= M_1 = \rho u_x & M_2^{\text{eq}} &= M_2 = \rho u_y \\
M_3^{\text{eq}} &= \rho u_x u_y & M_4^{\text{eq}} &= \frac{1}{3} (3\rho u_x^2 + \rho) \\
M_5^{\text{eq}} &= \frac{1}{3} (3\rho u_y^2 + \rho) & M_6^{\text{eq}} &= \frac{1}{3} \rho u_y \\
M_7^{\text{eq}} &= \frac{1}{3} \rho u_x & M_8^{\text{eq}} &= \frac{1}{9} \rho (1 + 3u_x^2 + 3u_y^2)
\end{aligned} \tag{3.8}$$

### 3.4 Derivation of the Navier-Stokes Equations

Using Chapman-Enskog Expansion, it is possible to derive the macroscopic Navier-Stokes equations from the mesoscopic moments of (3.8). We begin by Taylor expanding the left hand side of the LBE (3.1). The precise definition of this terms is

$$f_i(\vec{x} + \vec{c}_i \Delta t, t + \Delta t) = \sum_{k=0}^{\infty} \frac{1}{k!} (\partial_t + \vec{c}_i \cdot \nabla)^k f_i(\vec{x}, t). \tag{3.9}$$

Substituting this expansion into the LBE, we find the lowest order equation yields no information, and we proceed to first order.

$$\sum_{k=1}^{\infty} \frac{1}{k!} (\partial_t + \vec{v} \cdot \nabla)^k f_i(\vec{x}, t) = -\frac{1}{\tau} (f_i - f_i^{\text{eq}}) \tag{3.10}$$

The LBE is now defined solely in terms of derivatives in (3.10), allowing the expansion of the time derivatives and  $f$ 's into smaller contributions. The contribution of each term will be relative to the smallness parameter  $\varepsilon$  for ( $\varepsilon \ll 1$ ). This breaks down the LBE into contributions from various time scales where the lowest time scale is Euler (ideal), and

then follows the transport time scale.

$$\partial_t \rightarrow \varepsilon \partial_t^{(0)} + \varepsilon^2 \partial_t^{(1)} + \dots \quad (3.11a)$$

$$\partial_\alpha \rightarrow \varepsilon \partial_\alpha \quad (3.11b)$$

$$f \rightarrow f^{(0)} + \varepsilon f^{(1)} + \varepsilon^2 f^{(2)} + \dots \quad (3.11c)$$

In this notation, the  $\mathcal{O}(1)$  terms in the LBE (3.10) provide the equation

$$\mathcal{O}(1) : \quad 0 = -\frac{1}{\tau} \left( f_i^{(0)} - f_i^{\text{eq}} \right) . \quad (3.12)$$

proving the relationship  $f^{\text{eq}} \equiv f^{(0)}$ .

Conserved quantities such as  $\rho$  and  $\rho \vec{u}$  are collisional invariants, meaning that they remain unchanged (conserved) during particle collisions. In order to preserve these quantities, they are solely defined by the lowest order distributions  $f^{\text{eq}}$ . Specifically,

$$\rho = \sum_i f_i^{\text{eq}} \quad (3.13a)$$

$$\rho \vec{u} = \sum_i \vec{c}_i f_i^{\text{eq}} \quad (3.13b)$$

with

$$0 = \sum_i f_i^{(k)} \quad (3.14a)$$

$$0 = \sum_i \vec{c}_i f_i^{(k)} \quad (3.14b)$$

for  $k > 0$ .

Inserting these expanded terms (3.11) into (3.10) we find the next two lowest order equations corresponding to the ideal evolution (without dissipation) time scale and the

dissipative time scale respectively are

$$\mathcal{O}(\varepsilon) : \quad \partial_t^{(0)} f_i^{(0)} + \vec{c}_i \cdot \nabla f_i^{(0)} = -\frac{1}{\tau} f_i^{(1)} \quad (3.15)$$

$$\mathcal{O}(\varepsilon^2) : \quad \partial_t^{(0)} f_i^{(1)} + \vec{c}_i \cdot \nabla f_i^{(1)} + \partial_t^{(1)} f_i^{(0)} + \frac{1}{2} \left( \partial_t^{(0)} + \vec{c}_i \cdot \nabla \right)^2 f_i^{(0)} = -\frac{1}{\tau} f_i^{(2)} \quad (3.16)$$

The  $\mathcal{O}(\varepsilon^2)$  equation can be further simplified by substituting the  $\mathcal{O}(\varepsilon)$  equation into the fourth term resulting in

$$\partial_t^{(0)} f_i^{(1)} + \vec{c}_i \cdot \nabla f_i^{(1)} + \partial_t^{(1)} f_i^{(0)} + \frac{1}{2} \left( \partial_t^{(0)} + \vec{c}_i \cdot \nabla \right) \left( -\frac{1}{\tau} f_i^{(1)} \right) = -\frac{1}{\tau} f_i^{(2)} \quad (3.17)$$

Simplified, the  $\mathcal{O}(\varepsilon^2)$  equation becomes

$$\mathcal{O}(\varepsilon^2) : \quad \partial_t^{(1)} f_i^{(0)} + \left( 1 - \frac{1}{2\tau} \right) \left( \partial_t^{(0)} + \vec{c}_i \cdot \nabla \right) f_i^{(1)} = -\frac{1}{\tau} f_i^{(2)} \quad (3.18)$$

If the  $\mathcal{O}(\varepsilon)$  (3.15) and  $\mathcal{O}(\varepsilon^2)$  (3.18) equations are now recombined we get

$$\left( \partial_t + \vec{c}_i \cdot \nabla \right) f_i^{(0)} + \left( 1 - \frac{1}{2\tau} \right) \left( \partial_t^{(0)} + \vec{c}_i \cdot \nabla \right) f_i^{(1)} = -\frac{1}{\tau} \left( f_i^{(1)} + f_i^{(2)} \right) \quad (3.19)$$

the final combined evolution equation with ideal and dissipative terms.

## Derivation of the Continuity Equation

Now, we can recover the Navier-Stokes equations by taking the conserved moments from the combined evolution equation (3.19). We will start with the zeroth moment to recover the density equation. It should be noted that  $\vec{c}_i$  commutes with the  $\partial_t$  and  $\nabla$  operators and the partial derivatives can be factored out of the sum. Taking the moments

term by term, and using (3.13) and (3.14) we find that

$$\sum_i \left[ \partial_t f_i^{(0)} + \nabla \cdot \vec{c}_i f_i^{(0)} + \left(1 - \frac{1}{2\tau}\right) \left( \partial_t^{(0)} f_i^{(1)} + \nabla \cdot \vec{c}_i f_i^{(1)} \right) = -\frac{1}{\tau} \left( f_i^{(1)} + f_i^{(2)} \right) \right] \quad (3.20)$$

$$\partial_t \rho + \nabla \cdot \rho \vec{u} + \left(1 - \frac{1}{2\tau}\right) (0 + 0) = 0 \quad (3.21)$$

Simplified, the continuity equation is

$$\partial_t \rho + \nabla \cdot \rho \vec{u} = 0 \quad (3.22)$$

which is the Navier-Stokes equation governing the evolution of fluid density.

### Derivation of the Momentum Equation

Next, the first conserved moment of (3.19) will prove to be the more difficult equation but will result in the Navier-Stokes momentum equation. To begin, we take the first moment of (3.19) by multiplying through by  $\vec{c}_i$  and then summing over  $i$ . The momentum equation initially takes the form

$$\begin{aligned} & \sum_i \partial_t \vec{c}_i f_i^{(0)} + \sum_i \nabla \cdot \vec{c}_i \vec{c}_i f_i^{(0)} \\ & + \sum_i \left(1 - \frac{1}{2\tau}\right) \left( \partial_t^{(0)} \vec{c}_i f_i^{(1)} + \nabla \cdot \vec{c}_i \vec{c}_i f_i^{(1)} \right) = - \sum_i \frac{1}{\tau} \left( \vec{c}_i f_i^{(1)} + \vec{c}_i f_i^{(2)} \right) \end{aligned} \quad (3.23)$$

$$\partial_t \rho \vec{u} + \nabla \cdot \Pi^{(0)} + \left(1 - \frac{1}{2\tau}\right) (0 + \nabla \cdot \Pi^{(1)}) = 0 \quad (3.24)$$

In order to evaluate the non-conserved moments that have appeared  $\Pi^{(0)}$  and  $\Pi^{(1)}$ , we need to be able to evaluate a moment's equilibrium. The second and third moment equilibria are evaluated below using (3.5). Henceforth, Greek indices will be used for vector components and Roman indices will be used for lattice components. It is important to note here that

$c_{\alpha i} c_{\alpha i} c_{\alpha i} = c_{\alpha i}$  for some dimension  $\alpha$ .

$$\sum_i c_{\alpha i} c_{\beta i} f_i^{\text{eq}} = \Pi_{\alpha\beta}^{\text{eq}} = \rho \left( \delta_{\alpha\beta} \frac{1}{3} + u_\alpha u_\beta \right) \quad (3.25)$$

$$\sum_i c_{\alpha i} c_{\beta i} c_{\gamma i} f_i^{\text{eq}} = \delta_{\alpha\gamma} \frac{\rho u_\beta}{3} + \delta_{\beta\gamma} \frac{\rho u_\alpha}{3} + \delta_{\alpha\beta} \frac{\rho u_\gamma}{3} \quad (3.26)$$

With  $\Pi^{\text{eq}}$  evaluated above (3.25) and set to  $\Pi^{(0)}$  via (3.12), we simply need to determine  $\Pi^{(1)}$ . This is found by taking the second moment of the  $\mathcal{O}(\varepsilon)$  equation (3.15) which appears as

$$\sum_i \partial_t^{(0)} \vec{c}_i \vec{c}_i f_i^{(0)} + \sum_i \vec{c}_i \vec{c}_i \vec{c}_i \cdot \nabla f_i^{(0)} = - \sum_i \frac{1}{\tau} \vec{c}_i \vec{c}_i f_i^{(1)} \quad (3.27)$$

and solving for  $\sum_i \vec{c}_i \vec{c}_i f_i^{(1)}$ . The first term in (3.27) is found by applying the chain rule to the specified non-conserved equilibrium in terms of the conserved equilibria as shown in (3.28). The solutions to the resulting time derivatives of the conserved quantities are then plugged in from their corresponding  $\mathcal{O}(\varepsilon)$  moment equation (3.15). Summation convention is used only over the Greek indices which give the vector nature of the fields. Because LB functions in the low velocity limit ( $|\vec{u}| \ll \text{Ma}$ ), simplification of these derivatives to  $\mathcal{O}(u^2)$  is allowed.

$$\sum_i \partial_t^{(0)} c_{\alpha i} c_{\beta i} f_i^{(0)} = \partial_t^{(0)} \Pi_{\alpha\beta}^{\text{eq}} = \frac{\partial \Pi_{\alpha\beta}^{\text{eq}}}{\partial \rho} \partial_t^{(0)} \rho + \frac{\partial \Pi_{\alpha\beta}^{\text{eq}}}{\partial \rho u_\gamma} \partial_t^{(0)} \rho u_\gamma \quad (3.28)$$

$$\partial_t^{(0)} \Pi_{\alpha\beta}^{\text{eq}} = \left( \delta_{\alpha\beta} \frac{1}{3} + u_\alpha u_\beta \right) (-\nabla \cdot \rho \vec{u}) + (\delta_{\alpha\gamma} u_\beta + \delta_{\beta\gamma} u_\alpha) \left( -\nabla_\lambda \rho \left( \delta_{\lambda\gamma} \frac{1}{3} + u_\lambda u_\gamma \right) \right) \quad (3.29)$$

$$\partial_t^{(0)} \Pi_{\alpha\beta}^{\text{eq}} \approx -\frac{1}{3} (\delta_{\alpha\beta} \nabla \cdot \rho \vec{u} + u_\beta \nabla_\alpha \rho + u_\alpha \nabla_\beta \rho) + \mathcal{O}(u^3) \quad (3.30)$$

Now that the first term of (3.27) is determined, the second term can be found by simply substituting in the equilibrium term (3.26) found previously. And so the final

solution to  $\Pi^{(1)}$  is found by substituting (3.30) and (3.26) into (3.27).

$$\Pi_{\alpha\beta}^{(1)} = -\frac{\tau}{3} [-(\delta_{\alpha\beta}\nabla \cdot \rho\vec{u} + u_\beta\nabla_\alpha\rho + u_\alpha\nabla_\beta\rho) + \nabla_\alpha\rho u_\beta + \nabla_\beta\rho u_\alpha + \delta_{\alpha\beta}\nabla \cdot \rho\vec{u}] \quad (3.31)$$

$$\Pi_{\alpha\beta}^{(1)} = -\frac{\tau}{3} [-u_\beta\nabla_\alpha\rho - u_\alpha\nabla_\beta\rho + \nabla_\alpha\rho u_\beta + \nabla_\beta\rho u_\alpha] \quad (3.32)$$

$$\Pi_{\alpha\beta}^{(1)} = -\frac{\tau}{3}\rho[\nabla_\alpha u_\beta + \nabla_\beta u_\alpha] \quad (3.33)$$

The LB derived momentum evolution equation is now solved by substituting  $\Pi^{(0)}$  (3.25) and  $\Pi^{(1)}$  (3.33) into (3.24).

$$\partial_t\rho u_\beta + \nabla_\alpha\rho\left(\delta_{\alpha\beta}\frac{1}{3} + u_\alpha u_\beta\right) - \frac{\tau}{3}\left(1 - \frac{1}{2\tau}\right)\nabla_\alpha\rho(\nabla_\alpha u_\beta + \nabla_\beta u_\alpha) = 0 \quad (3.34)$$

$$\partial_t\rho\vec{u} + \nabla \cdot \rho(\vec{u}\vec{u}) = -\nabla\frac{\rho}{3} + \frac{1}{3}\left(\tau - \frac{1}{2}\right)\nabla_\alpha\rho(\nabla_\alpha u_\beta + \nabla_\beta u_\alpha) \quad (3.35)$$

The form of the LB derived momentum evolution equation can be further simplified below to precisely match the Navier-Stokes momentum equation

$$\partial_t\rho\vec{u} + \rho(\vec{u} \cdot \nabla)\vec{u} = -\nabla P + 2\nabla \cdot \nu\rho\mathbf{S} \quad (3.36)$$

where  $\mathbf{S}$  is the strain rate tensor with  $S_{\alpha\beta} = \frac{1}{2}(\nabla_\alpha u_\beta + \nabla_\beta u_\alpha)$ ,  $P$  is the pressure evaluated as  $P = \frac{\rho}{3}$ , and  $\nu$  is the kinematic viscosity evaluated as  $\nu = \frac{1}{3}\left(\tau - \frac{1}{2}\right)$ .

It is possible to further simplify the momentum equation if we assume incompressible Navier-Stokes with uniform density ( $\rho$ ). Separating out the diffusive term

$$\partial_t\rho\vec{u} + \nabla \cdot \rho(\vec{u}\vec{u}) = -\nabla P + \nu((\nabla\rho) \cdot (\nabla\vec{u}) + (\nabla\vec{u}) \cdot (\nabla\rho) + \rho(\nabla^2\vec{u} + \nabla\nabla \cdot \vec{u})) \quad (3.37)$$

and applying the assumption that  $\nabla\rho \rightarrow 0$  and  $\nabla \cdot \vec{u} \rightarrow 0$ , we find a simpler form to the

momentum equation for a given problem.

$$\partial_t \rho \vec{u} + \rho (\vec{u} \cdot \nabla) \vec{u} = -\nabla P + \nu \rho (\nabla^2 \vec{u}) \quad (3.38)$$

This chapter has shown how LB functions as an extremely parallelizable fluid simulation method and has even proven its accuracy in reproducing the well-known Navier-Stokes equations. In CFD, one has to deal with the nonlinear convective derivative  $(\vec{u} \cdot \nabla) \vec{u}$ , while in LB one is dealing with the passive linear advection  $c_i \cdot \nabla$  for the fixed lattice vector  $c_i$ . As mentioned in chapter 1, parallelization is a critical factor which sets LB apart from other CFD methods, allowing it to maximize the use of modern HPC's.

# CHAPTER 4

## Magnetohydrodynamics

Plasma is a state of matter in which the constituents of a gas are ionized typically into electrons and ions. What makes the description of a plasma difficult is the huge range in both length and time scales that are possible. For a simple hydrogen plasma with densities  $10^{19} \text{ m}^{-3}$ , temperatures of 1 keV, magnetic fields of 3 T and plasma lengths of 0.5 m, one finds that length scales range from the 0.5 m down to the Debye length of  $7 \times 10^{-5} \text{ m}$ , while time scales range from the electron times  $3.5 \times 10^{-11} \text{ s}$  to ion cyclotron and Alfvén times of  $2 \times 10^{-8} \text{ s}$ , to resistive time scales of 2 ms and Ohmic decay times of 3 s [12].

This makes it impossible to devise a practical computationally feasible model to cover all the parameters ranges. Hence one is forced into simplified restricted subsets of models, with some overlapping others. The BBGKY hierarchy is unmanageable and so some form of low order closure is hoped for. One of the simplest BBGKY closure models is to ignore all binary-particle interactions, while retaining the collective effects in the system. This will lead to the Vlasov equation, coupled to the Maxwell equations. One of the difficulties of the Vlasov model is that it is still time-reversible (as is the underlying equations of motion of all the particles underlying the plasma) and hence no H-theorem exists nor the



tendency for the plasma to move towards a thermal equilibrium. In the time scales longer than the particle collision times, one must now consider equilibration effects, typically requiring (kinetic) velocity-space diffusion. This requires the consideration of binary particle collisions. At this order of closure, the BBGKY hierarchy leads to the Fokker-Planck equation and to its plasma cousin, the Balescu-Lenard equations. The Balescu-Lenard extension of the Fokker-Planck equation now includes renormalized potential interactions terms due to the collective nature of the plasma. These equations do possess an H-theorem and can (in principle) lead to thermal equilibrium. Generally these equations are too complex and computationally straining, leaving one to seek other models if near-equilibrium problems are of interest.

The simpler models are the fluid representations of the plasma. Binary collisions and (non-destructive) plasma instabilities will typically drive a plasma to relaxation in the kinetic-velocity space while maintaining spatial gradients that resolve on longer time scales. Within these time scales the plasma is well approximated by local Maxwellian velocity distributions [viewing binary collisions as local]. These quasi-Maxwellian distributions have the nice feature of being described by the first few moments: mean density, mean velocity and thermal (kinetic) temperature. An attempt is made to take moments of the kinetic equations and form a hierarchy of moment equations which themselves need further closure approximations. This description is now in the realm of fluid equations. One would expect that the simplest accurate plasma model would be the two-fluid MHD model, made up of one set of fluid equations for the ions which is coupled to the fluid equations for the electrons. The neutral particles which exist can be marginalized, treating them as higher order effects. Beyond this two-fluid MHD model, the one-fluid MHD model is an even simpler plasma model that is remarkably robust in its predictions. The one-fluid MHD model, where the different species are averaged, is the model that is of interest in this thesis.

The previously derived Boltzmann equation (2.5), altered to include the long-range forces will serve as the basis for deriving the MHD equations

$$\frac{d}{dt}f = \left( \frac{\partial}{\partial t} + \vec{v}_i \cdot \nabla_{\vec{x}} + \frac{\vec{F}}{m} \cdot \nabla_{\vec{v}} \right) f_i = (\partial_t f_i)_{col} \quad (4.1)$$

In MHD, the long range forces are governed by the Lorentz force. Rewriting the Boltzmann equation, we have

$$\left( \frac{\partial}{\partial t} + \vec{v}_i \cdot \nabla_{\vec{x}} + \frac{q}{m} \left( \vec{E} + \frac{\vec{u}}{c} \times \vec{B} \right) \cdot \nabla_{\vec{v}} \right) f = (\partial_t f_i)_{col} \quad (4.2)$$

where  $\vec{E}$  is the electric field,  $\vec{u}$  is the macroscopic plasma velocity, and  $\vec{B}$  is the magnetic field.

## 4.1 MHD Magnetic Equation

Deriving an equation governing the evolution of the magnetic field begins with Ohm's law, assumed to state that the Lorentz force is equivalent to the product of resistivity and current density.

$$\vec{E} + \frac{\vec{u}}{c} \times \vec{B} = \eta \vec{J}. \quad (4.3)$$

where  $\vec{J}$  is the current density and  $\eta$  is the resistivity. Substituting Ohm's law (4.3) into Ampere's law

$$\nabla \times \vec{B} = \frac{4\pi \vec{J}}{c} + \frac{1}{c} \frac{\partial \vec{E}}{\partial t} \quad (4.4)$$

we have a new relation for the current density

$$\nabla \times \vec{B} = \frac{4\pi\vec{J}}{c} - \frac{1}{c^2} \frac{\partial (\vec{u} \times \vec{B} - c\eta\vec{J})}{\partial t} \quad (4.5)$$

In non-relativistic simulations,  $c \gg |\vec{u}|$ , or considering only low frequencies, the second term on the RHS is negligible. We can absorb the remaining coefficients into the current, defining it in terms of “natural” units as

$$\nabla \times \vec{B} = \vec{J} \quad (4.6)$$

From here, Ohm’s law (4.3) can be combined with Faraday’s law

$$\nabla \times \vec{E} = -\frac{1}{c} \frac{\partial \vec{B}}{\partial t} \quad (4.7)$$

to recover the induction equation in MHD

$$\frac{\partial \vec{B}}{\partial t} = \nabla \times (\vec{u} \times \vec{B}) - \nabla \times \eta \vec{J} \quad (4.8)$$

where “natural” units are used,  $\vec{J}$  is the current density and  $\eta$  is the resistivity.  $\vec{J}$  can be replaced with the previous solution for the current density (4.6), simplifying the induction equation to

$$\frac{\partial \vec{B}}{\partial t} = \nabla \times (\vec{u} \times \vec{B}) + \eta \nabla^2 \vec{B} . \quad (4.9)$$

where  $\eta$  is considered to be constant.

The induction equation provides the evolution of the magnetic field over time in MHD. It is worth noting that  $\nabla \cdot \nabla \times (\vec{u} \times \vec{B}) = 0$ , making  $\nabla \cdot \vec{B} = 0$  automatically satisfied for

all future time when no resistivity is present.

## 4.2 MHD Fluid Equations

The MHD fluid equations are recovered from the MHD Boltzmann equation (4.2) by taking moments (2.12) according to the procedure mentioned in sec 3.3.

### 4.2.1 Continuity Equation

The zeroth moment of the Boltzmann equation (4.2) becomes, term by term

$$\int_{-\infty}^{\infty} d^3v \partial_t f = \partial_t \int_{-\infty}^{\infty} d^3v f = \partial_t \rho \quad (4.10)$$

where  $\rho$  is the macroscopic fluid density. The second term is

$$\int_{-\infty}^{\infty} d^3v \vec{v} \cdot \nabla_x f = \nabla_x \cdot \int_{-\infty}^{\infty} d^3v (\vec{v} f) = \nabla \cdot (\rho \vec{u}) \quad (4.11)$$

where  $\vec{u}$  is the macroscopic fluid velocity. This relation exists because  $\nabla \cdot \vec{v} = 0$ . The third term is

$$\int_{-\infty}^{\infty} d^3v \frac{\vec{F}}{m} \cdot \nabla_v f = \sum_{\alpha} \int_{-\infty}^{\infty} d^2v \left[ \frac{\vec{F}_{\alpha}}{m} f \right]_{v_{\alpha}=-\infty}^{v_{\alpha}=\infty} - \int_{-\infty}^{\infty} d^3v \frac{f}{m} \nabla_v \cdot \vec{F} = 0 \quad (4.12)$$

which goes to 0 because  $f \rightarrow 0$  as  $v \rightarrow \pm\infty$  and  $\nabla_v \cdot \vec{F} = 0$  for the Lorentz force.

Finally, the collision term defines the relationship between particles of different species. Two defining rates are the rate of ionization and the rate of change in momentum. The rate of ionization/recombination describes the production or annihilation of particle number/mass. The ionization rate for all species modeled must sum to zero. Also, the rate

of change in momentum occurs due to collisions with other particle species and will be set to zero if all species modeled have the same mass. Since the current MHD model consists of only one species, these values are set to zero and the collision term can be replaced by the simple BGK operator used in LB just as before (2.13). All orders of contribution in Chapman-Enskog of the collision term for the zeroth moment are zero according to the procedure outlined in sec. 3.4.

The resulting MHD continuity equation can thus be written as

$$\frac{\partial \rho}{\partial t} + \nabla \cdot (\rho \vec{u}) = 0 \quad (4.13)$$

## 4.2.2 Momentum Equation

The momentum equation exists as the first moment of (4.2). Similar to the continuity equation, term by term, the first term is

$$\int_{-\infty}^{\infty} d^3v \partial_t \vec{v} f = \partial_t \int_{-\infty}^{\infty} d^3v \vec{v} f = \partial_t \rho \vec{u} \quad (4.14)$$

The second term is the divergence of the second moment of  $f_i$  (2.12c)

$$\int_{-\infty}^{\infty} d^3v \vec{v} \cdot \nabla_x \vec{v} f = \nabla_x \cdot \int_{-\infty}^{\infty} d^3v (\vec{v} \vec{v} f) = \nabla \cdot (\rho \vec{u} \vec{u}) + \nabla P \quad (4.15)$$

where  $P$  is the macroscopic fluid pressure  $P = 2\rho RT$ . The third term representing the Lorentz force is

$$\begin{aligned}
\int_{-\infty}^{\infty} d^3v \vec{v} \frac{\vec{F}}{m} \cdot \nabla_v f &= \sum_{\alpha} \int_{-\infty}^{\infty} d^2v \left[ \vec{v} \frac{\vec{F}_{\alpha}}{m} f \right]_{v_{\alpha}=-\infty}^{v_{\alpha}=\infty} - \int_{-\infty}^{\infty} d^3v \frac{f}{m} \nabla_v \cdot (\vec{F} \vec{v}) \\
&= 0 - \left( \int_{-\infty}^{\infty} d^3v \frac{f}{m} \vec{v} \nabla_v \cdot \vec{F} + \int_{-\infty}^{\infty} d^3v \frac{f}{m} \vec{F} \cdot \nabla_v \vec{v} \right) \\
&= 0 - \left( 0 + \frac{\rho}{m} \vec{F} \right) = -n\vec{F}
\end{aligned} \tag{4.16}$$

where  $n$  is the number density. The first term on the right-hand side of (4.16) is zero since  $f$  scales as  $\exp(-v^2)$  near equilibrium according to (2.11). The second term of (4.16) is zero since  $\nabla_v \cdot \vec{F} = 0$ , leaving the solution  $-n\vec{F}$ .

MHD is prone to quasi-neutrality, meaning that locally the number density of ions is approximately equal to the number density of electrons,  $n_{ion} \approx n_{elec}$ . Since the charge of ions and electrons are opposite, this implies that  $\vec{E}$  is balanced and can be equated to zero ( $\vec{E} \rightarrow 0$ ), leaving  $n\vec{F} = nq\frac{\vec{u}}{c} \times \vec{B} = \vec{J} \times \vec{B}$  where  $\vec{J}$  is the current density. The Lorentz force can be further simplified using (4.6). In “natural” units, the third term is

$$\vec{F} = \vec{J} \times \vec{B} = \left( \vec{B} \cdot \nabla \right) \vec{B} - \frac{1}{2} \nabla B^2 \tag{4.17}$$

As stated before, the collision term is replaced with the BGK operator according to (2.13). The first moment of this operator at the hydrodynamic time scale equals zero, however, following the same procedure in sec. 3.4, the viscosity shows itself at the viscous time scale in Chapman-Enskog expansions of order  $\mathcal{O}(\varepsilon^2)$ . Following the Chapman-Enskog procedure as before, the viscosity can be inserted with the same result as for Navier-Stokes into the momentum equation as  $2\nabla \cdot \nu \rho \mathbf{S}$  where  $\nu$  is the dissipation rate and  $\mathbf{S}$  is the strain-rate tensor with  $S_{\alpha\beta} = \frac{1}{2} (\nabla_{\alpha} u_{\beta} + \nabla_{\beta} u_{\alpha})$ .

The resulting MHD momentum equation is

$$\rho \frac{\partial \vec{u}}{\partial t} + \rho (\vec{u} \cdot \nabla) \vec{u} = -\nabla P + \left( \vec{B} \cdot \nabla \right) \vec{B} - \frac{1}{2} \nabla B^2 + 2\nabla \cdot \nu \rho \mathbf{S} \quad (4.18)$$

In summation, the dissipative, resistive MHD equations are

$$\frac{\partial \rho}{\partial t} + \nabla \cdot \vec{u} = 0 \quad \nabla \cdot \vec{B} = 0 \quad (4.19a)$$

$$\rho \frac{\partial \vec{u}}{\partial t} + (\vec{u} \cdot \nabla) \vec{u} = -\nabla p + \left( \vec{B} \cdot \nabla \right) \vec{B} + 2\nabla \cdot \nu \rho \mathbf{S} \quad (4.19b)$$

$$\frac{\partial \vec{B}}{\partial t} = \left( \vec{B} \cdot \nabla \right) \vec{u} - (\vec{u} \cdot \nabla) \vec{B} + \eta \nabla^2 \vec{B} \quad (4.19c)$$

$$d_t \left( \frac{p}{\rho^\gamma} \right) = 0 \quad (4.19d)$$

where  $\nabla \cdot \vec{B}$  is included from Gauss's law for magnetism, the  $\frac{1}{2}B^2$  term is combined with the pressure  $P$  to become a new pressure  $p$ , and the evolution of pressure is stated in the adiabatic case with  $\gamma$  as the ratio of specific heats taken to be 5/3. The stated energy equation is only applicable in the absence of shocks and heat conduction.

### 4.3 Dellar's lattice Boltzmann MHD model

Lattice Boltzmann has been extended to include MHD by Dellar [13]. Because MHD includes a third evolution equation which governs the magnetic field, his concept was to create a magnetic distribution which evolves alongside the fluid and governs the magnetic field. This new distribution would have only the magnetic field as a conserved moment and would evolve in the same manner as the fluid. Ideally, the conserved moments make up the lowest moments of a distribution. In order to accommodate the vector magnetic field in the zeroth moment, Dellar made the distribution a vector distribution. This means that in 3D, there would be three magnetic distributions evolving alongside each other and

the fluid.

Dellar’s magnetic field LB equation is

$$\partial_t \vec{g}_i + \partial_\alpha e_{\alpha i} \vec{g}_i = \frac{1}{\tau_g} (\vec{g}_i - \vec{g}_i^{\text{eq}}) \quad (4.20)$$

where  $\vec{g}_i$  is a vector distribution with  $i$  denoting the discrete velocity component of the magnetic lattice  $\vec{e}_i$  (similar to  $\vec{c}_i$ ),  $\vec{g}_i^{\text{eq}}$  is the value of  $\vec{g}_i$  at equilibrium, and  $\tau_g$  is the relaxation rate related to resistivity by  $\eta = c_s^2 (\tau_g - \frac{1}{2})$  and  $c_s$  is the speed of sound of the lattice. The importance of the vector magnetic distribution approach is that it is able to enforce the critical  $\nabla \cdot \vec{B} = 0$  constraint automatically and not need divergence cleaning as required by standard CFD algorithms.

Physically, this kinetic model for the magnetic field has no direct analog, especially since “collisional” effects in the magnetic field represent the resistivity. A simplistic approach to rationalizing the concept is to imagine that the individual particles create their own magnetic field which follow them as they move through space. The fluid distribution describing the collection of particles can be mimicked for the collection of corresponding magnetic fields. The total contribution of generated magnetic fields in a local region sum to represent the macroscopic magnetic field of that region. Lattice Boltzmann is not attempting to model the true kinetics of the system, instead it tries to model the MHD equations at the macroscopic scale in a mesoscopic kinetic form. Some butchering of the kinetics is justifiable as long as they recover the MHD equations in a Chapman Enskog expansion.

The fluid equilibrium must be modified such that a force balance occurs between the pressure gradient and the quasi-neutral Lorentz force ( $\nabla P - \vec{J} \times \vec{B} = 0$ ) with  $\vec{J}$  defined in (4.6). The equilibrium is then expanded in Hermite polynomials as found in [9]. In 2D,



the new fluid equilibrium appears as

$$f_i^{\text{eq}} = w_i \rho \left( 1 + \frac{1}{c_s^2} \vec{c}_i \cdot \vec{u} + \frac{1}{2c_s^4} (\vec{c}_i \cdot \vec{u})^2 - \frac{1}{2c_s^2} \vec{u}^2 \right) + \frac{w_i}{2c_s^4} \left( \frac{1}{2} |\vec{B}|^2 |\vec{c}_i|^2 - (\vec{c}_i \cdot \vec{B})^2 \right) \quad (4.21)$$

where  $c_s$  is the speed of sound of the lattice and is typically set to  $c_s = \frac{1}{\sqrt{3}}$ .

The magnetic equilibrium can be set to any simple distribution where the zeroth moment is equal to the magnetic field

$$\sum_i g_{\alpha i} = B_\alpha \quad (4.22)$$

and the first moment is equal to the Lorentz tensor

$$\sum_i c_{\alpha i} g_{\beta i}^{\text{eq}} = u_\alpha B_\beta - B_\alpha u_\beta . \quad (4.23)$$

This distribution in 2D is

$$g_{\beta i}^{\text{eq}} = w_i \left( B_\beta + \frac{c_{\alpha i}}{c_s^2} [u_\alpha B_\beta - B_\alpha u_\beta] \right) \quad (4.24)$$

to cubic error in terms of  $\vec{u}$  and  $\vec{B}$ .

### 4.3.1 Lattice Velocities

The new magnetic vector distribution only has one conserved moment per vector component in any dimensional space. Following the rules from sec. 3.2, in 2D, only three moments are required from each vector component to reproduce the induction equation (1 magnetic field and 2 elements from the quasi-neutral Lorentz tensor). In 3D, this becomes four moments (1 magnetic and 3 elements from the Lorentz tensor). As can be seen, the magnetic vector distribution requires fewer moments and can take advantage of a smaller

number of lattice vectors than the scalar fluid distribution. It is then possible to run a simulation with the fluid on one type of lattice and the magnetic field simultaneously on a second type of lattice, as long as the conserved moments  $(\rho, \vec{u}, \vec{B})$  can be defined at all points on both lattice types. An example would be if the fluid is run on the D2Q9 lattice while the magnetic field is run on the D2Q5 (with missing corner velocities from D2Q9) lattice. The points on the D2Q5 and D2Q9 lattices overlap, allowing the macroscopic variables to be easily defined at every point in both lattices.

## 4.4 Return to MHD equations

Recovering all three MHD equations from the new distributions is performed just as before in sec. 3.4. The scalar fluid distribution reproduces the continuity and momentum equation in the same way as before since the only change is in the equilibrium. One notable change is that the second moment's equilibrium has become

$$\sum_i c_{\alpha i} c_{\beta i} f_i^{\text{eq}} = \Pi_{\alpha\beta}^{\text{eq}} = \rho \left( \delta_{\alpha\beta} \frac{1}{3} + u_\alpha u_\beta \right) + \frac{1}{2} B^2 \delta_{\alpha\beta} - B_\alpha B_\beta . \quad (4.25)$$

The induction equation is found in the same manner as the fluid by following the steps found in sec. 3.4 for the magnetic vector distribution at the zeroth moment.

### 4.4.1 $\nabla \cdot \mathbf{B} = 0$

In general, when dealing with ideal MHD, the Maxwell equation,  $\nabla \cdot \vec{B} = 0$ , tends to be satisfied implicitly. As resistivity is incorporated, we typically find that  $\nabla \cdot \vec{B} = 0$  must be manually enforced in simulations. In order to enforce this physical law in resistive MHD, a process called divergence cleaning must be employed. Divergence cleaning is performed by subtracting the “unphysical” part of the magnetic field represented as  $\nabla\phi$  where the

magnetic field is represented as  $\vec{B} = \nabla \times \vec{A} + \nabla\phi$ . Subtracting this unphysical quantity requires the Fourier transform, a bottleneck step in parallel computation.

Divergence is satisfied automatically in Dellar's model. According to [13], the divergence of the magnetic field was found to be  $< 10^{-16}$  in numerical experiments using 64-bit (17 digit) IEEE floating point arithmetic. This precision is explained by maintaining that the trace of the first moment is zero to second order in the Chapman-Enskog expansion. At third order, a lack of isotropy occurs, but as stated, this error was found to be incredibly small and thus negligible. This automatic precision of  $\nabla \cdot \vec{B}$  in resistive MHD is an important improvement over CFD for extreme parallelizability.

# CHAPTER 5

## Characteristics of Simulations

This chapter will focus on some of the simulation characteristics used to verify the accuracy of the new LB models expressed in this thesis. Two important characteristics explored here are related to the energy spectrum of turbulent flows and the Kelvin-Helmholtz instability. Firstly, the energy spectrum of turbulent flows in 2D and 3D for both Navier-Stokes and MHD are expected to carry certain predictable quantitative and qualitative attributes, if enough time to evolve has elapsed. These attributes exist regardless of a flow's initial conditions.

The second set of characteristics used pertain to the simulation of the Kelvin-Helmholtz (KH) instability. The early time evolution of many instabilities can be predicted analytically with a certain level of accuracy by linearization. Given that these instabilities are some of the only ways to analytically predict the evolution of turbulent flows, they are crucial in verifying the accuracy of turbulence models and simulations. In this thesis, the Kelvin-Helmholtz instability is used to verify accuracy in each model.

## 5.1 Energy Spectrum

The energy spectrum of an evolved turbulent system can be an important indicator of simulation accuracy. As new models are created, they are typically expected to follow “universal” spectral forms. A simulation without these expected spectral forms can be ruled as not modeling physical fluids unless a theory predicts otherwise. Much work has gone into predicting the spectra of evolved turbulent systems.

The energy spectrum of a spatial simulation can be generated by taking the Fourier transform of the full simulation space. This is done separately for each vector component of the fluid momentum (square root of kinetic energy  $\sqrt{\rho}u_\alpha$ ) and magnetic field (square root of magnetic energy  $B_\alpha$ ) to obtain the kinetic spectrum and magnetic spectrum respectively. The Fourier transform has changed the grid dimensions from spatial position  $(x, y, z)$  to wavenumber  $(k_x, k_y, k_z)$ . The square root of the total energy for a particular wavenumber is then the surface elements drawn out by some radius  $k$  from wavenumber  $(0, 0, 0)$ . The components of the kinetic spectrum can then be squared (multiplied by its own conjugate), added to other components, and normalized for the one-dimensional kinetic spectrum of the system. The same steps can be done for the magnetic spectrum and adding the two spectra together provides the total energy spectrum of the system.

An example of a total energy spectrum is presented in Fig. 5.1 with log-log scaling, allowing the spectra in the inertial subrange to be exhibited by a straight line. The plot shows three basic regions of motion: the energy containing range made up of large scale mixing in the fluid, the inertial subrange at the intermediate scale, and the dissipation range where fluid motion is dissipated into heat. Each range plays an important role in the evolution of the system but none are as frequently used in verifying simulation accuracy as the inertial subrange; since the inertial subrange is the only range that has “universal” characteristics for all simulations.

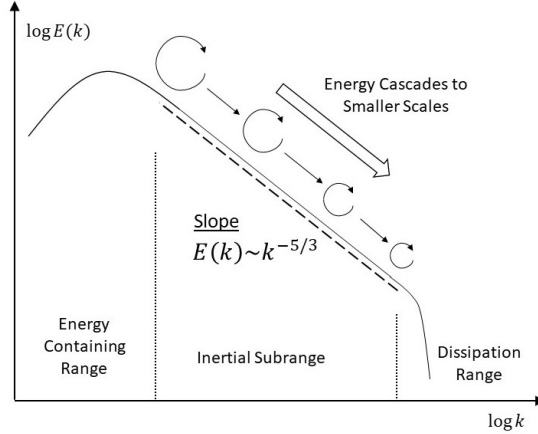


FIG. 5.1: **A model energy spectrum.** Most of the energy is in large scales on the left side while the dissipative range on the right has very little energy. In the inertial subrange, energy cascades over time to smaller scales and maintains an average slope of  $k^{-5/3}$ .

According to the second Kolmogorov similarity hypothesis, any turbulent flow at sufficiently high Reynold's number will produce an energy-spectrum function in the inertial subrange equal to

$$E(k) = C\varepsilon^{2/3}k^{-5/3} \quad (5.1)$$

where  $C$  is a universal Kolmogorov constant supported by experimental data to be  $C = 1.5$  and  $\varepsilon$  is the rate of dissipation [14]. This slope is well accepted and frequently used as a measure of model/simulation accuracy.

Similarly, the energy containing range at small  $k$  is expected to have a slope of  $k^{p_0}$  with  $p_0 = 2$ , while the dissipation range is expected to decay very rapidly at large  $k$ ,  $E(k) \sim k^{-5/3}e^{-k}$  [14]. These slopes are much more difficult to measure since the slope approaches  $k^{-5/3}$  as  $k$  approaches the inertial subrange and so they are not typically used to verify model accuracy.

The inertial subrange is an intermediate scale in which energy is typically transferred from the large-scale energy containing range to the small-scale dissipation range. This

cascading of energy to smaller scales explains why larger vortices typically break up into smaller vortices. The exception to the rule occurs in 2D Navier-Stokes where inverse cascading occurs transferring energy from small scales to large scales. In 2D Navier-Stokes, small vortices with the same spin direction will join over time until only two large vortices of opposite spin remain due to the existence of enstrophy as a conserved quantity (as viscosity  $\rightarrow 0$ ), where enstrophy is the mean square vorticity. This implies that models designed to measure the small scales more accurately are better used in direct cascade systems rather than 2D Navier-Stokes. Simply changing the 2D Navier-Stokes model into a 2D MHD model allows direct cascading to occur.

## 5.2 Kelvin-Helmholtz Instability

A Kelvin-Helmholtz instability is one that exists due to a shear velocity difference. The simplest picture of such an instability (Fig. 5.2) can be imagined as a fluid that has been separated into a lower and upper portion, labeled 1 and 2 respectively. The two fluids are separated vertically ( $\hat{z}$ ) with their own respective density ( $\rho$ ) and velocity ( $\vec{u}$ ). To create the Kelvin-Helmholtz instability in this model, the velocity of each fluid is assumed to be mainly in the horizontal ( $\hat{x}$ ) direction parallel to the plane of separation of the fluids ( $z_s$ ). As the two fluids move past each other, vortices begin to form from variations in the fluid velocity which signify an unstable flow. This instability will continue to grow and incite turbulence in Navier-Stokes fluids. However, a MHD fluid can be stabilized amidst a Kelvin-Helmholtz instability if a strong magnetic field exists parallel to the direction of flow. This stability can be explained by the fact that  $(\vec{u} \times \vec{B}) = 0$  when the vectors  $\vec{u}$  and  $\vec{B}$  are parallel. When  $\vec{u}$  begins a transverse flow, those particles will begin cyclotronic motion about the magnetic field lines, while the overall flow velocity will be maintained. The size of the cyclotronic orbits will be determined by a ratio of flow velocity vs magnetic field

strength. A weak magnetic field will allow large cyclotronic orbits which result in wider vortices and greater instability of MHD flow while a strong magnetic field will enforce tight cyclotronic orbits and prevent wide vortices from manifesting. The derivation of the analytic solution for the dispersion relation of the KH instability of a MHD fluid follows.

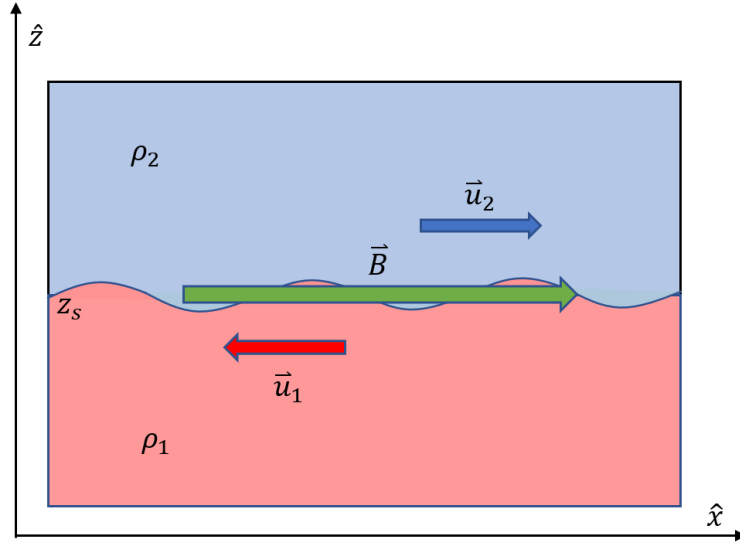


FIG. 5.2: Diagram of two-fluid Kelvin-Helmholtz instability for MHD fluid.

### 5.2.1 Analytic Solution

The linear stability of the KH instability can be determined analytically via the dispersion relation. A perturbed plane wave solution is assumed for the MHD quantities



$$\vec{u} \rightarrow U\hat{x} + \varepsilon \delta\vec{u}e^{i(k_x x + k_y y - \omega t)} \quad (5.2a)$$

$$\vec{B} \rightarrow B_0\hat{x} + \varepsilon \vec{h}e^{i(k_x x + k_y y - \omega t)} \quad (5.2b)$$

$$p \rightarrow p + \varepsilon \delta p e^{i(k_x x + k_y y - \omega t)} \quad (5.2c)$$

$$\rho \rightarrow \rho + \varepsilon \delta\rho e^{i(k_x x + k_y y - \omega t)} \quad (5.2d)$$

$$z_s \rightarrow z_s + \varepsilon \delta z_s e^{i(k_x x + k_y y - \omega t)} \quad (5.2e)$$

where  $\mathcal{O}(1)$  terms only vary with respect to  $\hat{z}$  and  $z_s$  is the vertical position of the boundary between the two fluids. The perturbed plane wave solutions are inserted into the MHD evolution equations from Chapter 4 but slightly edited to include the effects of gravity

$$\frac{d}{dt}\rho = \frac{\partial}{\partial t}\rho + (\vec{u} \cdot \nabla)\rho = 0 \quad (5.3a)$$

$$\frac{\partial}{\partial t}\rho\vec{u} + \rho(\vec{u} \cdot \nabla)\vec{u} = -\frac{1}{\rho}\nabla p + (\nabla \times \vec{B}) \times \vec{B} + \vec{g}\delta\rho \quad (5.3b)$$

$$\frac{\partial}{\partial t}\vec{B} = (\vec{B} \cdot \nabla)\vec{u} - (\vec{u} \cdot \nabla)\vec{B} \quad (5.3c)$$

$$\frac{d}{dt}\delta z_s = \frac{\partial}{\partial t}\delta z_s + (\vec{u} \cdot \nabla)\delta z_s = w(z_s) \quad (5.3d)$$

where  $\vec{g}$  is the gravitational acceleration equal to  $-g\hat{z}$ , the  $z_s$  equation is derived using the derivative chain rule, and  $w(z)$  is the vertical component of the perturbed velocity  $\delta\vec{u} = (u, v, w)$  of the fluid at height  $z$ . After inserting (5.2) into (5.3) while ignoring  $\mathcal{O}(\varepsilon^2)$  terms, the MHD equations become

$$i(k_x U - \omega) \delta \rho + w \partial_z \rho = 0 \quad (5.4a)$$

$$i \rho (k_x U - \omega) u + \rho (\partial_z U) w = -i k_x \delta p \quad (5.4b)$$

$$i \rho (k_x U - \omega) v - i B_0 (k_x h_y - k_y h_x) = -i k_y \delta p \quad (5.4c)$$

$$i \rho (k_x U - \omega) w - B_0 (i k_x h_z - \partial_z h_x) = -\partial_z \delta p - g \delta \rho \quad (5.4d)$$

$$-i \omega \mathbf{h} = i B_0 k_x \mathbf{u} + h_z \partial_z U \hat{x} - i U k_x \mathbf{h} \quad (5.4e)$$

$$i (U k_x - \omega) \delta z_s = w(z_s) \quad (5.4f)$$

Following the procedure in Chandrasekhar [15], the momentum equations are further simplified through linear combinations of (5.4) and the incompressibility equation  $\nabla \cdot \vec{u} = 0$ . Equation (5.4e) can be written explicitly for each component of the magnetic field  $\vec{h}$  as

$$h_x = \frac{k_x B_0}{k_x U - \omega} \left( u - \frac{i \partial_z U}{k_x U - \omega} w \right) \quad (5.5a)$$

$$h_y = \frac{k_x B_0}{k_x U - \omega} v \quad (5.5b)$$

$$h_z = \frac{k_x B_0}{k_x U - \omega} w \quad (5.5c)$$

The expressions for  $\vec{h}$  (5.5) and the continuity equation (5.4a) are then inserted into the  $v$

(5.4c) and  $w$  (5.4d) momentum equations

$$i\rho(k_x U - \omega)v - \frac{k_x B_0^2}{k_x U - \omega} \left( \xi - \frac{k_y \partial_z U}{k_x U - \omega} w \right) = -ik_y \delta p \quad (5.6a)$$

$$i\rho(k_x U - \omega)w + k_x B_0^2 \partial_z \left( \frac{1}{k_x U - \omega} \left( u - \frac{i \partial_z U}{k_x U - \omega} w \right) \right) - \frac{ik_x^2 B_0^2}{k_x U - \omega} w = -\partial_z \delta p - ig \frac{\partial_z \rho}{k_x U - \omega} w \quad (5.6b)$$

$$\text{where } \xi = ik_x v - ik_y u \quad (5.6c)$$

and  $\xi$  represents the vorticity of the fluid. The vorticity can be rewritten in terms of the  $w$  momentum by multiplying the  $u$  (5.4b) and  $v$  (5.6a) momentum equations by  $-ik_y$  and  $+ik_x$  respectively, then adding the equations together so that

$$\xi = \frac{k_y \partial_z U}{k_x U - \omega} w . \quad (5.7)$$

Substituting the vorticity in terms of the  $w$  momentum (5.7) back into the  $v$  momentum equation (5.6a) reduces it to

$$i\rho(k_x U - \omega)v = -ik_y \delta p \quad (5.8)$$

Now that the  $v$  momentum equation is simplified, we will combine the  $u$  (5.4b) and  $v$  (5.8) momentum equations by multiplying them respectively by  $-k_x$  and  $-k_y$  and then adding them together to obtain

$$\rho(k_x U - \omega) \partial_z w - \rho k_x (\partial_z U) w = ik^2 \delta p . \quad (5.9)$$

Using the two definitions of vorticity, (5.6c) and (5.7), as well as the incompressibility

equation,  $\nabla \cdot \vec{u} = 0$ , we can build a useful relation relating  $ik^2u$  to the  $w$  momentum for further simplifications.

$$ik^2u = -(k_x \partial_z w + k_y \xi) = - \left( k_x \partial_z w + \frac{k_y^2 \partial_z U}{k_x U - \omega} w \right) \quad (5.10)$$

Now this new relation can be used to simplify the  $w$  momentum equation (5.6b) further by first multiplying (5.6b) by  $-ik^2$  as

$$ik^2 \partial_z \delta p = \rho k^2 (k_x U - \omega) w - k_x k^2 B_0^2 \partial_z \left( \frac{1}{k_x U - \omega} \left( iu + \frac{\partial_z U}{k_x U - \omega} w \right) \right) - \frac{k_x^2 k^2 B_0^2}{k_x U - \omega} w + gk^2 \frac{\partial_z \rho}{k_x U - \omega} w \quad (5.11)$$

and then applying the  $ik^2u$  relation (5.10). The new  $w$  momentum is

$$ik^2 \partial_z \delta p = \rho k^2 (k_x U - \omega) w + k_x^2 B_0^2 \left\{ \partial_z \left( \frac{\partial_z w}{k_x U - \omega} \right) - \frac{k^2 w}{k_x U - \omega} \right\} - k_x^3 B_0^2 \partial_z \left( \frac{\partial_z U}{(k_x U - \omega)^2} w \right) + gk^2 \frac{\partial_z \rho}{k_x U - \omega} w. \quad (5.12)$$

Finally, the  $v$  and  $w$  momentum equations are combined by replacing the  $\delta p$  term in (5.12) by (5.9), producing

$$\begin{aligned} & \partial_z \{ \rho (k_x U - \omega) \partial_z w - \rho k_x (\partial_z U) w \} \\ &= \rho k^2 (k_x U - \omega) w + k_x^2 B_0^2 \left\{ \partial_z \left( \frac{\partial_z w}{k_x U - \omega} \right) - \frac{k^2 w}{k_x U - \omega} \right\} \\ & \quad - k_x^3 B_0^2 \partial_z \left( \frac{\partial_z U}{(k_x U - \omega)^2} w \right) + gk^2 \frac{\partial_z \rho}{k_x U - \omega} w. \end{aligned} \quad (5.13)$$

This is the ultimate MHD evolution equation for the KH instability where all MHD equations have been combined into one, allowing the production of a dispersion relation. Inte-

grating this equation (5.13) over  $z$  at  $z = 0$ , we get the final dispersion relation.

$$\Delta_0 \{ \rho (k_x U - \omega) \partial_z w \} = k_x^2 B_0^2 \Delta_0 \left( \frac{\partial_z w}{k_x U - \omega} \right) + g k^2 \Delta_0(\rho) \left( \frac{w}{k_x U - \omega} \right)_0 \quad (5.14)$$

where  $\Delta_0(x)$  defines a difference of the parameter  $x$  across the boundary layer at  $z = 0$ .

In order to solve this equation across the fluid border, a general solution is needed for the  $w$  momentum. The general solution is found by identifying the quantity conserved across the fluid border. Using equation (5.4f), we find the conserved change over the boundary  $\delta z_s = \frac{w}{U k_x - \omega}$ . The boundary conditions are then defined for the general solution such that the extreme upper ( $z = +\infty$ ) and lower ( $z = -\infty$ ) boundaries reduce  $w$  to 0 and  $\delta z_{s1} = \delta z_{s2}$  at the boundary where  $z = 0$ . With these boundary conditions, the general solutions for the lower and upper  $w$  are respectively

$$w_1 = A (k_x U_1 - \omega) e^{+kz} \quad (z < 0) \quad (5.15)$$

$$w_2 = A (k_x U_2 - \omega) e^{-kz} \quad (z > 0) \quad (5.16)$$

The  $\Delta_0$  functions can now be solved across the fluid border using the general solution to  $w$ . The dispersion relation is simplified to become

$$\rho_1 (k_x U_1 - \omega)^2 + \rho_2 (k_x U_2 - \omega)^2 = g k (\rho_2 - \rho_1) + 2 k_x^2 B_0^2 \quad (5.17)$$

as we assign subscripts distinguishing the quantities of the two fluids (1 for lower fluid and 2 for upper fluid).

At this point, I will set  $\rho_1 = \rho_2 = \rho_0$  as the fluid density is unchanged across the boundary layer ( $z = 0$ ) for all problems modeled in this thesis. Under these conditions, the gravitational field plays no role. The KH dispersion relation with a uniform magnetic

field parallel to fluid flow is then

$$\frac{\omega}{k_x} = \frac{1}{2} (U_1 + U_2) \pm \sqrt{\frac{B_0^2}{\rho_0} - \frac{1}{4} (U_1 - U_2)^2} \quad (5.18)$$

This relation shows that  $\frac{\omega}{k_x}$  will remain strictly real and thus stable under the condition

$$V_A = \frac{B_0}{\sqrt{\rho_0}} \geq \frac{1}{2} |U_1 - U_2| \quad (5.19)$$

where  $V_A$  is the Alfvén velocity (in simplified units). Further discussion on the Kelvin-Helmholtz instability for a MHD fluid can be found in Chandrasekhar [15].

### 5.2.2 KH Simulation Results

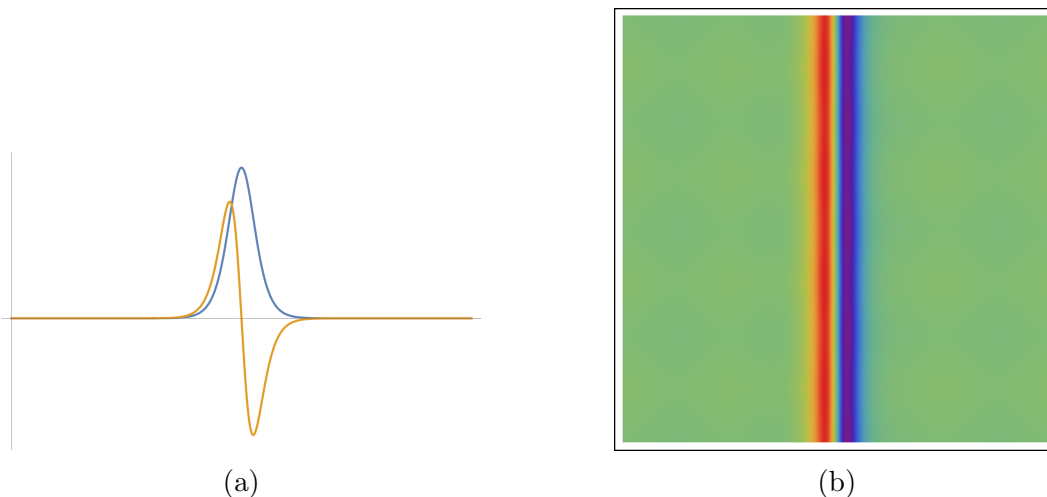


FIG. 5.3: **Initial profile of the KH jet instability simulated in LB.** (a) Profile of the initial jet's vertical speed  $[u_y(x) = U_0 \text{sech}^2(\frac{2\pi}{L}x)]$  (blue) and vorticity  $[\nabla \times \vec{u}]$  (orange) along the horizontal axis of the simulation grid. (b) A 2D plot of the initial vorticity of the KH jet (red is positive, blue is negative).

In this section, a basic proof of concept simulation for LB MHD is provided as an example of functionality. This example is also meant to be used for comparison against the LB MHD models presented later in this thesis, which all use the KH instability as

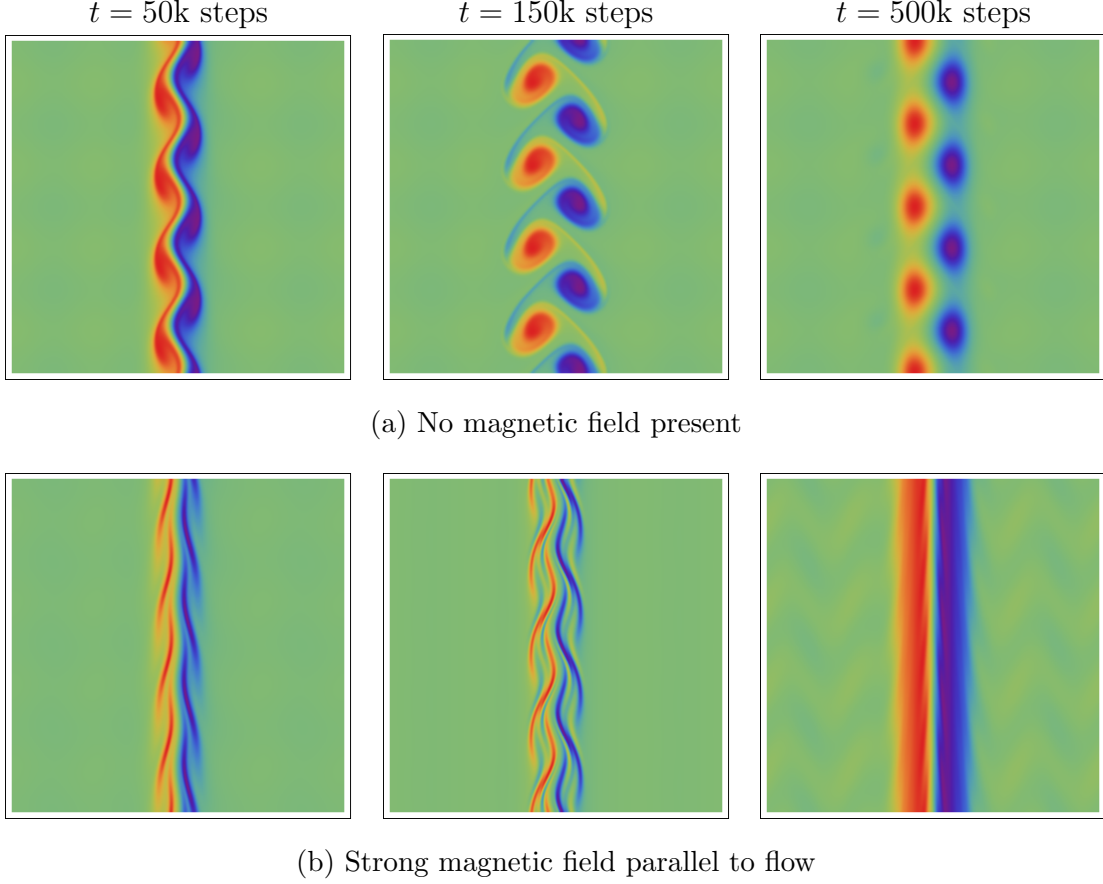


FIG. 5.4: **KH LB simulation of a moderate velocity jet** with gridsize  $L = 512$ , magnetic field strength  $B_0$  and fluid velocity  $U_0$ .

a measure of accuracy. The KH instability is modeled as a jet of fluid with an upward vertical velocity against a motionless fluid background. The initial profile of the jet is presented in figure 5.3 with velocity  $u_y(x) = U_0 \operatorname{sech}^2\left(\frac{2\pi}{L}x\right)$ . It is worth noting that in 2D MHD, the vorticity ( $\nabla \times \vec{u}$ ) and current ( $\nabla \times \vec{B}$ ) are solely in the  $\hat{z}$ -direction (in or out of the plane).

Figure 5.4a shows the evolution of the KH instability where no magnetic field is present. As can be seen, the jet eventually breaks up. Figure 5.4b shows the same simulation with a strong magnetic field parallel to the flow of the jet. The jet initially appears to become unstable but eventually stabilizes in a wider stance. The widening of

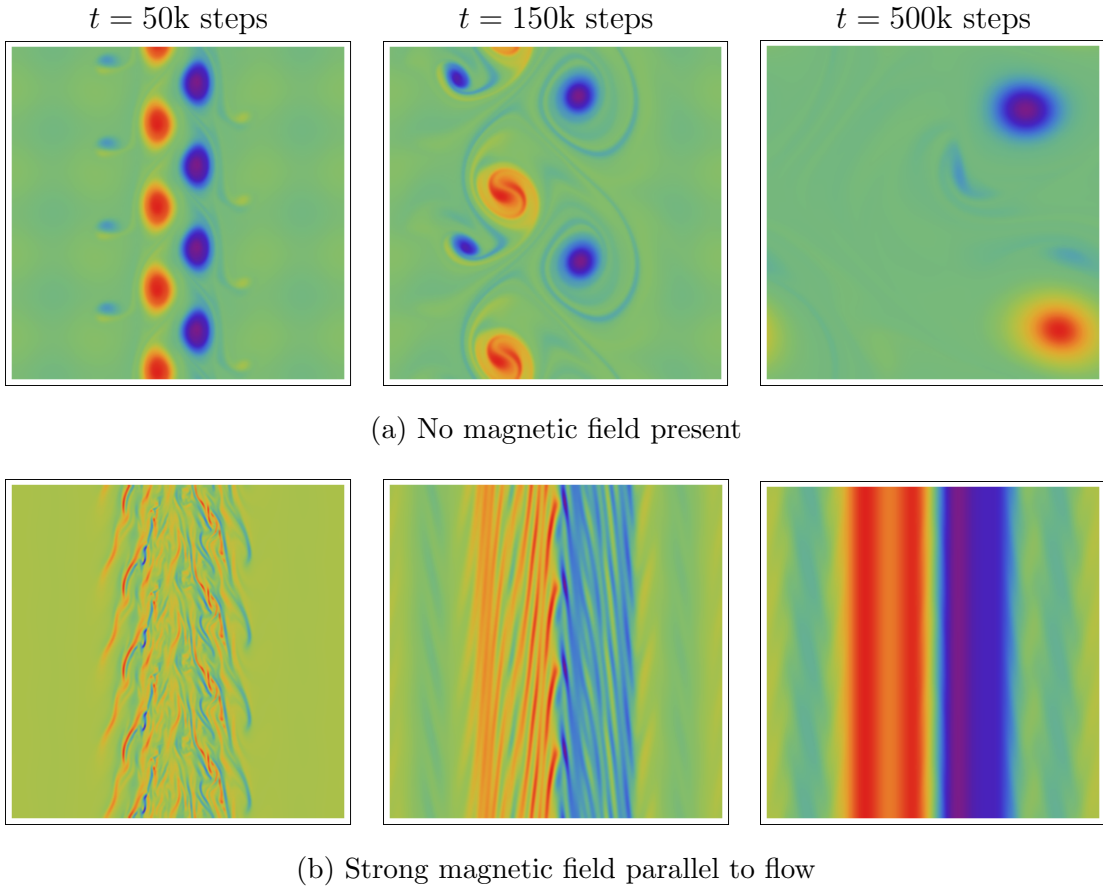


FIG. 5.5: **KH LB simulation of a high velocity jet** with gridsize  $L = 512$ , magnetic field strength  $B_0$  and fluid velocity  $2.5U_0$ . Numbers are compared against those used in figure 5.4.

the jet occurs when eq. (5.19) is not satisfied. Although the magnetic field is strong, it is not strong enough to stabilize the initial high velocity of the jet. As the instability grows, the kinetic energy of the jet is spread more thinly over the transverse space causing the maximum fluid velocity at the center to drop. Once the maximum fluid velocity drops to become equal with the Alfvén velocity, the jet finally stabilizes in its new, wider stance.

A second set of simulation results are shown in figure 5.5 with a much higher initial velocity ( $2.5U_0$ ) and the same magnetic field strength ( $B_0$ ). With no magnetic field present (Fig. 5.5a), the jet breaks up wildly to the point of breaking symmetry. The inverse cascading of 2D Navier-Stokes can also be clearly seen as the four small orange vortices at



$t = 50k$  combine into two moderate-sized orange vortices at  $t = 150k$  and finally into one large orange vortex at  $t = 500k$ . When the vertical magnetic field is present (Fig. 5.5b), small striating vortex bands can be seen initially at  $t = 50k$ . These bands result from direct cascading of energy to small scales in MHD and a lack of initial KH stabilization by the magnetic field. As mentioned in the previous paragraph, the jet velocity lowers as the jet widens until the jet velocity drops below the Alfvén velocity. Since the initial velocity was much higher, so is the final width of the jet.

# CHAPTER 6

## Partial Entropic MRT LB Model

The lattice Boltzmann (LB) algorithm has proven to be an extremely interesting method for the solution of Navier-Stokes [16] flows because of its simplicity, extreme parallelizability and accuracy. One of the major constraints on LB is that it is prone to numerical instability in certain parameter regimes. There is no inherent mechanism to enforce the LB distribution function to remain non-negative in time, particularly in strong turbulence simulations. In this chapter, a new entropic multiple relaxation time (MRT) model is presented for LB MHD with the goal of improving stability. While this new model will not enforce the scalar distribution to remain non-negative, it will reduce the tendency of certain distributions to become unstable without changing the MHD equations. This is done by dynamically adjusting the individual relaxation rates of certain distributions as a function of minimum fluid entropy without changing the transport coefficients in the MHD equations [3].

## 6.1 Multiple Relaxation Time (MRT)

The LB equation (3.1) and specifically, the collision step of the LB method (3.2a) assumes that all fluid distributions, regardless of velocity, approach equilibrium at the same rate. This single relaxation time (SRT) is represented by a single  $\tau$  used for all distributions. Although this approach has had great success and simplicity for the LB method, exploration of multiple relaxation times (MRT) has opened the door to greater stability improvements for the LB approach in general.

There are quite a few MRT extensions [17–20] of the original SRT LB-MHD model of Dellar [13]. However, for simplicity, we shall work with only an SRT model for the vector magnetic field distribution  $\vec{g}_k$ , and an MRT model for the scalar distribution function  $f_i$ , where the subscripts denote the velocity streaming directions

$$(\partial_t + \partial_\gamma c_{\gamma i}) f_i = \sum_j X'_{ij} (f_j^{\text{eq}} - f_j) \quad (6.1)$$

$$(\partial_t + \partial_\gamma c_{\gamma k}) \vec{g}_k = Y' (\vec{g}_k^{(\text{eq})} - \vec{g}_k) \quad (6.2)$$

with the moments

$$\sum_i f_i = \rho \quad , \quad \sum_i f_i \vec{c}_i = \rho \vec{u} \quad \text{and} \quad \sum_k \vec{g}_k = \vec{B} \quad (6.3)$$

It is convenient to employ the summation convention only over the Greek indices which give the vector nature of the fields ( $\gamma = 1, 2$  for 2D), while the Roman indices run over the corresponding (kinetic) lattice vectors  $\vec{c}_i, i = 0..8$  for the 9-bit model in 2D (see Fig. 3.1). Summation over the Roman indices will always be made explicit.  $X'_{ij}$  is the MRT collision operator for the evolution of  $f_i$  while  $Y'$  is the SRT for the evolution of  $\vec{g}_k$ . The MHD viscosity and resistivity transport coefficients are determined from these kinetic relaxation

rates.

It is well known that the minimal LB representation of MHD equations on a square lattice is a 9-bit velocity streaming for  $f_i$  and just 5-bit streaming for  $\vec{g}_k$ . This is because  $\vec{u}$  is defined from the first moment of  $f_i$  while  $\vec{B}$  is defined as the zeroth moment of  $\vec{g}_k$ . It is convenient (and helpful for numerical stability) to employ the 9-bit streaming model for both kinetic equations. To recover the MHD equations in the Chapman-Enskog limit of the (discrete) kinetic equations, we take the well-known choice of relaxation distribution functions  $f_i^{\text{eq}}$  and  $\vec{g}_k^{\text{eq}}$

$$f_i^{\text{eq}} = w_i \rho \left[ 1 + 3 (\vec{c}_i \cdot \vec{u}) + \frac{9}{2} (\vec{c}_i \cdot \vec{u})^2 - \frac{3}{2} \vec{u}^2 \right] + \frac{9}{2} w_i \left[ \frac{1}{2} \vec{B}^2 \vec{c}_i^2 - (\vec{B} \cdot \vec{c}_i)^2 \right] \quad (6.4)$$

$$\vec{g}_k^{\text{(eq)}} = w_k \left[ \vec{B} + 3 \left\{ (\vec{c}_k \cdot \vec{u}) \vec{B} - (\vec{c}_k \cdot \vec{B}) \vec{u} \right\} \right] \quad (6.5)$$

for  $i$  and  $k = 0..8$ .

In MRT-LB it is natural to perform the collisional relaxation in moment space (because of the local conservation of mass and momentum constraints) and the streaming in the distribution space  $f_i, \vec{g}_k$ . There is a 1-1 map between these spaces. For the moment basis it is obvious to include the conservation moments (the zeroth and first moments of the  $f_i$  and the zeroth moment of  $\vec{g}_k$ ), while the remaining higher moments are somewhat arbitrary [10, 11]. In particular, we consider the same constant  $9 \times 9$  T- matrix that connects the scalar distributions ( $f_i, i = 0..8$ ) to their moments ( $M_i, i = 0..8$ ) as for the vector magnetic distributions ( $\vec{g}_k, k = 0..8$ ) with their moments ( $\vec{N}_k, k = 0..8$ ). The transformation follows from section 3.3 and equations (3.4) and (3.6)

$$M_i = \sum_{j=0}^8 T_{ij} f_j \quad , \quad \vec{N}_k = \sum_{q=0}^8 T_{kq} \vec{g}_q \quad (6.6)$$

with

$$\mathbb{T} = \begin{pmatrix} \mathbf{1} \\ c_x \\ c_y \\ c_x c_y \\ c_x^2 \\ c_y^2 \\ c_x^2 c_y \\ c_x c_y^2 \\ c_x^2 c_y^2 \end{pmatrix} = \begin{pmatrix} 1 & 1 & 1 & 1 & 1 & 1 & 1 & 1 & 1 \\ 0 & 1 & 0 & -1 & 0 & 1 & -1 & -1 & 1 \\ 0 & 0 & 1 & 0 & -1 & 1 & 1 & -1 & -1 \\ 0 & 0 & 0 & 0 & 0 & 1 & -1 & 1 & -1 \\ 0 & 1 & 0 & 1 & 0 & 1 & 1 & 1 & 1 \\ 0 & 0 & 1 & 0 & 1 & 1 & 1 & 1 & 1 \\ 0 & 0 & 0 & 0 & 0 & 1 & 1 & -1 & -1 \\ 0 & 0 & 0 & 0 & 0 & 1 & -1 & -1 & 1 \\ 0 & 0 & 0 & 0 & 0 & 1 & 1 & 1 & 1 \end{pmatrix} \quad (6.7)$$

where the Cartesian components of the corresponding 9-dimensional lattice vectors are just

$$c_x = \{0, 1, 0, -1, 0, 1, -1, -1, 1\} \quad , \quad c_y = \{0, 0, 1, 0, -1, 1, 1, -1, -1\} \quad . \quad (6.8)$$

For the scalar distributions, the 1<sup>st</sup> row of the  $\mathbb{T}$ -matrix is just the conservation of density while the 2<sup>nd</sup> and 3<sup>rd</sup> rows are just the conservation of momentum (2D). For the vector magnetic distributions the 1<sup>st</sup> row of the  $\mathbb{T}$ -matrix is the only collisional invariant.

With this moment basis, the MRT collisional relaxation rate tensor  $X'_{ij}$  is diagonalized with the  $T$ - matrix as a similarity transformation. It is convenient to denote this diagonal matrix with elements  $X_i \delta_{ij}$ . In the  $D2Q9$  phase space, the relaxation rate  $X_j$  is associated with the corresponding moment  $M_j$ ,  $j = 0..8$ . Similarly for the magnetic distributions in SRT, there is just a single collisional relaxation rate for each magnetic moment  $\vec{N}_k$ , and this will be denoted by  $Y$ .

In particular, the equilibrium moments can be written in terms of the conserved

moments:

$$\begin{aligned}
M_0^{\text{eq}} &= M_0 = \rho & M_1^{\text{eq}} &= M_1 = \rho u_x & M_2^{\text{eq}} &= M_2 = \rho u_y \\
M_3^{\text{eq}} &= \rho u_x u_y - B_x B_y & M_4^{\text{eq}} &= \frac{1}{6} (6\rho u_x^2 + 2\rho - 3(B_x^2 - B_y^2)) \\
M_5^{\text{eq}} &= \frac{1}{6} (6\rho u_y^2 + 2\rho + 3(B_x^2 - B_y^2)) & M_6^{\text{eq}} &= \frac{1}{3} \rho u_y \\
M_7^{\text{eq}} &= \frac{1}{3} \rho u_x & M_8^{\text{eq}} &= \frac{1}{9} \rho (1 + 3u_x^2 + 3u_y^2)
\end{aligned} \tag{6.9}$$

$$\begin{aligned}
N_{\alpha 0}^{\text{eq}} &= N_{\alpha 0} = B_\alpha & N_{\alpha 1}^{\text{eq}} &= u_x B_\alpha - u_\alpha B_x & N_{\alpha 2}^{\text{eq}} &= u_y B_\alpha - u_\alpha B_y \\
N_{\alpha 3}^{\text{eq}} &= 0 & N_{\alpha 4}^{\text{eq}} &= \frac{B_\alpha}{3} & N_{\alpha 5}^{\text{eq}} &= \frac{B_\alpha}{3} \\
N_{\alpha 6}^{\text{eq}} &= \frac{1}{3} (u_y B_\alpha - u_\alpha B_y) & N_{\alpha 7}^{\text{eq}} &= \frac{1}{3} (u_x B_\alpha - u_\alpha B_x) & N_{\alpha 8}^{\text{eq}} &= \frac{B_\alpha}{9}, \quad \alpha = x, y
\end{aligned} \tag{6.10}$$

## 6.2 Entropic Method and its Partial Extension to MHD

The Karlin group [3, 21] introduces the entropic procedure for Navier-Stokes flows by separating the scalar lattice Boltzmann distribution into various moment-related groups.

In particular,

$$f_i = k_i + s_i + h_i \quad , \quad i = 0..8 \tag{6.11}$$

where the  $k_i$  distributions correspond to those distributions with conserved moments, the  $s_i$  distributions correspond to the stress/shear moments, and finally the  $h_i$  distributions correspond to the remaining higher order moments. Thus for the  $k_i$  distributions

$$k_i = \sum_{j=0}^8 \sum_{m=0}^2 T_{im}^{-1} T_{mj} f_j \quad , \quad i = 0..8 \tag{6.12}$$

with the  $m$ -summation running from  $m = 0, 1, 2$  since there are 3 conserved moments. Similarly for  $s_i$  and  $h_i$ . The  $s_i$  distributions corresponding to the stress/shear moments

will come from the set

$$s_i \in \{d, d \cup t, d \cup q, d \cup t \cup q\} \quad (6.13)$$

where  $d$  is the deviatoric stress,  $t$  is the trace of the stress tensor, and  $q$  represents the third order moments. Here we choose, for simplicity, the moment contributions  $s_i$  to be  $d \cup t$  so that

$$s_i = \sum_{j=0}^8 \sum_{m=3}^5 \mathbb{T}_{im}^{-1} \mathbb{T}_{mj} f_j \quad , \quad i = 0..8. \quad (6.14)$$

Moments 3, 4, and 5 are each second order moments in the  $D2Q9$  model, and thus represent the second order quantities ( $d \cup t$ ). The moment contributions to  $h_i$  are then all the remaining moments that do not contribute to either  $k_i$  or  $s_i$ . Thus

$$h_i = \sum_{j=0}^8 \sum_{m=6}^8 \mathbb{T}_{im}^{-1} \mathbb{T}_{mj} f_j \quad , \quad i = 0..8. \quad (6.15)$$

Karlin *et. al.* [3, 21] now consider the entropy of the post-collisional state, and introduce a parameter  $\gamma$  which yields an extremal to this entropy function. In MRT only some of the relaxation rates affect the transport coefficient under Chapman-Enskog expansions [14]. The transport coefficient in Navier-Stokes simulations is first affected by the stress related distributions ( $s_i$ ). The tunable parameter  $\gamma$  is introduced to replace the relaxation rates for the higher order moment effects arising from the ( $h_i$ ) distributions. In particular, one moves from the standard post-collisional distributions

$$f'_i \equiv f_i(t+1) = f_i + 2\beta(f_i^{\text{eq}} - f_i) \quad (6.16)$$

$$\text{to} \quad f'_i = f_i - 2\beta\Delta s_i - \beta\gamma\Delta h_i \quad (6.17)$$

where  $\beta$  is related to the kinematic viscosity as  $\nu = \frac{1}{6} \left( \frac{1}{\beta} - 1 \right)$  and  $\Delta s_i = s_i - s_i^{\text{eq}}$ ,  $\Delta h_i = h_i - h_i^{\text{eq}}$ , while for the conserved moments  $\Delta k_i = k_i - k_i^{\text{eq}} = 0$ .

In order to maximize the entropy  $S[f]$

$$S[f] = - \sum_i f_i \ln \left( \frac{f_i}{w_i} \right). \quad (6.18)$$

one now writes the entropy in terms of the post-collisional state and the  $\gamma$  parameter. The critical point of the entropy [3, 21] determines the tunable parameter  $\gamma$  from

$$\sum_i \Delta h_i \ln \left( 1 + \frac{(1 - \beta\gamma) \Delta h_i - (2\beta - 1) \Delta s_i}{f_i^{\text{eq}}} \right) = 0 \quad (6.19)$$

This is a rather computationally expensive root-finding procedure having to be done at every point of the grid and at every timestep. Karlin *et. al* [3, 21] noted that if one invokes the simple small argument expansion  $\log(1+x) = x + \dots$  one can then readily determine the entropic factor algebraically. The parameter determined algebraically is denoted by  $\gamma^*$ :

$$\gamma^* = \frac{1}{\beta} - \left( 2 - \frac{1}{\beta} \right) \frac{\langle \Delta s | \Delta h \rangle}{\langle \Delta h | \Delta h \rangle} \quad (6.20)$$

$$\text{where the inner product } \langle A | B \rangle = \sum_i \frac{A_i B_i}{f_i^{\text{eq}}}. \quad (6.21)$$

A more complete derivation is provided in Appendix C. On substituting  $\gamma^*$  back into the new post-collisional state (6.17), a maximal entropy state has been determined for Navier-Stokes flows. The Karlin group successfully tested this approximation for the tunable parameter  $\gamma^*(\vec{x}, t)$  in various simulations of 2D and 3D Navier-Stokes [3, 21]. One thus sees that this entropic algorithm is a subset of MRT - but it has a dynamic entropic parameter determined at every lattice point and every timestep algebraically for entropic stabilization as opposed to the static relaxation times for typical MRT models.

Clearly, this analysis does not simply carry over to LB-MHD with possible non-positive vector magnetic distributions. Hence we make the ansatz for our partial entropic algo-



rithm that the entropic parameter in LB-MHD is still determined by Eq. (6.20) for the corresponding LB-MHD  $\Delta h$  and  $\Delta s$ . The validity of our ansatz will now be tested against various 2D MHD simulations.

Summarizing, our partial entropic LB-MHD algorithm consists of the following steps (c.f., Karlin *et. al.* [3]):

1. Compute the conserved moments  $(\rho, \mathbf{u}, \mathbf{B})$  (Eq. 6.6, 6.9, 6.10)
2. Evaluate the equilibria  $(f_i^{\text{eq}}(\rho, \mathbf{u}, \mathbf{B}), \vec{g}_k^{\text{eq}}(\rho, \mathbf{u}, \mathbf{B}))$  (Eq. 6.4)
3. Compute  $s$  and  $s^{\text{eq}}$  (Eq. 6.12, 6.13)
4. Compute  $\Delta s_i = s_i - s_i^{\text{eq}}$
5. Compute  $\Delta h_i = h_i - h_i^{\text{eq}} = f_i - f_i^{\text{eq}} - \Delta s_i$
6. Evaluate  $\gamma^*$  (Eq. 6.20)
7. Relax (Collide):  $f_i'$  (Eq. 6.17), and corresponding  $\vec{g}_k'$ .

Standard LB-MHD is recovered for entropy parameter:  $\gamma(\vec{x}, t) = \text{const.} = 2$ . As mentioned earlier, there is no attempt made to find a corresponding maximal entropy state for the magnetic distribution function since the magnetic field in most problems of interest undergoes field reversal. (e.g., in magnetic field reconnection..). However the effect of working with the maximal entropy state for the particle distribution function will have direct effects on the evolution of the magnetic field due to the coupling of the  $\vec{B}$ -field in the relaxation distribution function  $f^{\text{eq}}$  as well as the coupling of the fluid velocity  $\vec{u}$  in  $\vec{g}^{\text{eq}}$ .

## 6.3 Partially Entropic LB-MHD Simulations

We first have benchmarked our partially entropic LB-MHD code against our earlier (totally non-entropic) MRT LB-MHD simulations of a Kelvin-Helmholtz jet instability in a magnetic field [17]. Here we show the physics recovered by the variations in the partially entropic parameter  $\gamma^*$  and its variations away from the MRT value of  $\gamma^*(\vec{x}, t) \equiv 2.0$  for sufficiently weak axial  $\vec{B}$  that the jet is unstable. Some runs were then performed to examine the increased numerical stability in the parameter regime of the mean velocity  $\vec{u}$  and magnetic field  $\vec{B}$  due to the partially entropic algorithm. Following this we consider the interplay between Kelvin-Helmholtz instability and the tearing mode instability and qualitatively compare our results to that of Chen *et. al.* [22]. Finally we qualitatively compare our simulations with the Biskamp-Welter profile.

### 6.3.1 Magnetized Kelvin-Hemholtz Jet Instability

We now consider the partially entropic-LB-MHD algorithm for the breakdown of a Kelvin-Helmholtz jet in a weak magnetic field. In our simulations, the initial parameters are so chosen that there is a direct cascade of energy to small spatial scales (indicating the existence of a magnetic field) but the magnetic field is sufficient weak so as not to stabilize the jet. This simulation in general is to be compared with the KH simulation in section 5.2.2. The initial conditions are given as

$$\vec{u}(t = 0) = U_0 \operatorname{sech}^2(x)\hat{y}, \quad \vec{B}(t = 0) = B_0\hat{y} \quad (6.22)$$

see figure 5.3 for a graphic profile of initial conditions.

The evolution of the vorticity,  $\omega$ , the current,  $j$ , and the entropic stabilization parameter  $\gamma^*$  for this 2D jet is plotted in Fig. 6.1. With the (dimensionless) choice of

$B_0 = 0.005U_0$ , the jet breaks into a Kelvin-Helmholtz vortex street ( $t \leq 266k$ ). There is then further symmetry breaking as the vortex street is broken up, leading to vortex-vortex reconnection (ala 2D Navier-Stokes turbulence), as well as the generation of small scales eddies (characteristic of 2D MHD) for  $t > 266k$ . One notices that the partial entropy parameter  $\gamma^*$  in Fig. 6.1 deviates from the ordinary LB-MHD value of  $\gamma^*(\vec{x}, t) = 2$  wherever there are significant number of small eddies. These are regions of steep gradients and it is in these regions where the partial entropic stabilization of the simulation occurs. It is important to note that this partial entropy stabilization is occurring from local information at each lattice site. This is reminiscent of LB where gradients can be computed from local moments of perturbed distributions: e.g., in large eddy simulation modelings in the Smagorinsky model, the mean velocity gradients are determined from simple local moments. For stronger magnetic fields, the jet will be stabilized and is of little interest for our partial entropic-LB-MHD model, [17]. A spectral plot of the total energy of the Kelvin-Helmholtz simulation at  $t = 500k$  is presented in Fig. 6.2 with a slope of  $k^{-\frac{5}{3}}$ . This spectral plot corresponds to the final timestep in Fig. 6.2.

### Stability Improvements from the Entropic Algorithm

Some numerical stability boundaries were investigated between ordinary LB-MHD and our partial entropic-LB-MHD with the  $\gamma^*$  parameter on a grid of  $1024^2$  for the Kelvin-Helmholtz jet. We found that the partial entropic-LB-MHD algorithm permitted a maximal mean velocity  $\vec{U}_{0,max}$  to be increased by a factor of 2 in a purely Navier-Stokes turbulence simulation (i.e., no  $\vec{B}$ -field) while the velocity maximum could be increased by a factor of 8 when there was a strong stabilizing  $\vec{B}$ -field. As regards the magnetic field (at fixed  $\vec{U}_0$ ), the partial entropic-LB-MHD algorithm permitted an increase by a factor of 2 in  $\vec{B}_0$ . In the partial entropic-LB-MHD algorithm the viscosity could become arbitrary small, while ordinary LB-MHD the minimum stable viscosity was  $10^{-5}$  when  $\vec{B}_0 = 0$ , and

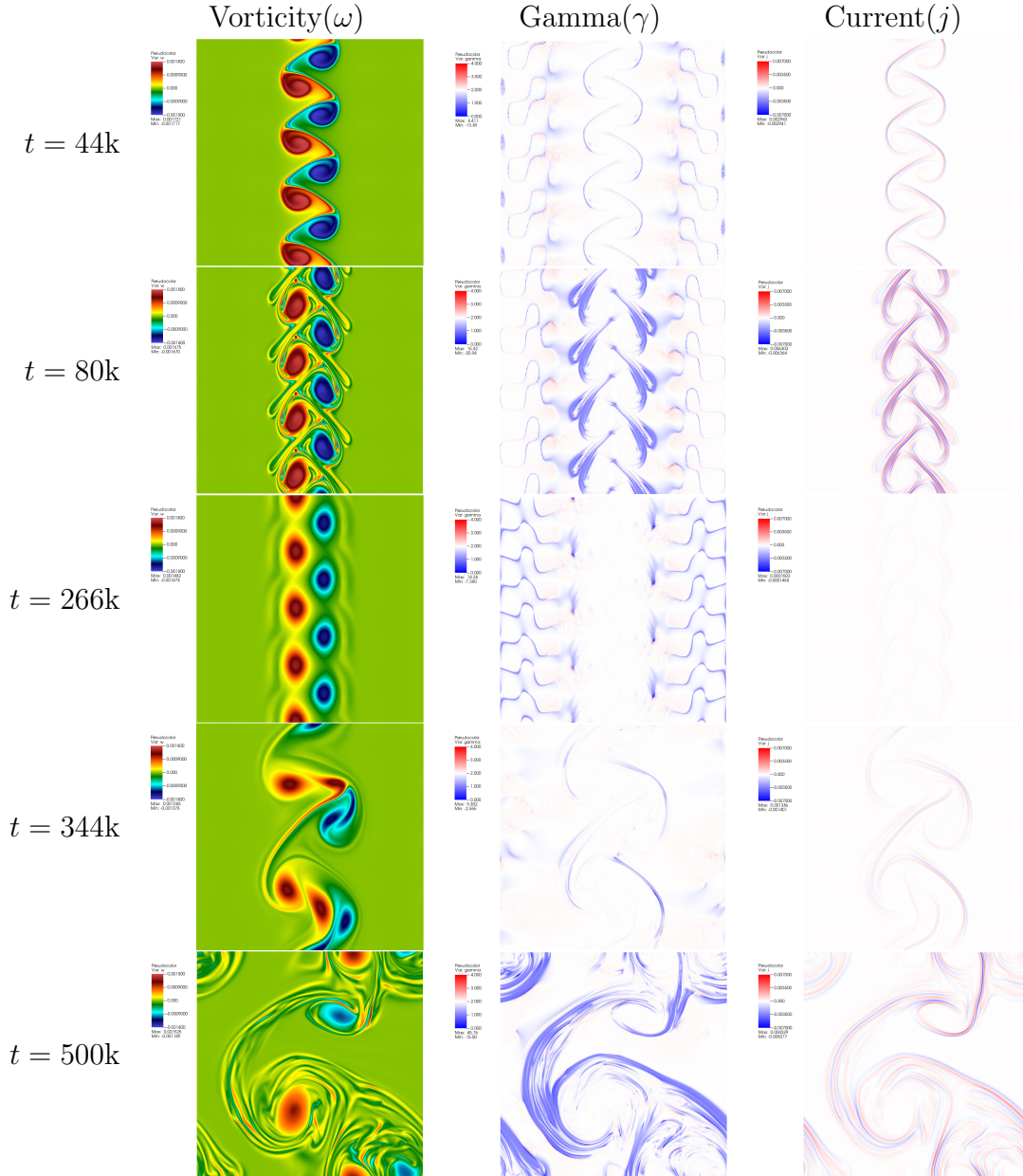


FIG. 6.1: Entropic MRT evolution of a Kelvin-Helmholtz jet with very weak axial magnetic field:  $B_0 = 0.005U_0$ . The column 2D plots are the vorticity  $\omega$ , the entropy parameter  $\gamma^*$ , and the current  $j$ . The jet is unstable forming a von-Karman like vortex street (time  $t = 44k$ ). These vortices start to generate secondary smaller vortex streaks ( $t = 80k$ ) - where the entropy factor becomes important. The vortex street then becomes unstable ( $t = 344k$ ) with vortex-vortex reconnection dominating shortly after the break-up of the vortex street. However by  $t = 500k$  strong subsidiary vortices are generated because of the 2D MHD turbulence with significant corresponding regions of variations of the entropic parameter away from 2. Note that the color scheme is held constant for all time snapshots. Spatial grid  $1024^2$

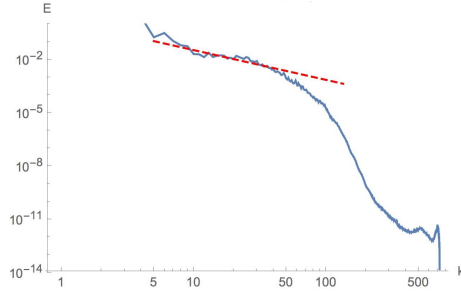


FIG. 6.2: Spectral plot of the Entropic MRT Kelvin-Helmholtz simulation at  $t = 500k$  where gridsize is  $1024^2$  and the slope of the dashed line is  $k^{-1.67}$ .

$10^{-2}$  when there was a strong stabilizing  $\vec{B}_0$ . No substantial stability limits were found on the achievable minimum resistivity.

It should be stressed that the computational overhead of computing this entropic parameter  $\gamma^*$  is quite small, primarily because it is determined algebraically from local information only.

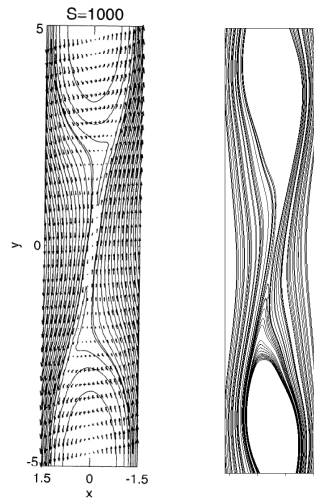


FIG. 6.3: Magnetic field line comparison in EMRT simulation against Chen Fig. 6a. A snapshot of the (a) magnetic field lines (and velocity fields) from a Chen *et. al.* [22] supersonic Alfvénic simulation, their Fig. 6a, compared to our (b) entropic LB-MHD simulation on  $1024^2$  grid for the same initial profiles.

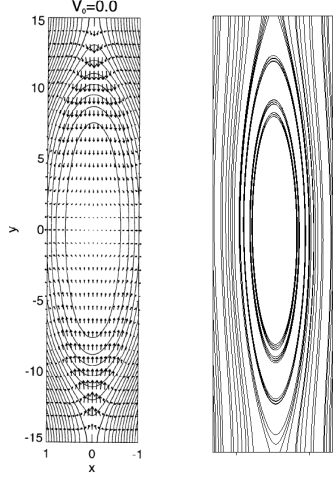


FIG. 6.4: **Magnetic field line comparison in EMRT simulation against Chen Fig. 4a.** A snapshot of (a) the magnetic field line contours (and velocity field) for zero initial shear, Chen *et. al.* [22] Fig. 4a, and (b) from our entropic LB-MHD algorithm on a  $1024^2$  grid.

### 6.3.2 Chen *et. al.* Profile

Chen *et. al.* [22] has considered the linear and nonlinear evolution of Kelvin-Helmholtz (velocity shear) vs. the tearing mode (magnetic shear) instabilities in 2D compressible MHD. Their closure includes an evolution equation for the enthalpy as well as various resistivity profiles using standard CFD techniques. Their initial profiles are

$$u_y(x, t = 0) = -U_0 \tanh(x), \quad B_y(x, t = 0) = B_0 \tanh(x). \quad (6.23)$$

Thus our comparisons can only be qualitative, and we only consider the Chen *et. al.* [22] simulations when they keep their resistivity constant. Typically, when the velocity is below the Alfvén speed, it stabilizes the tearing mode and so reduces the reconnection rate. However, if the velocity is above the Alfvén speed the Kelvin-Helmholtz instability sets in. In our first partial entropic LB-MHD simulation, we consider super-Alfvén velocity shear flow and the Kelvin-Helmholtz induced magnetic islands due to reconnection in Fig.

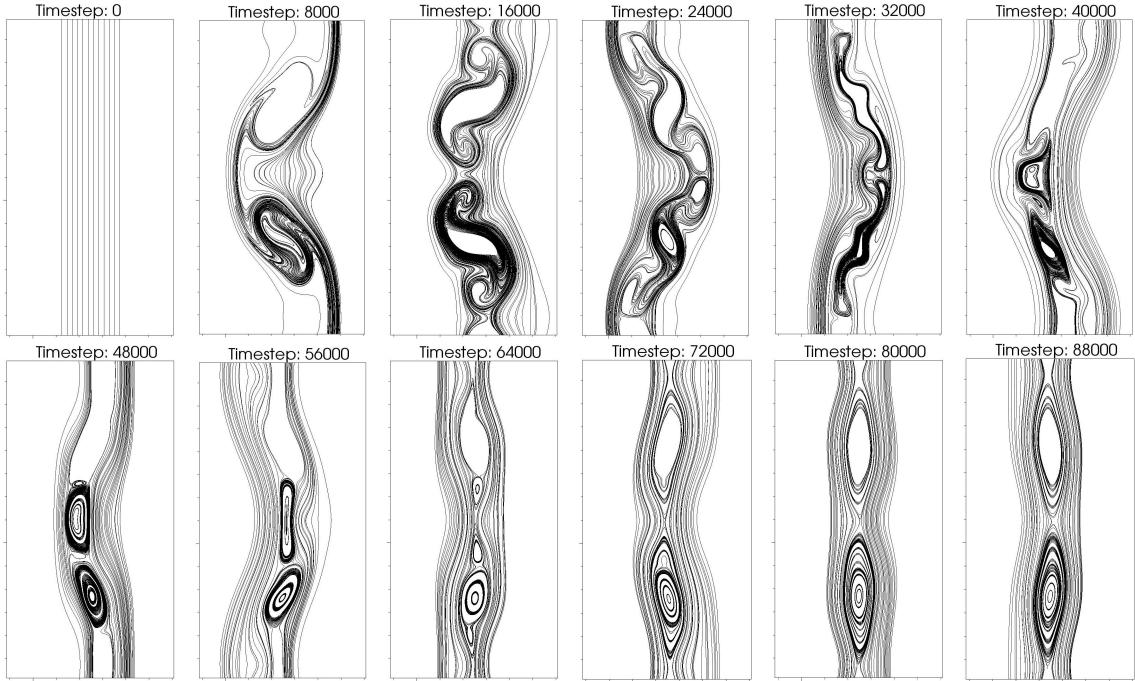


FIG. 6.5: Evolution of the magnetic field lines from our partial entropic LB-MHD code of Chen *et. al.* [22] Fig. 4a with zero initial shear velocity in a uniform magnetic field. Snapshots of the field lines are presented at each 8000 (8k) LB timesteps. Grid  $1024^2$ .

6.3. In Fig. 6.3a we show the simulation results of case 13 in Chen *et. al.* for the magnetic field lines and compare them to those arising from our partial entropic LB-MHD model for resistivity  $\eta = 0.001$ , Fig. 6.3b.

For the case of no initial shear, large magnetic islands are formed. A corresponding snapshot is given of the magnetic field lines from the case 5 simulation in Chen *et. al.*, Fig. 6.4a, and from our entropic LB-MHD model, Fig. 6.4b. In Fig. 6.5 we show the partial entropic LB-MHD evolution of the magnetic field lines for this initial zero velocity shear flow parameter set of Fig. 6.4. It seems for the case considered here, the enthalpy equation in Chen [22] does not play a significant role.

### 6.3.3 Biskamp-Welter Profile

We now consider the model of Biskamp and Welter [23] for decaying 2D MHD turbulence, using their initial profiles

$$\vec{u}(x, y, t = 0) = U_0 [\sin(y + 0.5)\hat{x} - \sin(x + 1.4)\hat{y}] \quad (6.24)$$

$$\vec{B}(x, y, t = 0) = B_0 [\sin(y + 4.1)\hat{x} - 2\sin(2x + 2.3)\hat{y}] \quad (6.25)$$

(These are a generalization of the canonical Orszag-Tang vortex). A snapshot of the current lines are shown in Fig. 6.6 and compared with those from the Biskamp-Welter simulation. In Fig. 6.7 we plot the corresponding 2D entropy parameter  $\gamma^*(x, y)$  at this

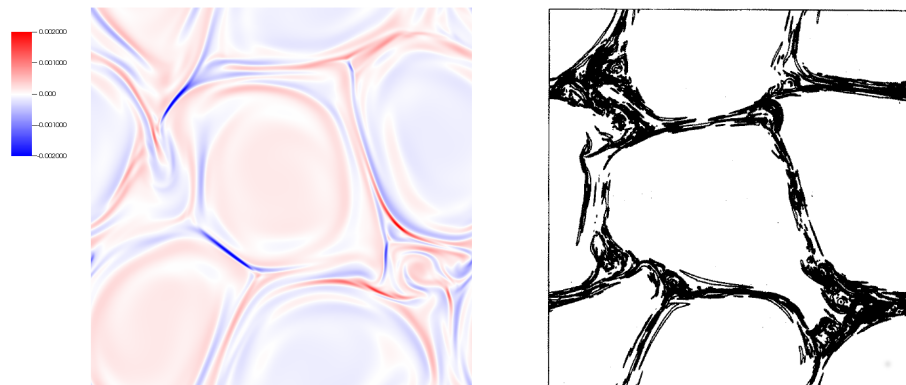


FIG. 6.6: **Comparison of current lines in Entropic MRT simulation of Biskamp [23] case A<sub>1</sub>.** Snapshot of the current lines from (a) partial entropic LB-MHD code on a grid of  $1024^2$  at time = 226k, (b) Biskamp-Welter, Fig. 11a

time snapshot. The lattice points at which  $\gamma^*(x, y) \neq 2$  correspond to points where there are effects of in our partial entropic LB-MHD algorithm. The energy dissipation rate for this Biskamp-Welter case is shown in Fig. 6.8. This can be compared with figure 20 in [23].



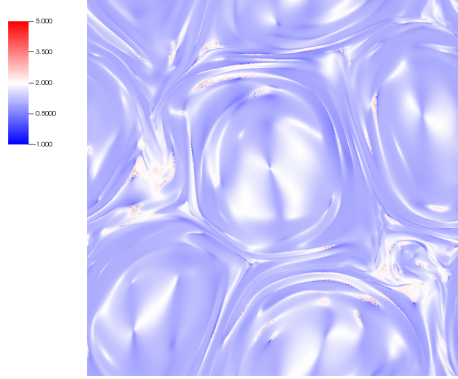


FIG. 6.7: Plot of the entropic parameter  $\gamma^*$  in an entropic MRT simulation of Biskamp [23] case  $A_1$  after 226k timesteps on a  $1024^2$  grid.  $\gamma = 2.0$  corresponds to ordinary LB-MHD. Lattice points with  $\gamma^* \neq 2.0$  correspond to the effects of the partial entropic LB-MHD algorithm.

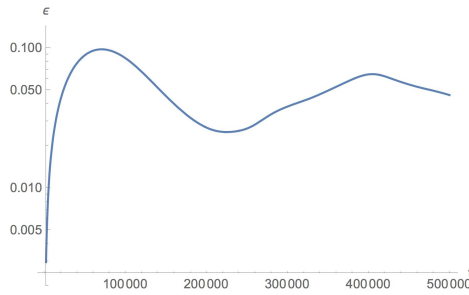


FIG. 6.8: Plot of energy dissipation over time for the Biskamp-Welter profile.

## 6.4 Conclusion

The Karlin [3, 21] entropic Navier-Stokes algorithm has been extended to LB-MHD and tested on 3 different problems: velocity shear flows exhibiting Kelvin-Helmholtz and/or tearing instability, a generalized Orszag-Tang vortex and magnetized jet instability. The partial entropy algorithm is applied only to the particle distributions while in using a vector distribution for the magnetic field one must allow for magnetic field reversals. Hence, the new partial entropic MRT LB MHD model is not fully entropic. The algorithm clearly extends immediately to 3D, but because of the much greater computational costs we have restricted our simulations to 2D for we can still capture turbulence effects of the

generation of small scale motions since in 2D MHD energy cascades to small scales. Good agreement has been found with the CFD simulations of Chen *et. al.* and Biskamp and Welter. The partial entropic algorithm permits much larger ranges of velocity and magnetic field amplitudes than could be found in standard LB-MHD algorithms. This greater numerical stability is achieved at a quite small increase in computational costs since Karlin *et. al.* have determined a simple algebraic approximation to the full entropic parameter. This approximation is then carried over as an ansatz for our 2D LB-MHD model. Moreover the extreme parallelization of this partial entropic LB-MHD algorithm is retained since this algebraic entropic parameter  $\gamma^*$  is determined purely from local information at each lattice site. The accuracy of the under-resolved Navier-Stokes simulations of Bösch *et. al.* [24] portend that this new (partial) entropy method could be a possible subgrid model in itself. In some sense, this is the spirit behind pushing the magnitude of  $U_0$  and  $B_0$ . There is no claim on improved accuracy for this model. This partial entropic LB-MHD algorithm is a subset of MRT models in which there is now a dynamical relaxation rate determined for quasi-stabilization of the fluid flow by a well-defined procedure as opposed to the standard static MRT relaxation rates.

# CHAPTER 7

## Large Eddy Simulations

In the previous chapter, the partial entropic MRT method was introduced to improve the stability and the possible accuracy of the LBM. In this chapter, large eddy simulations (LES) are introduced to address the specific problem of computational cost of simulations. A brief history and explanation for the need of LES are covered.

### 7.1 Relative Scales

Passing a problem from the physical world into an LB simulation requires an understanding of relative scales. To simplify the relationship between physical (with subscript  $p$ ) and LB (no subscript) scales, the non-dimensional scales (with subscript  $d$ ) are introduced. The relationship between the physical and non-dimensional scales is

$$t_0 = \frac{t_p}{t_d} \quad , \quad r_0 = \frac{r_p}{r_d} \quad , \quad u_p = \frac{r_0}{t_0} u_d \quad , \quad \nu_p = \frac{r_0^2}{t_0} \nu_d \quad (7.1)$$

where  $t_0$  and  $r_0$  are scaling factors between physical and dimensionless values which are typically set to 1 and  $\nu$  is the viscosity. The relationship between the non-dimensional and

LB scaled counterparts is

$$r_1 = \frac{L}{r_d} \quad , \quad t_1 = \frac{t}{t_d} \quad , \quad U = \frac{r_1}{t_1} u_d \quad , \quad \nu = \frac{r_1^2}{t_1} \nu_d \quad (7.2)$$

where  $L$  is the number of LB cells required to equal length  $r_d$  and  $t$  is the number of timesteps required to equal time  $t_d$ . Similar to  $t_0$  and  $r_0$ , the non-dimensional variables  $r_d$  and  $t_d$  are arbitrarily set to 1 for simplicity when no physical scale is being referenced.

## 7.2 Cost of DNS

A proper choice of  $L$  is necessary in order to fully resolve the dynamics of a problem. A typical, fully resolved ( $L \geq L_{min}$ ) simulation is considered a direct numerical simulation (DNS).  $L_{min}$  needs to be large enough that all scales of motion are included down to the dissipation of kinetic motion into heat. The smallest microscale where this occurs is known as the Kolmogorov length scale, defined as

$$\eta_k = \left( \frac{\nu_d^3}{\epsilon} \right)^{1/4} \quad \text{for} \quad \epsilon = \frac{u_d^3}{r_d} \quad . \quad (7.3)$$

where  $\epsilon$  is the dissipation rate. The Kolmogorov length scale ( $\eta_k$ ) can be used to find the lowest required resolution and thus the minimum required length to fully resolve a problem. In LB units,  $\eta_k$  becomes

$$\eta_{LB} = \frac{1}{r_1} \left( \frac{\nu^3 L}{U^3} \right)^{1/4} \quad (7.4)$$

Since  $\eta_{LB}$  represents the smallest turbulent motions with units one over length, this value provides the lowest resolution required for a fully resolved DNS. The minimum

gridsize for said resolution is

$$L_{min} = \frac{r_d}{\eta_{LB}} = \left( \frac{UL}{\nu} \right)^{3/4} = \text{Re}^{3/4} \quad (7.5)$$

with the Reynold's number defined as

$$\text{Re} = \frac{UL}{\nu} \quad (7.6)$$

where  $U$  is the fluid velocity,  $L$  is the characteristic linear dimension (typically width) and the Reynolds number (Re) is a dimensionless ratio which characterizes a specific problem. In 2D LB, the minimum number of required gridpoints is  $(L_{min})^2 = \text{Re}^{3/2}$  and for 3D LB,  $(L_{min})^3 = \text{Re}^{9/4}$ . This is problem for turbulent simulations as the Reynolds number can be very large for physical turbulent flows. For example, the red spot in Jupiter's atmosphere has  $\text{Re} = 10^{12}$  by estimating the velocity on the order of 100 m/s, the kinematic viscosity of hydrogen on the order of  $10^{-5} \text{m}^2/\text{s}$ , and a height of the atmosphere on the order of 100 km.

Along with the minimum gridsize required to use in memory, the computational cost of a DNS scales as  $\text{Re}^3$  according to Pope [14]. This shows that a DNS generally has a very high computational cost. In general, the computational cost to simulate any system is proportional to the full number of cells ( $L^D$  for a cubic grid) times the number of timesteps ( $t$ ). This formula can be written as

$$C = L^D t = L^D \left( L^2 \frac{\nu_d}{\nu} \right) = L^{D+2} \frac{\nu_d}{\nu} . \quad (7.7)$$

If, for example, the number of cells along each dimension were doubled ( $L \rightarrow 2L$ ) for increased accuracy in a 2D system without changing the Reynold's number ( $\nu \rightarrow 2\nu$ ), the

computational cost would be

$$C = (2L)^2 t = 4L^2 \left( (2L)^2 \frac{\nu_d}{2\nu} \right) = 8L^4 \frac{\nu_d}{\nu}. \quad (7.8)$$

Just doubling the linear size of a 2D LB grid without changing the Reynold's number will quadruple the amount of computational time spent calculating one timestep and halve the value of a single timestep, making the total computational cost 8 times greater!

At this point, it is important to note that nearly all computational effort in DNS is expended on the smallest dissipative motions. Figure 7.1 shows the ratio of energy scales in a full DNS. Notice that the dissipation range takes up 99.98% of the phase space while the energy containing range and the inertial subrange which carry most of the energy and anisotropy take up only a small portion at the center. A standard energy spectrum is presented in Fig. 5.1 showing the amount of energy in each of these ranges. Although most of the energy is found at large scales and cascades to smaller scales, some energy backscattering occurs. This means energy at smaller scales can affect larger scales due to nonlinearity in the convective term and qualitatively explains why high resolution in the dissipative range is required.

## 7.3 Filtering

One approach to further reducing the minimum required gridsize is a technique called Large Eddy Simulation (LES). This technique applies low-pass filters to all fields, removing the high frequency scales and lowering their perceived resolution. An example of filtering 1D data is shown in Fig. 7.2. As can be seen, the filtered field line  $\bar{U}$  has smoothed the field line  $U$ , allowing the representation of  $\bar{U}$  to be shown on a low resolution plot. Similarly, an example of 2D filtering is shown in Fig. 7.3. As the DNS data in Fig. 7.3a is filtered, the

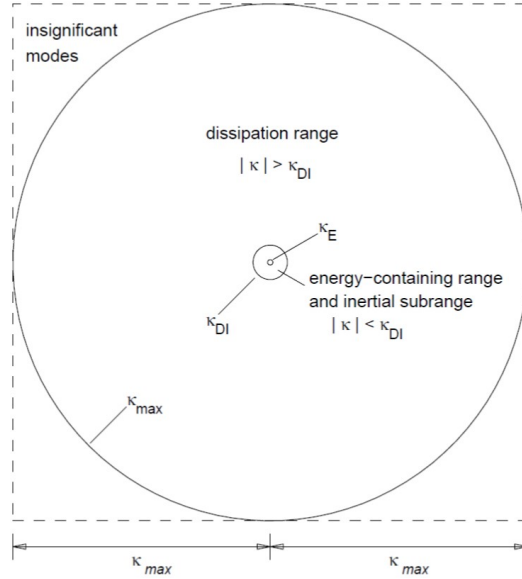


FIG. 7.1: **Diagram showing the relative size of the energy scales in a full DNS** [Cited from Pope [14], Fig. 9.4].

filtered data in figs. 7.3b and 7.3c is perceived to be of lower resolution and can actually be represented on lower resolution grids. The definition of filtered quantity  $\bar{\mathbf{U}}$  relative to its counterpart  $\mathbf{U}$  is

$$\bar{\mathbf{U}} = \int G(\mathbf{r}, \mathbf{x}) \mathbf{U}(\mathbf{x} - \mathbf{r}, t) d\mathbf{r} \quad (7.9)$$

where  $G(\mathbf{r}, \mathbf{x})$  is some filter function normalized such that

$$\int G(\mathbf{r}, \mathbf{x}) d\mathbf{r} = 1 . \quad (7.10)$$

A very commonly used filter function is the Gaussian. It is favorable because of its similarity in both real space and phase space. The normalized Gaussian is defined as

$$G(r) = \left( \frac{6}{\pi \Delta^2} \right)^{D/2} \exp \left( -\frac{6r^2}{\Delta^2} \right) \quad (7.11)$$

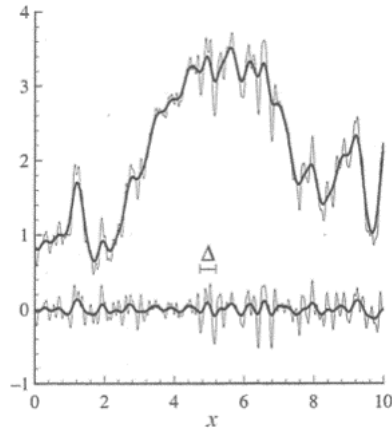


FIG. 7.2: **1D Filter Example cited from Pope [14].**

The upper thin curve corresponds to the exact field  $U$ , and the upper bold curve corresponds to filtered field  $\bar{U}$ . The lower thin curve around 0 is the deviation  $u' = U - \bar{U}$ . Note that the filtered fluctuations  $\bar{u}'$  are nonzero as shown by the bold curve around 0.

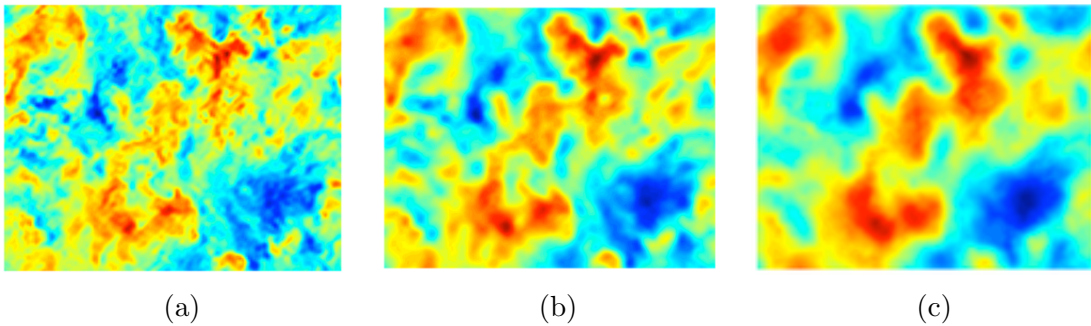


FIG. 7.3: **2D filtering example.** Velocity field of DNS simulation from Lu *et. al.* [25]. (a) DNS without a filter applied. (b) DNS filtered using Box filter with filter width  $\Delta = \frac{L}{32}$ . (c) DNS filtered using a Box filter with a coarser filter width  $\Delta = \frac{L}{16}$ .

where  $D$  is the number of dimensions of the Gaussian and  $\Delta$  is the filter width which defines the strength of the filter. The Gaussian filter is also used for its nice isotropic



properties where the zeroth, first, and second moments have known simple values

$$\int G(\mathbf{r}, \mathbf{x}) d\mathbf{r} = 1 \quad (7.12a)$$

$$\int \mathbf{r} G(\mathbf{r}, \mathbf{x}) d\mathbf{r} = 0 \quad (7.12b)$$

$$\int r_\alpha r_\beta G(\mathbf{r}, \mathbf{x}) d\mathbf{r} = \frac{\Delta^2}{12} \delta_{\alpha\beta} . \quad (7.12c)$$

Other filter functions can be ideal for certain simulation or LES techniques. The sharp spectral filter is a simple cutoff filter in phase space but is entirely non-local in physical space and the converse is true of the box filter. Filtering does not automatically provide closure to LES, as will soon be discussed, and so some filters have specific analytic approximations to closure, such as the Pao filter, but can be difficult to use.

For reference, the difference in a field before and after it is filtered is defined as

$$\mathbf{u}'(\mathbf{x}, t) \equiv \mathbf{U}(\mathbf{x}, t) - \bar{\mathbf{U}}(\mathbf{x}, t) \quad (7.13)$$

and it is important to note that a filtered difference is not zero (as it would be if the filter was an averaging procedure)

$$\overline{\mathbf{u}'(\mathbf{x}, t)} = \overline{\mathbf{U}(\mathbf{x}, t) - \bar{\mathbf{U}}(\mathbf{x}, t)} = \bar{\mathbf{U}}(\mathbf{x}, t) - \bar{\bar{\mathbf{U}}}(\mathbf{x}, t) \neq 0 . \quad (7.14)$$

## 7.4 Early LES

Applying a filter to a field will lower the field's resolution but does not change the minimum resolution required of the simulation. So in order to perform a filtered simulation with a lower resolution, we need to know how to evolve the subgrid elements (those required elements in the dissipation range removed by the low-pass filter). Essentially, in

filtered Navier-Stokes, the gridsize would be reduced according to the filter width. Each filtered field would evolve as standard Navier-Stokes at each grid point, then an additional evolution term would be included to evolve the subgrid motions and maintain the accuracy of a higher resolution simulation. This approach was pioneered by Smagorinsky when he proposed an ad-hoc solution for the subgrid evolution. Creating the new evolution equations requires the existing equations to be filtered.

$$\overline{\partial_t \mathbf{u} + (\mathbf{u} \cdot \nabla) \mathbf{u}} = \overline{-\nabla P + \nu \nabla^2 \mathbf{u}} \quad (7.15)$$

$$\partial_t \bar{\mathbf{u}} + \overline{(\mathbf{u} \cdot \nabla) \mathbf{u}} = \overline{-\nabla P} + \nu \nabla^2 \bar{\mathbf{u}} \quad (7.16)$$

To provide closure to the filtered Navier-Stokes equations above and to have standard evolution in the filtered terms as described above,  $\overline{(\mathbf{u} \cdot \nabla) \mathbf{u}}$  needs to be replaced such that

$$\overline{(\mathbf{u} \cdot \nabla) \mathbf{u}} = (\bar{\mathbf{u}} \cdot \nabla) \bar{\mathbf{u}} + \partial_j \tau_{ij} \quad (7.17)$$

where  $\tau_{ij} = \overline{u_i u_j} - \bar{u}_i \bar{u}_j$ .  $\tau_{ij}$  now presents a closure problem whose solution is now assumed by Smagorinsky to be related to the rate of strain tensor  $S_{ij}$  such that

$$\tau_{ij} = -2C_s \Delta^2 \left| \bar{S} \right| \bar{S}_{ij} = -2\nu_T \bar{S}_{ij} \quad (7.18)$$

where  $\bar{S}_{ij} = \frac{1}{2} (\partial_j \bar{u}_i + \partial_i \bar{u}_j)$ ,  $\left| \bar{S} \right| = \sqrt{2 \bar{S}_{ij} \bar{S}_{ij}}$ ,  $\nu_T$  is a parameter representing the “subgrid viscosity”, and  $C_s$  is the unknown Smagorinsky constant which is a factor specific to each problem. This definition was chosen for the subgrid evolution because the small scale regime is dominated by diffusion. Determining this Smagorinsky constant was originally determined through trial and error. However, much work has gone into a mathematical approach to finding  $C_s$  with previous LB-LES-NS modeling [26, 27] concentrating on the

Smagorinsky closure for the subgrid stresses.

## 7.5 Advances in LES

Early advances in LES were quickly made to find a solution to  $C_s$  for specific filters, such as the sharp spectral filter and Pao filter. The drawback here is that many of these filters can be difficult to use in certain circumstances and typically requires some level of approximation. Further advances in LES would determine  $C_s$  by limiting the filter width.

A very large filter width where  $\frac{\Delta}{L} \rightarrow \infty$  has the property  $C_s \rightarrow 0$ . The filtered field  $\bar{\mathbf{U}}$  tends to the mean  $\langle \mathbf{U} \rangle$  with this approach and is very inaccurate at higher Reynold's numbers [14]. At high Reynold's number, the large filter width forces the inertial subrange to be modeled inaccurately by the subgrid evolution terms.

The Clark model requires a very small filter width ( $\frac{\Delta}{\eta_k} \ll 1$ ) allowing the filter function to be Taylor expanded about the filter width. When a Gaussian filter is used, the second order subgrid term (according to the Gaussian isotropic properties (7.12)) becomes

$$\tau_{ij} = \overline{u_i u_j} - \bar{u}_i \bar{u}_j = \frac{\Delta^2}{12} \partial_k \bar{U}_i \partial_k \bar{U}_j \quad (7.19)$$

removing the need for Smagorinsky's constant altogether. When Smagorinsky's model is used with the same small filter width, conflicting values for  $C_s$  are found for different filter functions [14]. These conflicting results show that the Smagorinsky model provides a poor description of the residual stresses at a detailed level. However, the wide usage and success of the Smagorinsky model and its derivative models have shown that the ad-hoc form is relatively accurate.

Recent advances [28, 29] in LES have found a general solution numerically for the Smagorinsky constant, regardless of filter function. The approach applies a test filter  $\widetilde{\bar{\mathbf{U}}}$

to the filtered evolution equations to yield doubly filtered equations. The error between the first filter and the test filter is then minimized to precisely calculate  $C_s$  at every timestep. Although a general solution provides the most accurate results for a given LES problem, the computational cost is comparatively high since the filtering and minimization is recalculated at every timestep.

Mixed models are another recent advancement which attempts to combine various LES models for greater accuracy and lower computational cost. LES is a useful and almost necessary extension to Navier-Stokes and MHD for simulating physical flows since DNS can require high computational cost to be fully resolved.

# CHAPTER 8

## LES model for LB MHD

Computational methods are stretched to the limit in trying to solve problems of strong turbulence [4, 28, 30–32]. Direct numerical simulations (DNS) attempt to solve the evolution equations by resolving all the scales excited in the turbulence. Hence, in strong turbulence, DNS will quickly run into resolution problems: one will not be able to resolve all the excited scales all the way down to the dissipation scales. Basically, the computational cost of DNS scales as the  $Re^3$ , where  $Re$  is the Reynolds number of the flow. (The Reynolds number is basically the ratio of the nonlinear to linear terms in the equations).

There have been attempts to extend Smagorinsky's ideas to MHD, similar to those in section 7.4 [29, 33–36]. The filtered MHD equations, Eqs. (8.1–8.3), contain the unknown

subgrid stress tensors (8.4, 8.5),  $\tau_{\alpha\beta}^{(v)}$  and  $\tau_{\alpha\beta}^{(b)}$ .

$$\nabla \cdot \bar{\mathbf{u}} = 0 \quad , \quad \nabla \cdot \bar{\mathbf{B}} = 0 \quad (8.1)$$

$$\partial_t \bar{\mathbf{u}} + (\bar{\mathbf{u}} \cdot \nabla) \bar{\mathbf{u}} = -\nabla \bar{p} + (\bar{\mathbf{B}} \cdot \nabla) \bar{\mathbf{B}} + \nu \nabla^2 \bar{\mathbf{u}} + \nabla \cdot \tau^{(v)} \quad (8.2)$$

$$\partial_t \bar{\mathbf{B}} = (\bar{\mathbf{B}} \cdot \nabla) \bar{\mathbf{u}} - (\bar{\mathbf{u}} \cdot \nabla) \bar{\mathbf{B}} + \eta \nabla^2 \bar{\mathbf{B}} + \nabla \cdot \tau^{(b)}, \quad (8.3)$$

$$\text{where } \nabla \cdot \tau^{(v)} = [(\bar{\mathbf{u}} \cdot \nabla) \bar{\mathbf{u}} - \overline{(\mathbf{u} \cdot \nabla) \mathbf{u}}] - [(\bar{\mathbf{B}} \cdot \nabla) \bar{\mathbf{B}} - \overline{(\mathbf{B} \cdot \nabla) \mathbf{B}}] \quad (8.4)$$

$$\nabla \cdot \tau^{(b)} = [(\bar{\mathbf{u}} \cdot \nabla) \bar{\mathbf{B}} - \overline{(\mathbf{u} \cdot \nabla) \mathbf{B}}] - [(\bar{\mathbf{B}} \cdot \nabla) \bar{\mathbf{u}} - \overline{(\mathbf{B} \cdot \nabla) \mathbf{u}}]. \quad (8.5)$$

As a first step one could invoke the Smagorinsky's ad-hoc closure scheme to the filtered MHD equations and so resolve the subgrid stress tensors, Eqs. (8.6) and (8.7), by relating them to the mean strain rate tensor, Eq. (7.18), and the mean current, Eq. (8.8) :

$$\tau_{\alpha\beta}^{(v)} = -2C_{Sv} \Delta^2 \left| \bar{S} \right| \bar{S}_{\alpha\beta} = -2\nu_t \bar{S}_{\alpha\beta} \quad (8.6)$$

$$\tau_{\alpha\beta}^{(b)} = -2C_{Sb} \Delta^2 \left| \bar{j} \right| \bar{J}_{\alpha\beta} = -2\eta_t \bar{J}_{\alpha\beta} \quad (8.7)$$

$$\bar{J}_{\alpha\beta} = \frac{1}{2} \left( \partial_\beta \bar{B}_\alpha - \partial_\alpha \bar{B}_\beta \right) \quad (8.8)$$

Another closure scheme proposed by Carati *et. al* [29] permits the backscatter of energy from the subgrid to resolved scales. This cross-helicity based closure takes the form

$$\tau_{\alpha\beta}^{(v)} = -2C_{Sv} \Delta^2 \left| \bar{S}_{\alpha\beta}^v \bar{S}_{\alpha\beta}^b \right|^{1/2} \bar{S}_{\alpha\beta} = -2\nu_t \bar{S}_{\alpha\beta} \quad (8.9)$$

$$\tau_{\alpha\beta}^{(b)} = -2C_{Sb} \Delta^2 \text{sgn}(\bar{j} \cdot \bar{\omega}) \left| \bar{j} \cdot \bar{\omega} \right|^{1/2} \bar{J}_{\alpha\beta} = -2\eta_t \bar{J}_{\alpha\beta} \quad (8.10)$$

$$\text{where } \bar{S}_{\alpha\beta}^v = \bar{S}_{\alpha\beta} \quad , \quad \bar{S}_{\alpha\beta}^b = \frac{1}{2} \left( \partial_\beta \bar{B}_\alpha + \partial_\alpha \bar{B}_\beta \right) \quad , \quad \bar{\omega} = \nabla \times \bar{\mathbf{u}} \quad (8.11)$$

Ansumali *et al.* [4] realized that the 2 limit processes in LES for a LB representation of Navier-Stokes turbulence (the Chapman-Enskog expansion in the Knudsen number,

Kn, and an expansion in the filter width,  $\Delta$ ) do not commute. The typical approach of first performing the Chapman-Enskog limit on LB (to reproduce the fluid equations) and then perform the filtering will lead to the closure problem. However, Ansumali *et al.* [4] first performed the filter-width  $\Delta$  expansion directly on the LB equations. This was then followed by the usual Chapman-Enskog expansion to recover the final fluid equations. By requiring that the effects of the subgrid stresses first enter the evolution equations at the transport level one can get a closed form final expression for the LES equations as well as determining the required scaling of the filter width  $\Delta$  in terms of the Knudsen number Kn. It should be noted that Ansumali *et al.* [4] restricted their analysis to 2D Navier-Stokes turbulence in which the energy is inverse cascaded to large scales. It is also interesting to note that Pope [14], has discussed the expansion of the filtered Navier-Stokes equation in terms of the filter width  $\Delta$ . The practical problem is that this would force us to perform filtering in the dissipate range - and thereby placing a very heavy burden on the LES solution to be useful in turbulence simulations, basically turning the LES into a DNS.

Here we extend the ideas of Ansumali *et al.* [4] to MHD. For simplicity, we restrict our analysis to 2 dimensional (2D) MHD - since in 2D MHD turbulence energy is cascaded to small scales as in 3D MHD turbulence. Hence there is a need for subgrid modeling in 2D MHD unlike 2D Navier-Stokes turbulence in which there is an inverse cascade of energy to large scales. In Sec. 8.1, we introduce the Gaussian filter and perform expansions in the filter width  $\Delta$  to evaluate nonlinear filter averages. In Sec. 8.2, we discuss the transformation of the LB-MHD algorithm into the moment basis, permitting a multi-relaxation collision model for the density/velocity distributions while we use a single-relaxation model for the vector magnetic distribution function first introduced by Dellar [13]. In Sec. 8.3, the MHD equations are derived from the new LES-LB-MHD model. We first filter the LB-moment equations and present the details, for brevity, of the 3rd moment,  $\overline{M}_3$ . An expansion is then made in the usual Knudsen number, Kn, to move

from the LB-MHD representation to the macroscopic dissipative equations for MHD. In order that the subgrid effects first affect the dynamics at the transport time scales one must scale the filter width  $\Delta \simeq \mathcal{O}(\text{Kn}^{1/2})$ . Sec. 8.4 then discusses preparations of the LES-LB-MHD model for actual simulation. And finally, Sec. 8.5 discusses the simulation results of the LES-LB-MHD model in 2D.

## 8.1 Filters and Filter Widths

The backbone of any LES [14, 26–44] is the introduction of a spatial filter function to smooth out field fluctuations on the order of the filter width  $\Delta$ . Consider a filter function,  $G(\vec{r}, \Delta)$ , which averages over scales of width  $\Delta$ , so that the filtered field  $\bar{X}$  is given by the convolution integral, as found in Eq. (7.9)

$$\bar{X}(\vec{r}', \Delta) = \int_{-\infty}^{\infty} X(\vec{r}' - \vec{r}) G(\vec{r}, \Delta) d\vec{r} \quad (8.12)$$

where  $\vec{r}$  and  $\Delta$  defines a location on the lattice and the filter width respectively. For convenience, we shall use the Gaussian filter function (7.11) which is sharply peaked about  $r = 0$

$$G(\vec{r}, \Delta) = \left( \frac{6}{\pi \Delta^2} \right)^{\frac{1}{2}} \exp\left( -\frac{6r^2}{\Delta^2} \right) \quad (8.13)$$

with the isotropic properties

$$\int_{-\infty}^{\infty} G(\vec{r}, \Delta) d\vec{r} = 1, \quad \int_{-\infty}^{\infty} G(\vec{r}, \Delta) \vec{r} d\vec{r} = 0, \quad \int_{-\infty}^{\infty} G(\vec{r}, \Delta) r_{\alpha} r_{\beta} d\vec{r} = \frac{\Delta^2}{12} \delta_{\alpha\beta} \quad (8.14)$$

Taylor expanding the dynamical field  $X(\vec{r}' - \vec{r})$  about  $\vec{r} = \vec{r}'$  in Eq. (8.12) and then



performing the Gaussian weighted polynomial integrals one immediately finds [14]

$$\bar{X} = X + \frac{\Delta^2}{24} \partial_\beta^2 X + \mathcal{O}(\Delta^4) \quad (8.15)$$

Similarly, it can be shown

$$\overline{(XY)} = \bar{X} \bar{Y} + \frac{\Delta^2}{12} (\partial_\beta \bar{X}) (\partial_\beta \bar{Y}) + \mathcal{O}(\Delta^4) \quad (8.16)$$

and

$$\begin{aligned} \overline{\left(\frac{XY}{Z}\right)} &= \frac{\bar{X}\bar{Y}}{\bar{Z}} + \frac{\Delta^2}{12\bar{Z}} \left[ (\partial_\beta \bar{X}) (\partial_\beta \bar{Y}) \right. \\ &\quad \left. - \frac{(\partial_\beta \bar{Z})}{\bar{Z}} \left( \bar{X} (\partial_\beta \bar{Y}) + \bar{Y} (\partial_\beta \bar{X}) - \frac{\bar{X}\bar{Y} (\partial_\beta \bar{Z})}{\bar{Z}} \right) \right] + \mathcal{O}(\Delta^4) \end{aligned} \quad (8.17)$$

for arbitrary fields  $X$ ,  $Y$ , and  $Z$ .

## 8.2 Moment Basis Representation for LES LB-MHD

The single relaxation LB-MHD model of Dellar [13] is extended to incorporate multiple relaxation times (MRT) similar to section 6.1 but with a different transformation matrix used for simplicity in the derivation. The derivation is done in 2D for simplicity, and it is readily extended to 3D, but with the complications of a larger number of lattice velocities. However, unlike the 2D Navier-Stokes work of Ansumali *et. al.*, 2D MHD exhibits the same energy cascade to small scales as in 3D. The LB equations for the distribution functions

$f_i$ , of the density and mean velocity, and  $\vec{g}_k$ , for the magnetic field are

$$(\partial_t + \partial_\gamma c_{\gamma i}) f_i = \sum_j s'_{ij} (f_j^{\text{eq}} - f_j) \quad (8.18)$$

$$(\partial_t + \partial_\gamma C_{\gamma k}) \vec{g}_k = s'_m (\vec{g}_k^{\text{eq}} - \vec{g}_k) \quad (8.19)$$

with the moments  $\sum_i f_i = \rho$ ,  $\sum_i f_i \vec{c}_i = \rho \vec{u}$ , and  $\sum_k \vec{g}_k = \vec{B}$ . In these equations the summation convention is employed on the vector nature of the fields (using Greek indices). Roman indices correspond to the corresponding lattice vectors for the kinetic velocities  $\vec{c}_i$  (Fig. 3.1) and  $\vec{C}_k$  (Fig. 8.1).  $s'_{ij}$  and  $s'_m$  are the collisional relaxation rate tensor for the density and the collisional relaxation rate scalar for the magnetic field distributions, respectively. The choice of these kinetic relaxation rates will determine the MHD viscosity and resistivity transport coefficients.

To recover the MHD equations, one must make an appropriate choice of phase space velocity/magnetic field lattice vectors and appropriate relaxation distribution functions. An appropriate choice for 2D MHD is the 9-bit phase space velocities (D2Q9) as seen in Fig. 3.1 for the density distribution and the simpler 5-bit velocities (D2Q5) for the magnetic field distribution as seen in Fig. 8.1. The simpler lattice for the magnetic field distribution arises since the magnetic field  $\vec{B}$  is the zeroth moment of  $\vec{g}_k$  while the mean fluid velocity is determined from the 1st moment of  $f_i$ . To recover the MHD equations in the Chapman-Enskog limit of the (discrete) kinetic equations, an appropriate choice of relaxation distribution functions  $f_i^{\text{eq}}$  and  $\vec{g}_k^{\text{eq}}$  is presented in equations (4.21) and (4.24)

and repeated here explicitly for the lattice systems

$$D2Q9 : \quad f_i^{\text{eq}} = w_i \rho \left[ 1 + 3(\vec{c}_i \cdot \vec{u}) + \frac{9}{2}(\vec{c}_i \cdot \vec{u})^2 - \frac{3}{2}u^2 \right] + \frac{9}{2}w_i \left[ \frac{1}{2}\vec{B}^2 \vec{c}_i^2 - (\vec{B} \cdot \vec{c}_i)^2 \right], i = 0, \dots, 8 \quad (8.20)$$

$$D2Q5 : \quad \vec{g}_k^{\text{eq}} = w'_k \left[ \vec{B} + 3 \left\{ (\vec{C}_k \cdot \vec{u}) \vec{B} - (\vec{C}_k \cdot \vec{B}) \vec{u} \right\} \right], k = 0, \dots, 4 \quad (8.21)$$

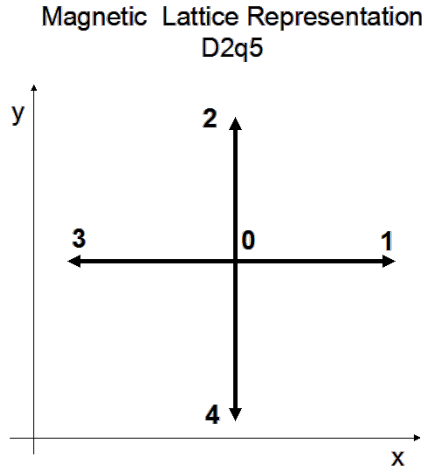


FIG. 8.1: **The magnetic lattice vectors (D2Q5) for LB-MHD in 2D** are  $\vec{C}_k = (0, 0), (0, \pm 1)$ ,  $k = 0 \dots 4$ .  $w_i$  are appropriate weight factors dependent on the choice of lattice: for speed 0,  $w_0 = \frac{1}{3}$ ; and for speed 1,  $w_i = \frac{1}{6}$  with lattice speed of sound  $c_s = \frac{1}{\sqrt{3}}$ .

Typically these equations are solved by split-operator methods: streaming and collisional relaxation. The 1-1 constant transformation matrices  $T$  and  $T_m$  chosen for convenience in derivation, permit the mapping between the distribution space  $(f_i, \vec{g}_k)$  and the moment space  $(M_i, \vec{N}_k)$ . The transformation equations are

$$M_i = \sum_{j=0}^8 T_{ij} f_j \quad , \quad \vec{N}_k = \sum_{q=0}^4 T_{m,kq} \vec{g}_q \quad (8.22)$$

with the choice of the moments

$$\mathbf{T} = \begin{pmatrix} \mathbf{1} \\ c_x \\ c_y \\ c_x c_y \\ c_x^2 - c_y^2 \\ 3c_x c_y^2 - 2c_x \\ 3c_y c_x^2 - 2c_y \\ 4 \cdot \mathbf{1} - 9(c_x^2 + c_y^2 - 2c_x^2 c_y^2) \\ 4 \cdot \mathbf{1} - 4(c_x^2 + c_y^2) + 3c_x^2 c_y^2 \end{pmatrix} = \begin{pmatrix} 1 & 1 & 1 & 1 & 1 & 1 & 1 & 1 & 1 \\ 0 & 1 & 0 & -1 & 0 & 1 & -1 & -1 & 1 \\ 0 & 0 & 1 & 0 & -1 & 1 & 1 & -1 & -1 \\ 0 & 0 & 0 & 0 & 0 & 1 & -1 & 1 & -1 \\ 0 & 1 & -1 & 1 & -1 & 0 & 0 & 0 & 0 \\ 0 & -2 & 0 & 2 & 0 & 1 & -1 & -1 & 1 \\ 0 & 0 & -2 & 0 & 2 & 1 & 1 & -1 & -1 \\ 4 & -5 & -5 & -5 & -5 & 4 & 4 & 4 & 4 \\ 4 & 0 & 0 & 0 & 0 & -1 & -1 & -1 & -1 \end{pmatrix} \quad (8.23)$$

and

$$\mathbf{T}_m = \begin{pmatrix} \mathbf{1} \\ C_x \\ C_y \\ C_x^2 \\ C_y^2 \end{pmatrix} = \begin{pmatrix} 1 & 1 & 1 & 1 & 1 \\ 0 & 1 & 0 & -1 & 0 \\ 0 & 0 & 1 & 0 & -1 \\ 0 & 1 & 0 & 1 & 0 \\ 0 & 0 & 1 & 0 & 1 \end{pmatrix}. \quad (8.24)$$

For 2D LB-MHD the  $\mathbf{T}$ -matrix is a  $9 \times 9$  matrix, due to the lattice choice  $D2Q9$ , and the  $\mathbf{T}_m$  matrix is a  $5 \times 5$  matrix, due to the lattice choice  $D2Q5$  for the magnetic field representation. The  $x$  and  $y$  components of the 9-dimensional lattice vectors are

$$c_x = \{0, 1, 0, -1, 0, 1, -1, -1, 1\} \quad , \quad c_y = \{0, 0, 1, 0, -1, 1, 1, -1, -1\} \quad (8.25)$$

while the  $x$  and  $y$  components of the 5-dimensional lattice vectors for the magnetic distribution are

$$C_x = \{0, 1, 0, -1, 0\} \quad , \quad C_y = \{0, 0, 1, 0, -1\} \quad . \quad (8.26)$$

In the moment basis, the collisional relaxation rate tensor in MRT is diagonalized from  $s'_{ij}$  to  $s_i$  similar to that in section 6.1 where the MRT collisional relaxation rate tensor  $s'_{ij}$  is diagonalized with the  $T$ -matrix as a similarity transformation. It is convenient to

denote this diagonal matrix with elements  $s_i \delta_{ij}$ . In the  $D2Q9$  phase space,  $i = 0..8$  for  $s_i$  corresponding to the respective moment  $M_i$ . The collisional relaxation rate scalar for the magnetic field in SRT,  $s'_m$ , is equal for all magnetic moments,  $\vec{N}_k$ , just as it has been for  $\vec{g}_k$ , so we will define the relaxation rate for the magnetic field in moment space to be  $s_m$  for completeness in notation where  $s_m = s'_m$ .

The first three fluid moments are nothing but the collisional invariants - being nothing but the conservation of density (the 1<sup>st</sup> row of the T-matrix) and the conservation of momentum (the 2<sup>nd</sup> and 3<sup>rd</sup> rows of T). For the  $T_m$  matrix only the 1<sup>st</sup> row is a collisional invariant. In particular, the moments can be written in terms of the conserved moments:

$$\begin{aligned}
M_0^{\text{eq}} = M_0 = \rho & & M_3^{\text{eq}} = \frac{\rho u_x \rho u_y}{\rho} - B_x B_y & & M_6^{\text{eq}} = -\rho u_y \\
M_1^{\text{eq}} = M_1 = \rho u_x & & M_4^{\text{eq}} = \frac{(\rho u_x)^2 - (\rho u_y)^2}{\rho} - B_x^2 + B_y^2 & & M_7^{\text{eq}} = -3 \frac{(\rho u_x)^2 + (\rho u_y)^2}{\rho} \\
M_2^{\text{eq}} = M_2 = \rho u_y & & M_5^{\text{eq}} = -\rho u_x & & M_8^{\text{eq}} = \frac{5}{3} \rho - 3 \frac{(\rho u_x)^2 + (\rho u_y)^2}{\rho}
\end{aligned} \tag{8.27}$$

$$\begin{aligned}
N_{\alpha 0}^{\text{eq}} = N_{\alpha 0} = B_\alpha & & N_{\alpha 1}^{\text{eq}} = \rho u_x B_\alpha - \rho u_\alpha B_x & & N_{\alpha 2}^{\text{eq}} = \rho u_y B_\alpha - \rho u_\alpha B_y \\
N_{\alpha 3}^{\text{eq}} = \frac{B_\alpha}{3} & & N_{\alpha 4}^{\text{eq}} = \frac{B_\alpha}{3}
\end{aligned} \tag{8.28}$$

## 8.3 Derivation of LES MHD Equations for LB MRT

### 8.3.1 Filter expansion

Using the transformations, Eq. (8.22), the LB Eqs. (8.18, 8.19) are transformed into the moment basis  $M_0, \dots, M_8$  and  $\vec{N}_0, \dots, \vec{N}_4$ . Thus there will be a set of 9 scalar moment evolution equations for the fluid ( $D2Q9$ ) and 5 vector equations for the magnetic field ( $D2Q5$ ). We present the details for just one of these moments, the time evolution of the 3<sup>rd</sup> fluid moment  $M_3$ , as the others are done similarly. Appendix A follows the procedure

below explicitly for every moment, not just the  $M_3$  moment. On filtering the evolution equation for  $M_3$

$$\partial_t \bar{M}_3 + \frac{1}{3} \partial_x (2 \bar{M}_2 + \bar{M}_6) + \frac{1}{3} \partial_y (2 \bar{M}_1 + \bar{M}_5) = s_3 (\bar{M}_3^{(\text{eq})} - \bar{M}_3) \quad (8.29)$$

where the problem of closure arises from the evaluation of the  $\bar{M}_3^{(\text{eq})}$  in the collision term. From Eq. (8.27) for  $\bar{M}_3^{(\text{eq})}$ , and the filtering expansions Eqs. (8.16, 8.17), we obtain

$$\begin{aligned} \bar{M}_3^{(\text{eq})} &= \overline{\left( \frac{\rho u_x \rho u_y}{\rho} \right)} - \overline{(B_x B_y)} \\ &= \frac{\overline{\rho u_x \rho u_y}}{\bar{\rho}} - \bar{B}_x \bar{B}_y + \frac{\Delta^2}{12 \bar{\rho}} [(\partial_\beta \overline{\rho u_x}) (\partial_\beta \overline{\rho u_y}) \\ &\quad - \frac{(\partial_\beta \bar{\rho})}{\bar{\rho}} \left( \overline{\rho u_x} (\partial_\beta \overline{\rho u_y}) + \overline{\rho u_y} (\partial_\beta \overline{\rho u_x}) - \frac{\overline{\rho u_x \rho u_y} (\partial_\beta \bar{\rho})}{\bar{\rho}} \right)] \\ &\quad - \frac{\Delta^2}{12} (\partial_\beta \bar{B}_x) (\partial_\beta \bar{B}_y) + \mathcal{O}(\Delta^4). \end{aligned} \quad (8.30)$$

It is convenient to rewrite this in the form (for a general moment)

$$\bar{M}_i^{(\text{eq})} = M_i^{(\text{eq})} (\bar{M}_0, \bar{M}_1, \bar{M}_2, \bar{N}_{x0}, \bar{N}_{y0}) + \Delta^2 \bar{M}_i^{(\Delta)} \quad (8.31)$$

where  $M_i^{(\text{eq})} (\bar{M}_0, \bar{M}_1, \bar{M}_2, \bar{N}_{x0}, \bar{N}_{y0})$  is just those moment expressions in Eq. (8.27, 8.28) but now a function of the filtered conserved moments rather than in their the unfiltered forms, while the  $\Delta^2 \bar{M}_i^{(\Delta)}$  is the term arising from the fact that  $\bar{M}_i^{(\text{eq})} \neq M_i^{(\text{eq})} (\bar{M}_0, \bar{M}_1, \bar{M}_2, \bar{N}_{x0}, \bar{N}_{y0})$ . Indeed for the 3rd moment we have

$$M_3^{(\text{eq})} (\bar{M}_0, \bar{M}_1, \bar{M}_2, \bar{N}_{x0}, \bar{N}_{y0}) = \frac{\overline{\rho u_x \rho u_y}}{\bar{\rho}} - \bar{B}_x \bar{B}_y \quad (8.32)$$

$$\begin{aligned}
\Delta^2 \bar{M}_3^{(\Delta)} &= \frac{\Delta^2}{12\bar{\rho}} [(\partial_\beta \bar{\rho} \bar{u}_x) (\partial_\beta \bar{\rho} \bar{u}_y) \\
&\quad - \frac{(\partial_\beta \bar{\rho})}{\bar{\rho}} \left( \bar{\rho} \bar{u}_x (\partial_\beta \bar{\rho} \bar{u}_y) + \bar{\rho} \bar{u}_y (\partial_\beta \bar{\rho} \bar{u}_x) - \frac{\bar{\rho} \bar{u}_x \bar{\rho} \bar{u}_y (\partial_\beta \bar{\rho})}{\bar{\rho}} \right)] - \\
&\quad \frac{\Delta^2}{12} (\partial_\beta \bar{B}_x) (\partial_\beta \bar{B}_y)
\end{aligned} \tag{8.33}$$

### 8.3.2 Knudsen expansion

We now expand the filtered LB Eqs. (8.29) in the standard way that the fluid equations are derived from the LB by introducing the small parameter  $\varepsilon$  which is just the Knudsen number (basically the ratio of the mean free path to the macroscopic length scales). Using multi-time scale analysis, with the advection time scale at  $\mathcal{O}(\varepsilon)$  and the transport time scale at  $\mathcal{O}(\varepsilon^2)$ , one has

$$\begin{aligned}
\partial_t &\rightarrow \varepsilon \partial_t^{(0)} + \varepsilon^2 \partial_t^{(1)} \quad , \quad \partial_\alpha \rightarrow \varepsilon \partial_\alpha \\
\bar{M}_i &\rightarrow \bar{M}_i^{(0)} + \varepsilon \bar{M}_i^{(1)} + \dots \quad , \quad \bar{N}_k \rightarrow \bar{N}_k^{(0)} + \varepsilon \bar{N}_k^{(1)} + \dots
\end{aligned} \tag{8.34}$$

In order that the eddy viscosity/resistivity terms come into the filtered fluid equations at the transport time scale and not earlier, one must choose  $\Delta^2$  to be on the order of the Knudsen number ( $\Delta \sim \sqrt{\text{Kn}}$ ), with  $\Delta^2 \bar{M}_3^{(\Delta)} \sim \varepsilon \bar{M}_3^{(\Delta)}$ .

The filtered LB equations are now separated into their respective order  $\varepsilon$ , and  $\varepsilon^2$  equations. For  $\bar{M}_3$  :

$$\begin{aligned}
\mathcal{O}(\varepsilon) : \partial_t^{(0)} \bar{M}_3^{(0)} + \frac{1}{3} \partial_x \left( 2 \bar{M}_2 + \bar{M}_6^{(0)} \right) + \frac{1}{3} \partial_y \left( 2 \bar{M}_1 + \bar{M}_5^{(0)} \right) \\
= s_3 \left( \bar{M}_3^{(\Delta)} - \bar{M}_3^{(1)} \right)
\end{aligned} \tag{8.35}$$

$$\begin{aligned}
\mathcal{O}(\varepsilon^2) : \partial_t^{(0)} \bar{M}_3^{(1)} + \frac{1}{3} \partial_x \left[ \left( 1 - \frac{1}{2} s_6 \right) \bar{M}_6^{(1)} \right] + \frac{1}{3} \partial_y \left[ \left( 1 - \frac{1}{2} s_5 \right) \bar{M}_5^{(1)} \right] \\
+ \partial_t^{(1)} \bar{M}_3^{(0)} = -s_3 \left( \bar{M}_3^{(2)} \right)
\end{aligned} \tag{8.36}$$

where at  $\mathcal{O}(1)$ ,  $M_i^{(\text{eq})}(\bar{M}_0, \bar{M}_1, \bar{M}_2, \bar{N}_{x0}, \bar{N}_{y0}) = \bar{M}_i^{(0)}$ .

In general, the unknown terms in the  $\mathcal{O}(\varepsilon)$  equations must now be determined:  $\bar{M}_i^{(0)}$ ,  $\bar{M}_i^{(\Delta)}$ ,  $\partial_t^{(0)} \bar{M}_i^{(0)}$ , and  $\bar{M}_i^{(1)}$ . The  $\bar{M}_i^{(0)}$  and  $\bar{M}_i^{(\Delta)}$  terms are determined as above in Eqs. (8.32, 8.33).

The zeroth order time derivatives of the conserved filtered moments  $\bar{M}_{0..2}$  and  $\bar{N}_{\alpha 0}$  can be determined by solving the  $\mathcal{O}(\varepsilon)$ , Eq. (8.35), in their corresponding moment representation

$$\partial_t^{(0)} \bar{M}_0 = -\partial_x \bar{M}_1 - \partial_y \bar{M}_2. \quad (8.37)$$

The remaining zeroth order time derivatives of the non-conserved filtered equilibria  $\bar{M}_{3..8}$  and  $\bar{N}_{\alpha 1..4}$  can then be found by differentiating with respect to the filtered conserved equilibria:

$$\begin{aligned} \partial_t^{(0)} \bar{M}_i^{(0)}(\bar{M}_0, \bar{M}_1, \bar{M}_2, \bar{N}_{x0}, \bar{N}_{y0}) &= \frac{\partial \bar{M}_i^{(0)}}{\partial \bar{M}_0} \partial_t^{(0)} \bar{M}_0 + \frac{\partial \bar{M}_i^{(0)}}{\partial \bar{M}_1} \partial_t^{(0)} \bar{M}_1 \\ &+ \frac{\partial \bar{M}_i^{(0)}}{\partial \bar{M}_2} \partial_t^{(0)} \bar{M}_2 + \frac{\partial \bar{M}_i^{(0)}}{\partial \bar{N}_{x0}} \partial_t^{(0)} \bar{N}_{x0} + \frac{\partial \bar{M}_i^{(0)}}{\partial \bar{N}_{y0}} \partial_t^{(0)} \bar{N}_{y0} \end{aligned} \quad (8.38)$$

Since our current LB algorithm itself is accurate to  $\mathcal{O}(\text{Ma}^3)$ , where Ma is the Mach number, these derivatives need only be evaluated to  $\mathcal{O}(\text{Ma}^3)$ . Having determined the zeroth order time derivatives of the conserved moments, one substitutes this into the appropriate equation. The solution for  $\partial_t^{(0)} \bar{M}_3^{(0)}$  is

$$\partial_t^{(0)} \bar{M}_3^{(0)} = \partial_t^{(0)} \left( \frac{\bar{M}_1 \bar{M}_2}{\bar{M}_0} - \bar{B}_x \bar{B}_y + \mathcal{O}(\varepsilon^2) \right) \rightarrow 0 + \mathcal{O}(\text{Ma}^3). \quad (8.39)$$

Finally, the perturbed moments,  $\bar{M}_i^{(1)}$ , can be calculated by substituting the previous results into the  $\mathcal{O}(\varepsilon)$  moment equation (8.35) and solving for  $\bar{M}_i^{(1)}$ . The solution for  $\bar{M}_3^{(1)}$



is (with  $\bar{M}_3^{(\Delta)} \simeq \Delta^2$ )

$$\begin{aligned}
\bar{M}_3^{(1)} &= -\frac{1}{s_3} \left( \partial_t^{(0)} \bar{M}_3^{(0)} + \frac{1}{3} \partial_x \left( 2 \bar{M}_2 + \bar{M}_6^{(0)} \right) + \frac{1}{3} \partial_y \left( 2 \bar{M}_1 + \bar{M}_5^{(0)} \right) \right) + \bar{M}_3^{(\Delta)} \\
&= -\frac{1}{3s_3} \left\{ \partial_x \bar{M}_2 + \partial_y \bar{M}_1 \right\} + \frac{\Delta^2}{12\bar{M}_0} \left[ \left( \partial_\beta \bar{M}_1 \right) \left( \partial_\beta \bar{M}_2 \right) \right. \\
&\quad \left. - \frac{\left( \partial_\beta \bar{M}_0 \right)}{\bar{M}_0} \left( \bar{M}_1 \left( \partial_\beta \bar{M}_2 \right) + \bar{M}_2 \left( \partial_\beta \bar{M}_1 \right) - \frac{\bar{M}_1 \bar{M}_2 \left( \partial_\beta \bar{M}_0 \right)}{\bar{M}_0} \right) \right] \\
&\quad - \frac{\Delta^2}{12} \left( \partial_\beta \bar{B}_x \right) \left( \partial_\beta \bar{B}_y \right).
\end{aligned} \tag{8.40}$$

With the  $\mathcal{O}(\varepsilon)$  equations for the conserved moments fully resolved, we must now determine the  $\mathcal{O}(\varepsilon^2)$  equations for the conserved moments by solving for the unknown  $\partial_t^{(1)} \bar{M}_i^{(0)}$ . This is determined by substituting these results into the  $\mathcal{O}(\varepsilon^2)$  moment equations and then solving for  $\partial_t^{(1)} \bar{M}_i^{(0)}$ . For  $\partial_t^{(1)} \bar{M}_0$  we find

$$\left( \partial_t^{(0)} \bar{M}_0 + \partial_x \bar{M}_1 + \partial_y \bar{M}_2 \right) + \partial_t^{(1)} \bar{M}_0 = 0 \quad \rightarrow \quad \partial_t^{(1)} \bar{M}_0 = 0 \tag{8.41}$$

### 8.3.3 Final filtered LES-MHD equations

Similarly one proceeds with these steps to determine the filtered MHD equations using the  $\mathcal{O}(\varepsilon)$  and  $\mathcal{O}(\varepsilon^2)$  equations for the conserved moments. The final evolution of the continuity ( $\bar{\rho}$ ), momentum ( $\bar{\rho}\bar{\mathbf{u}}$ ) and the magnetic field ( $\bar{\mathbf{B}}$ ) in our LB-LES-MHD model, after considerable algebra, are (with summation over repeated Greek subscripts)

$$\partial_t \bar{\rho} + \nabla \cdot \bar{\rho} \bar{\mathbf{u}} = 0, \quad \nabla \cdot \bar{\mathbf{B}} = 0 \quad (8.42a)$$

$$\begin{aligned} \partial_t (\bar{\rho} \bar{\mathbf{u}}) + \nabla \cdot \left( \frac{\bar{\rho} \bar{\rho} \bar{\mathbf{u}}}{\bar{\rho}} \right) &= -\nabla \bar{p} + \nabla \cdot (\bar{\mathbf{B}} \bar{\mathbf{B}}) - \frac{1}{2} \nabla (\bar{\mathbf{B}} \cdot \bar{\mathbf{B}}) + \left( \xi + \frac{1}{3} \nu \right) \nabla (\nabla \cdot \bar{\rho} \bar{\mathbf{u}}) + \nu \nabla^2 \bar{\rho} \bar{\mathbf{u}} \\ -\nabla \cdot \left\{ \frac{6\nu}{6\nu+1} \frac{\Delta^2}{12\bar{\rho}} \left[ (\partial_\beta (\bar{\rho} \bar{\mathbf{u}})) (\partial_\beta (\bar{\rho} \bar{\mathbf{u}})) - \frac{\partial_\beta \bar{p}}{\bar{p}} \left( \bar{\rho} \bar{\mathbf{u}} (\partial_\beta (\bar{\rho} \bar{\mathbf{u}})) + (\partial_\beta (\bar{\rho} \bar{\mathbf{u}})) \bar{\rho} \bar{\mathbf{u}} - \bar{\rho} \bar{\mathbf{u}} \bar{\rho} \bar{\mathbf{u}} \frac{\partial_\beta \bar{p}}{\bar{p}} \right) \right] \right\} \\ -\nabla \cdot \left\{ \left( \frac{s_4}{4} + \frac{s_7}{20} - \frac{3s_8}{10} \right) \frac{\Delta^2}{12\bar{\rho}} \left[ (\partial_\beta (\bar{\rho} \bar{\mathbf{u}})) \cdot (\partial_\beta (\bar{\rho} \bar{\mathbf{u}})) - \frac{\partial_\beta \bar{p}}{\bar{p}} \left( 2 \bar{\rho} \bar{\mathbf{u}} \cdot (\partial_\beta (\bar{\rho} \bar{\mathbf{u}})) - \bar{\rho} \bar{\mathbf{u}} \cdot \bar{\rho} \bar{\mathbf{u}} \frac{\partial_\beta \bar{p}}{\bar{p}} \right) \right] \right\} \\ -\frac{6\nu}{6\nu+1} \frac{\Delta^2}{12} \left\{ \frac{1}{2} \nabla [(\partial_\beta \bar{\mathbf{B}}) \cdot (\partial_\beta \bar{\mathbf{B}})] - \nabla \cdot [(\partial_\beta \bar{\mathbf{B}}) (\partial_\beta \bar{\mathbf{B}})] \right\} \end{aligned} \quad (8.42b)$$

$$\begin{aligned} \partial_t \bar{\mathbf{B}} &= \nabla \times \left( \frac{\bar{\rho} \bar{\mathbf{u}} \times \bar{\mathbf{B}}}{\bar{\rho}} \right) + \eta \nabla^2 \bar{\mathbf{B}} + \nabla \times \left[ \frac{\Delta^2}{12\bar{\rho}} \frac{6\eta}{6\eta+1} \{ (\partial_\beta (\bar{\rho} \bar{\mathbf{u}})) \times (\partial_\beta \bar{\mathbf{B}}) \right. \\ &\quad \left. - \frac{\partial_\beta \bar{p}}{\bar{p}} \left( (\bar{\rho} \bar{\mathbf{u}}) \times (\partial_\beta \bar{\mathbf{B}}) + (\partial_\beta (\bar{\rho} \bar{\mathbf{u}})) \times \bar{\mathbf{B}} - \frac{(\partial_\beta \bar{p})}{\bar{p}} (\bar{\rho} \bar{\mathbf{u}}) \times \bar{\mathbf{B}} \right) \right]. \end{aligned} \quad (8.42c)$$

In this isothermal model, the equation of state connecting the pressure to the density is  $p = \rho c_s^2 = \frac{\rho}{3}$ , in lattice units ( $c_s$  is the sound speed). The transport coefficients (shear viscosity  $\nu$ , bulk viscosity  $\xi$  and resistivity  $\eta$ ) are determined from the LB-MRT relaxation rates:

$$\nu = \frac{1}{3s_3} - \frac{1}{6} = \frac{1}{3s_4} - \frac{1}{6} \quad (8.43)$$

$$\xi = -\frac{1}{9} - \frac{1}{9s_4} - \frac{1}{15s_7} + \frac{2}{5s_8} \quad (8.44)$$

$$\eta = \frac{1}{3s_m} - \frac{1}{6} \quad (8.45)$$

## 8.4 Preparing LES for Simulation

The LES model has now been derived by first filtering the lattice Boltzmann (LB) representation of MHD [13, 17, 18, 45–49] after which one applies the Chapman-Enskog

limits to recover the final LES-MHD fluid equations, in essence extending to MHD the 2D Navier-Stokes (NS) LES-LB model of Ansumali *et. al.* [4]. A technical difficulty with the Ansumali *et. al.* model is that in 2D NS there is an inverse energy cascade to large spatial scales thereby rendering subgrid modeling non-essential. In 2D MHD, however, the energy cascades to small spatial scales as in 3D - and so makes it attractive to perform the LES-LB-MHD simulations in which there can be a substantial amount of excited subgrid modes. Here we present some preliminary LES-LB-MHD simulations of our model and compare the results with some direct numerical simulations (DNS). As Ansumali *et. al.* [4] did not perform any simulations on their LES-LB-NS model, these are the first such LES-LB simulations when one has first filtered the underlying LB representation, followed by the conventional small Knudsen number expansion.

If one wished to restrict oneself to a single relaxation (SRT) LB model for the particle distribution function, then  $(\frac{s_4}{4} + \frac{s_7}{20} - \frac{3s_8}{10}) = 0$  since  $s_3 = s_4 = s_5 = s_6 = s_7 = s_8$ , and the subgrid  $\nabla \cdot (\overline{\rho \mathbf{u}} \cdot \overline{\rho \mathbf{u}})$  terms of order  $\Delta^2$  cancel. It should also be noted that one recovers the standard (quasi-incompressible) LB model for the particle distribution function by setting  $\xi = \frac{2}{3}\nu$  with  $\Delta \rightarrow 0$ .

The order  $\Delta^2$ -terms in the above equations are the new subgrid closure terms determined by the LES-LB-MHD. We just note  $\nabla \cdot \overline{\mathbf{B}} = 0$  is maintained automatically to machine accuracy [13]. The nonlinearities in the MHD equations are recovered by polynomial powers of  $\mathbf{u}$  and  $\mathbf{B}$  in the relaxation distribution functions.

This model has some similarity to the Clark model [37] because we have also expanded the closure term over a small filter width. The main difference is that Clark applies an ad-hoc closure approximation for the eddy viscosity, however our method approaches the problem from kinematic first principles to solve for the eddy viscosity leaving only the filter width as a variable. While Vreman *et al.* [38] suggests that all LES based on Clark model will be inaccurate, Girimaji [43] also suggests that the availability of nonhydrodynamic

variables can potentially lead to a more accurate closure in LBM-LES.

We now summarize our computational LB-LES-MHD model that underlies Eqs. (8.42). For the 2D MHD simulation, we consider an LB model with 9-bit lattice

$$(\partial_t + \partial_\gamma c_{\gamma i}) f_i = \sum_j s'_{ij} (f_j^{\text{eq}} - f_j), \quad i = 0 \dots 8 \quad (8.46)$$

$$(\partial_t + \partial_\gamma c_{\gamma i}) \vec{g}_i = s'_m (\vec{g}_i^{\text{eq}} - \vec{g}_i), \quad i = 0 \dots 8 \quad (8.47)$$

with the moments  $\sum_i f_i = \rho$ ,  $\sum_i f_i \vec{c}_i = \rho \vec{u}$ , and  $\sum_k \vec{g}_k = \vec{B}$ . Here the summation convention is employed on the vector nature of the fields (using Greek indices) while for Roman indices, correspond to the corresponding lattice vectors for the kinetic velocities  $\vec{c}_i$ , there is no implicitly implied summation. The lattice is D2Q9 (Fig. 3.1) which are just the axes and diagonals of a square (along with the rest particle  $i = 0$ ).  $s'_{ij}$  are the MRT collisional relaxation rate tensor for the  $f_i$  while the SRT  $s'_m$  is the collisional relaxation rate for  $\vec{g}_i$ . These kinetic relaxation rates determine the MHD viscosity and resistivity transport coefficients. (Of course, more sophisticated LB models can be formed by MRT on the  $\vec{g}_k$  equations, but for this first reported LB-LES-MHD simulation we will restrict ourselves to the simpler SRT model)

A convenient choice of the relaxation distribution functions, will under Chapman-Enskog, yield the MHD equations

$$f_i^{\text{eq}} = w_i \rho \left[ 1 + 3 (\vec{c}_i \cdot \vec{u}) + \frac{9}{2} (\vec{c}_i \cdot \vec{u})^2 - \frac{3}{2} \vec{u}^2 \right] + \frac{9}{2} w_i \left[ \frac{1}{2} \vec{B}^2 \vec{c}_i^2 - (\vec{B} \cdot \vec{c}_i)^2 \right], \quad i = 0, \dots, 8 \quad (8.48)$$

$$\vec{g}_i^{\text{eq}} = w'_i \left[ \vec{B} + 3 \left\{ (\vec{c}_i \cdot \vec{u}) \vec{B} - (\vec{c}_i \cdot \vec{B}) \vec{u} \right\} \right], \quad i = 0, \dots, 8 \quad (8.49)$$

where the  $w'$ s are appropriate lattice weights. In the operator-splitting solution method of

collide-stream, it is most convenient to perform the collision step in moment-space (because of collisional invariants of the zeroth and 1st moment of  $f_i$ , and the zeroth moment of  $\vec{g}_i$ ), while the streaming is optimally done in the  $(f_i, \vec{g}_i)$ -space. Moment space  $(M_i, \vec{N}_i)$  is defined by

$$M_i = \sum_{j=0}^8 T_{ij} f_j \quad , \quad \vec{N}_i = \sum_{q=0}^8 T_{m,iq} \vec{g}_q \quad (8.50)$$

with the 1-1 constant transformation matrices,  $T$  given by Eq. (8.23) and  $T_m$  given by

$$T_m = \begin{pmatrix} \mathbf{1} \\ c_x \\ c_y \\ c_x c_y \\ c_x^2 \\ c_y^2 \\ c_x^2 c_y \\ c_x c_y^2 \\ c_x^2 c_y^2 \end{pmatrix} = \begin{pmatrix} 1 & 1 & 1 & 1 & 1 & 1 & 1 & 1 & 1 \\ 0 & 1 & 0 & -1 & 0 & 1 & -1 & -1 & 1 \\ 0 & 0 & 1 & 0 & -1 & 1 & 1 & -1 & -1 \\ 0 & 0 & 0 & 0 & 0 & 1 & -1 & 1 & -1 \\ 0 & 1 & 0 & 1 & 0 & 1 & 1 & 1 & 1 \\ 0 & 0 & 1 & 0 & 1 & 1 & 1 & 1 & 1 \\ 0 & 0 & 0 & 0 & 0 & 1 & 1 & -1 & -1 \\ 0 & 0 & 0 & 0 & 0 & 1 & -1 & -1 & 1 \\ 0 & 0 & 0 & 0 & 0 & 1 & 1 & 1 & 1 \end{pmatrix} \quad (8.51)$$

The  $x$  and  $y$  components of the 9-dimensional lattice vectors are

$$c_x = \{0, 1, 0, -1, 0, 1, -1, -1, 1\} \quad , \quad c_y = \{0, 0, 1, 0, -1, 1, 1, -1, -1\} \quad (8.52)$$

In terms of conserved moments, we can write

$$\begin{aligned}
M_0^{\text{eq}} = M_0 = \rho & & M_3^{\text{eq}} = \frac{\rho u_x \rho u_y}{\rho} - B_x B_y & & M_6^{\text{eq}} = -\rho u_y \\
M_1^{\text{eq}} = M_1 = \rho u_x & & M_4^{\text{eq}} = \frac{(\rho u_x)^2 - (\rho u_y)^2}{\rho} - B_x^2 + B_y^2 & & M_7^{\text{eq}} = -3 \frac{(\rho u_x)^2 + (\rho u_y)^2}{\rho} \\
M_2^{\text{eq}} = M_2 = \rho u_y & & M_5^{\text{eq}} = -\rho u_x & & M_8^{\text{eq}} = \frac{5}{3} \rho - 3 \frac{(\rho u_x)^2 + (\rho u_y)^2}{\rho}
\end{aligned} \tag{8.53}$$

$$\begin{aligned}
N_{\alpha 0}^{\text{eq}} = N_{\alpha 0} = B_\alpha & & N_{\alpha 3}^{\text{eq}} = 0 & & N_{\alpha 6}^{\text{eq}} = \frac{1}{3} (\rho u_y B_\alpha - \rho u_\alpha B_y) \\
N_{\alpha 1}^{\text{eq}} = \rho u_x B_\alpha - \rho u_\alpha B_x & & N_{\alpha 4}^{\text{eq}} = \frac{B_\alpha}{3} & & N_{\alpha 7}^{\text{eq}} = \frac{1}{3} (\rho u_x B_\alpha - \rho u_\alpha B_x) \\
N_{\alpha 2}^{\text{eq}} = \rho u_y B_\alpha - \rho u_\alpha B_y & & N_{\alpha 5}^{\text{eq}} = \frac{B_\alpha}{3} & & N_{\alpha 8}^{\text{eq}} = \frac{B_\alpha}{9}
\end{aligned} \tag{8.54}$$

### 8.4.1 Filtering LB

In applying filtering to the LB Eqs. (8.46) and (8.47), only the nonlinear terms in the relaxation distributions, Eqs. (8.48) and (8.49), require further attention. Moreover since collisions are performed in moment space, we need first to transform from  $f^{\text{eq}}$ ,  $\vec{g}^{\text{eq}}$  to  $M^{(\text{eq})}$ ,  $\vec{N}^{(\text{eq})}$  and then apply filtering in terms of the filtered collisional invariants  $\bar{M}_0, \bar{M}_1, \bar{M}_2, \bar{N}_{x0}, \bar{N}_{y0}$  using the perturbations in the filter width  $\Delta$  from equations (8.16) and (8.17). This produces a filtered moment equilibrium which can now be written in the same form as in Eq. (8.31)

$$\bar{M}_i^{(\text{eq})} = M_i^{(\text{eq})} \left( \bar{M}_0, \bar{M}_1, \bar{M}_2, \bar{N}_{x0}, \bar{N}_{y0} \right) + \Delta^2 \bar{M}_i^{(\Delta)} \quad i = 0 \dots 8 \tag{8.55}$$

where the  $O(\Delta^2)$  term arises from the nonlinearities. In particular for the  $\overline{M}_3^{(\text{eq})}$  term, the equilibrium for the third moment in the simulation's collision step would be defined as

$$\begin{aligned} \overline{M}_3^{(\text{eq})} &= \frac{\overline{\rho u_x \rho u_y}}{\overline{\rho}} - \overline{B_x} \overline{B_y} \\ &+ \frac{\Delta^2}{12 \overline{\rho}} \left[ (\partial_\beta \overline{\rho u_x}) (\partial_\beta \overline{\rho u_y}) - \frac{(\partial_\beta \overline{\rho})}{\overline{\rho}} \left( \overline{\rho u_x} (\partial_\beta \overline{\rho u_y}) + \overline{\rho u_y} (\partial_\beta \overline{\rho u_x}) - \frac{\overline{\rho u_x \rho u_y} (\partial_\beta \overline{\rho})}{\overline{\rho}} \right) \right] \\ &- \frac{\Delta^2}{12} \left( \partial_\beta \overline{B_x} \right) \left( \partial_\beta \overline{B_y} \right) + \mathcal{O}(\Delta^4) . \end{aligned} \tag{8.56}$$

just as in Eq. (8.30). Similar definitions would exist for the other filtered equilibrium moments. These new definitions for the equilibrium allow the LES-LB-MHD model to be simulated.

## 8.5 LES-LB-MHD Simulation

The filtered LB equations are now solved, with streaming performed in distribution space and collisions in moment space. As this is the first simulation on the LB-filtered-LES approach, a significant number of simplifications have been made. The first thing is to restrict the evolution of the filtered scalar distribution function to an SRT collision operator. In this case the relaxation rates  $s_i$  are all equal so that the 3rd term in Eq. (8.42b) is automatically zero. Moreover since nearly all LB simulations are quasi-incompressible at the fluid level, the (filtered) density gradients in the moment representation of the collision operator are neglected. Thus, for example,  $\overline{M}_3^{(\text{eq})}$  is now approximated in simulation by

$$\begin{aligned} \overline{M}_3^{(\text{eq})} &= \frac{\overline{\rho u_x \rho u_y}}{\overline{\rho}} - \overline{B_x} \overline{B_y} \\ &+ \frac{\Delta^2}{12 \overline{\rho}} (\partial_\beta \overline{\rho u_x}) (\partial_\beta \overline{\rho u_y}) - \frac{\Delta^2}{12} \left( \partial_\beta \overline{B_x} \right) \left( \partial_\beta \overline{B_y} \right) + \mathcal{O}(\Delta^4) . \end{aligned} \tag{8.57}$$

Also, since the last term in Eq. (8.42c) is dependent on the filtered density gradient, its effects at the filtered MHD level will not be significant when the filtered LB system is coded.

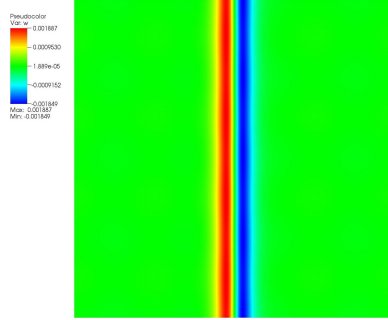


FIG. 8.2: **Initial vorticity profile of the LES-LB-MHD simulation:**  $U_y = U_0 \operatorname{sech}^2\left(\frac{2\pi}{L}4x\right)$  and  $B_y = B_0$  where  $B_0 = 0.005U_0$ . **Red** denotes positive vorticity, while **blue** denotes negative vorticity.

Many of the spatial derivatives in the filtered equilibria (as found in Eq. (8.57)) can be determined directly from strictly local, perturbed moments. An example procedure in finding a spatial derivative for this LES-LB-MHD algorithm from the local, perturbed moments can be found in Appendix B. There is a little subtlety in that not all the spatial derivatives in the filtered collision moments can be determined from local perturbed moments [13, 30]. This limitation is thought to arise from the low D2Q9 lattice. It is expected that on a D3Q27 lattice the linearly independent set of derivatives can be represented by the now larger number of local perturbed moments.

While the filtered LB equations are solved, resulting in the filtered LES MHD Eqs. (8.42), there is some similarity in the final MHD model with that of the “tensor diffusivity” model of Müller-Carati [29]. However it must be stressed that a first principles derivation of the eddy transport coefficients from a kinetic (LB) model is being performed while Muller-Carati propose an ad hoc scheme of minimizing the error between two filters at each time step in their determination of their model’s transport coefficients.



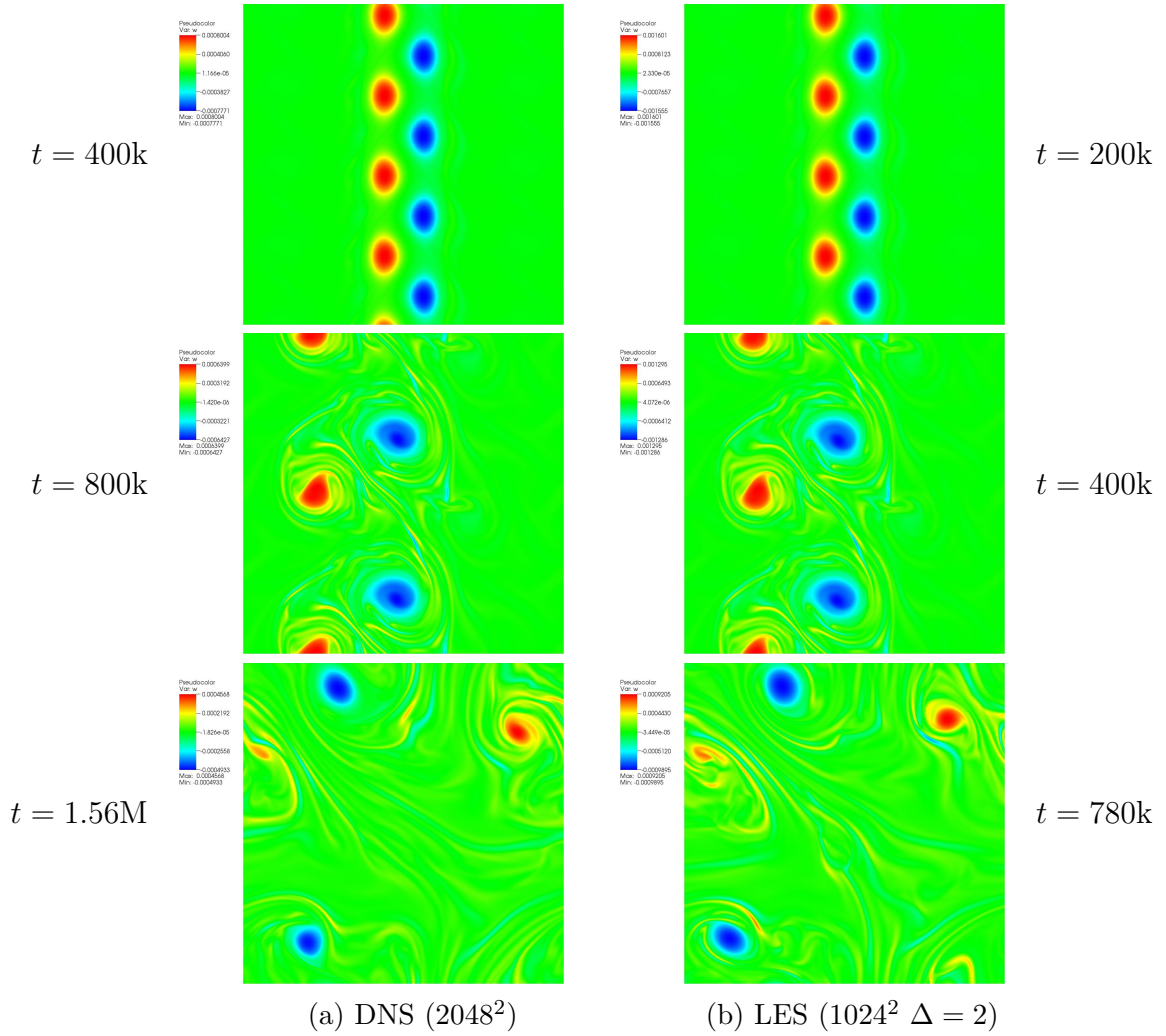


FIG. 8.3: Comparison of the vorticity evolution in the unstable magnetized KH jet between DNS and LES -LB-MHD simulations.

(a) On the left, the DNS simulation on grid =  $2048^2$ ;

(b) on the right, the LES simulation on grid =  $1024^2$  and  $\Delta = 2$ .

There is excellent agreement between DNS and LES simulations with time scaling  $t_{\text{DNS}} = 2t_{\text{LES}}$  due to the chosen grids.

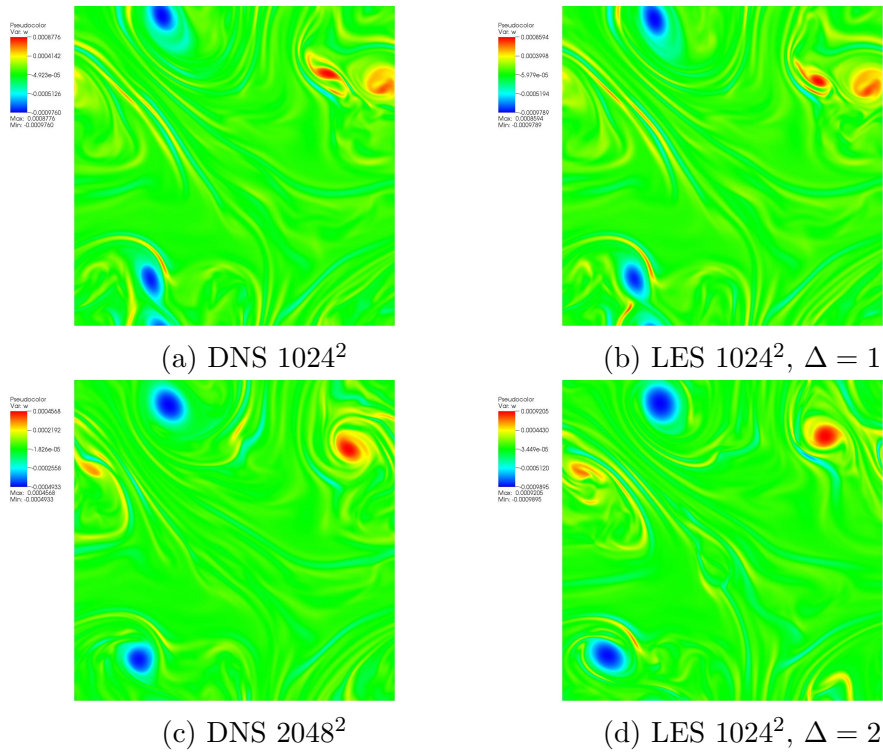


FIG. 8.4: **A late time vorticity snapshot comparison** between (a) DNS on grid =  $1024^2$  at  $t = 780k$ , (b) LES on grid =  $1024^2$  with  $\Delta = 1$ , at  $t = 780k$ , (c) DNS on grid =  $2048^2$  at  $t = 1.56M$ , and (d) LES on grid =  $1024^2$  at  $t = 780k$  but with filter width  $\Delta = 2$ .

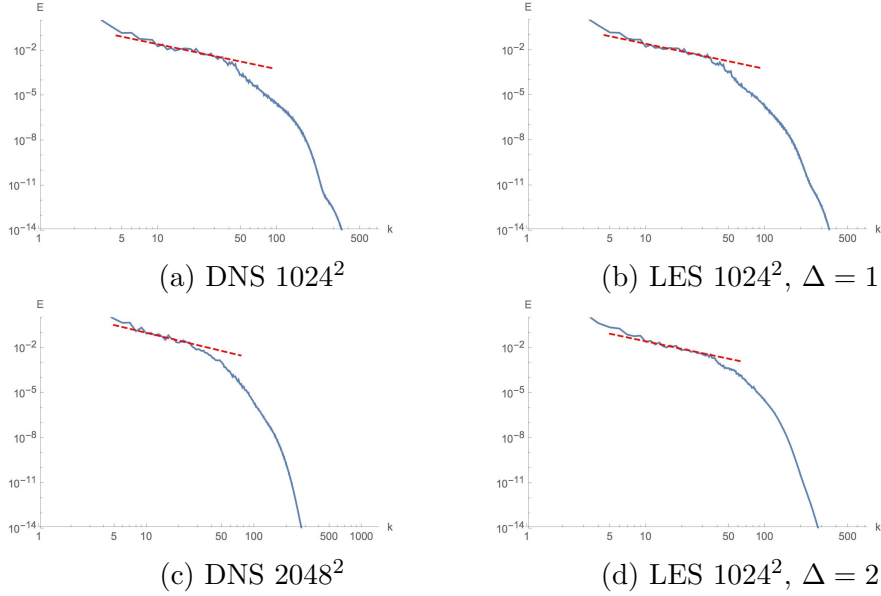


FIG. 8.5: **A late time spectral comparison** between (a) DNS on grid =  $1024^2$  with slope  $k^{-1.66}$  at  $t = 780k$ , (b) LES on grid =  $1024^2$  with  $\Delta = 1$  and slope  $k^{-1.66}$  at  $t = 780k$ , (c) DNS on grid =  $2048^2$  with slope  $k^{-1.71}$  at  $t = 1.56M$ , and (d) LES on grid =  $1024^2$  with slope  $k^{-1.66}$  at  $t = 780k$  but with filter width  $\Delta = 2$ .

The filtered LB equations are now evolved in time for the profile of a magnetized Kelvin-Helmholtz instability in a sufficiently weak magnetic field so that the 2D velocity jet is not stabilized [15]. The initial jet velocity profile is  $U_y = U_0 \operatorname{sech}^2\left(\frac{2\pi}{L}4x\right)$ . The corresponding vorticity is shown in Fig. 8.2. The initial Reynolds number is chosen to be  $\operatorname{Re} = U_0L/\nu = 50k = \text{const.}$ , with  $U_0 = 4.88 \times 10^{-2}$  and  $B_0 = 0.005U_0$ . The viscosity and resistivity on a grid of  $1024^2$  are  $\nu = \eta = 10^{-3}$  and scale with the grid to maintain a constant  $\operatorname{Re}$  and a constant magnetic Reynolds number  $U_0L/\eta$ . The initial perturbation to the fields are:  $U_y = 0.01U_0 \sin\left(\frac{2\pi}{L}4x\right)$ ,  $B_y = 0.01B_0 \sin\left(\frac{2\pi}{L}4x\right)$ ,  $U_x = 0.01U_0 \sin\left(\frac{2\pi}{L}4y\right)$ , and  $B_x = 0.01B_0 \sin\left(\frac{2\pi}{L}4y\right)$ . Note that initially  $\nabla \cdot \vec{B} = 0 = \nabla \cdot \vec{U}$ .

In Fig. 8.3, the evolution of vorticity in time is compared from DNS on a  $2048^2$  grid with that determined from the LES-LB-MHD model on a  $1024^2$  grid. The DNS simulations are determined by solving the direct unfiltered LB Eqs. (8.46) and (8.47). For constant Reynolds number simulations at different grid sizes, the kinematic viscosity is adjusted

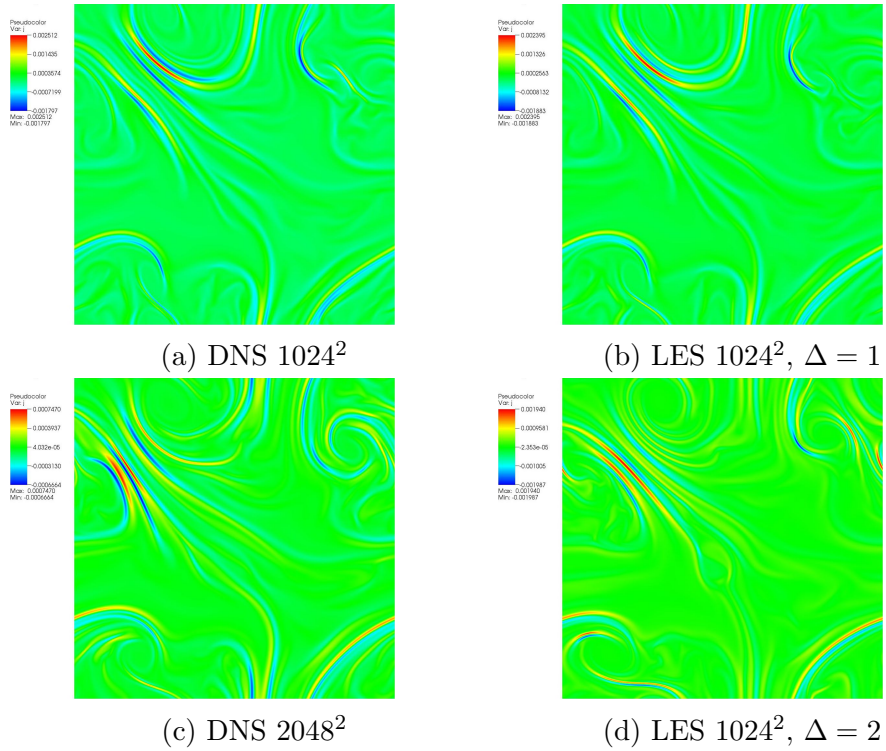


FIG. 8.6: **A late time snapshot current comparison** between (a) DNS on grid =  $1024^2$  at  $t = 780k$ , (b) LES on grid =  $1024^2$  with  $\Delta = 1$ , at  $t = 780k$ , (c) DNS on grid =  $2048^2$  at  $t = 1.56M$ , and (d) LES on grid =  $1024^2$  at  $t = 780k$  but with filter width  $\Delta = 2$ .

appropriately. Thus on halving the spatial grid, a DNS time step of  $2t_0$  corresponds to time step  $t_0$  in LES-LB-MHD.

At relatively early times the jet profile width slightly widens while within the vorticity layers the Kelvin-Helmholtz instability will break these layers into the familiar vortex street (Fig. 8.3). Since a weak magnetic field insufficient to stabilize the jet has been chosen, the vorticity streets break apart with like vortex-vortex reconnection (Fig. 8.3). There is very good agreement between DNS and LES-LB-MHD with filter width  $\Delta = 2$  (in lattice units) on a grid  $L/2$ .

Finally, the corresponding vorticity (Fig. 8.4), total energy spectrum (Fig. 8.5), and current (Fig. 8.6) plots are shown at  $t = 780k$  for simulations on  $1024^2$  grids and their counterparts on  $2048^2$  grids at time  $t = 1.56M$ . Four cases are considered: (a) DNS on  $1024^2$ , (b) filtered LB-LES-MHD on  $1024^2$  grid and small filter width,  $\Delta = 1$ , (c) DNS on  $2048^2$  and (d) filtered LES-LB-MHD on a  $1024^2$  grid but with filter width  $\Delta = 2$ . The effect of the filter width  $\Delta$  in our LB-LES-MHD model on the evolution of the vorticity is evident when comparing Fig. 8.4b to Fig. 8.4d - both in location and strength of the main vortices as well as in the fine grained small scale vorticity. As the filter width increases to  $\Delta = 2$  (Fig. 8.4d), there is stronger agreement now with the DNS (Fig. 8.4c) on  $L^2$  grid with the LES-LB-MHD filtered model on  $(L/2)^2$  grid. This shows that the subgrid terms are now influencing larger scales with some accuracy. The spectral plots (Fig. 8.5) are somewhat similar in all simulations with a very localized Kolmogorov energy spectrum. Presumably this is because the turbulence is limited and relatively weak. There appears to be good agreement in both the vorticity and current between DNS and LES-LB-MHD with  $\Delta = 2$  on half the grid.

## 8.6 Conclusion

Ansumali *et. al.* [4] have developed a rigorous closure model for 2D Navier-Stokes turbulence by first filtering the LB moment equations and then performing the long-wavelength long-time Knudsen expansion. The resulting closure model requires that the filter width  $\Delta \simeq \mathcal{O}(\text{Kn}^{1/2})$ . In principle their algorithm can be readily extended to the D3Q27 LB model of 3D Navier-Stokes turbulence where subgrid modeling is now critical. The Ansumali *et. al.* [4] LES-LB algorithm has been extended to 2D MHD by incorporating the vector distribution function LB representation of Dellar [13]. Because there is a direct energy cascade to small scales in 2D MHD, the model was restricted to 2D turbulence and the LB Navier-Stokes representation was extended to include multiple-collisional-relaxation rates. The development of a 3D LES-LB-MHD would be somewhat tedious but straightforward. In the new 2D-LES-LB-MHD model, the new subgrid-terms are written in vector form and one notes that they take the form of the Smagorinsky tensorial corrections. This is somewhat to be expected since Taylor expansions have been made in the filter width resulting in a similar closure term to the Clark model.

Some preliminary 2D filtered SRT LB-MHD simulation results have been presented based on an extension of ideas of Ansumali *et. al.* [4] that leads to a self-consistent LES-LB closure scheme based solely on expansions in the filter width  $\Delta$  and invoking the constraint that any eddy transport effects can only occur on the transport time scales. There is very good agreement between DNS and the LES-LB-MHD models. This warrants further investigation of other filters used in LES, as well as in dynamic subgridding commonly used in LES of Navier-Stokes turbulence. Finally, an exploration of the effects of MRT on this LES algorithm should be quite interesting as a somewhat unexpected term related to the gradient of a pressure appears in the subgrid viscosity. This term reveals that higher-order moments (not stress related) can have a first order effect on the subgrid viscosity

when MRT is employed. Given that this subgrid pressure term relies on the existence of higher order moments, it suggests that the extra parameters in lattice Boltzmann (ie. the distribution velocities/moments) are introducing new physics naturally absent from LES in computational fluid dynamics. It would be very interesting to see whether this new term enhances the LES accuracy or increases stability at even higher Reynold's flow. Further study could include how this term effects other, well-established LES approaches in computational fluid dynamics. These ideas are under consideration.

# CHAPTER 9

## Conclusion

As the future draws closer, plasmas can be modeled more accurately with better hardware and diligent research in modeling. Two new models have been presented which expand the previous capabilities of LB MHD. A partial entropic approach to MRT in LB MHD with the goal of increased stabilization will expand the domain applicability for the LB method. And an LES model for LB MHD will provide for more realistic, high accuracy problems to be modeled at a lower computational cost. These are the potentials of the new models but more work is still to be done in testing to find each model's relative accuracy and computational cost. Further work can also extend these models to 3D and determine whether local perturbed moments in 3D can fully describe every element of the fluid momentum gradient. This work will be under future consideration.



# APPENDIX A

## MRT Chapman-Enskog Expansion in LES MHD

A full derivation of the filtered MHD equations is provided in detail for the LES model found in chapter 8. Some equations are typed smaller so that they will fit on the page. The MHD LB equations are defined as

$$(\partial_t + \partial_\gamma e_{\gamma i}) f_i = \sum_j S_{ij} (f_i^{\text{eq}} - f_i) \quad (\text{A.1a})$$

$$(\partial_t + \partial_\gamma e_{\gamma i}) \vec{g}_i = \sum_j S_m (\vec{g}_i^{\text{eq}} - \vec{g}_i) \quad (\text{A.1b})$$

where  $S_{ij}$  is the fluid relaxation tensor in velocity space and  $S_m$  is magnetic relaxation tensor in velocity space.

Following the steps in section 3.4 to produce an  $\mathcal{O}(\varepsilon)$  and  $\mathcal{O}(\varepsilon^2)$  similar to (3.15) and

(3.18), the LB equations with separated scales appear as

$$\mathcal{O}(\varepsilon) : \partial_t^{(0)} f_i^{(0)} + \vec{c}_i \cdot \nabla f_i^{(0)} = -\frac{1}{\tau} f_i^{(1)} \quad (\text{A.2})$$

$$\mathcal{O}(\varepsilon^2) : \partial_t^{(1)} f_i^{(0)} + \left(1 - \frac{1}{2\tau}\right) \left(\partial_t^{(0)} + \vec{c}_i \cdot \nabla\right) f_i^{(1)} = -\frac{1}{\tau} f_i^{(2)} \quad (\text{A.3})$$

for the fluid and

$$\mathcal{O}(\varepsilon) : \partial_t^{(0)} \vec{g}_i^{(0)} + \vec{c}_i \cdot \nabla \vec{g}_i^{(0)} = -\frac{1}{\tau_g} \vec{g}_i^{(1)} \quad (\text{A.4})$$

$$\mathcal{O}(\varepsilon^2) : \partial_t^{(1)} \vec{g}_i^{(0)} + \left(1 - \frac{1}{2\tau_g}\right) \left(\partial_t^{(0)} + \vec{c}_i \cdot \nabla\right) \vec{g}_i^{(1)} = -\frac{1}{\tau_g} \vec{g}_i^{(2)} \quad (\text{A.5})$$

for the magnetic field.

The transformation matrix is defined for fluid in (8.23) and magnetic field (8.24). Using the transformation equation from (8.22), a change of basis in the LB equilibrium equations supplies a new set of equilibrium equations in the moment basis.

$$M_3^{(0)} = \frac{M_1 M_2}{M_0} - B_x B_y \quad (\text{A.6a})$$

$$M_4^{(0)} = \frac{M_1^2 - M_2^2}{M_0} - B_x^2 + B_y^2 \quad (\text{A.6b})$$

$$M_5^{(0)} = -M_1 \quad (\text{A.6c})$$

$$M_6^{(0)} = -M_2 \quad (\text{A.6d})$$

$$M_7^{(0)} = -3 \frac{M_1^2 + M_2^2}{M_0} \quad (\text{A.6e})$$

$$M_8^{(0)} = \frac{5}{3} M_0 - 3 \frac{M_1^2 + M_2^2}{M_0} \quad (\text{A.6f})$$

$$N_{x1}^{(0)} = N_{y2}^{(0)} = 0 \quad (\text{A.7a})$$

$$N_{y1}^{(0)} = \frac{M_1 B_y - M_2 B_x}{M_0} \quad (\text{A.7b})$$

$$N_{x2}^{(0)} = \frac{M_2 B_x - M_1 B_y}{M_0} \quad (\text{A.7c})$$

$$N_{x3}^{(0)} = N_{x4}^{(0)} = \frac{B_x}{3} \quad (\text{A.7d})$$

$$N_{y3}^{(0)} = N_{y4}^{(0)} = \frac{B_y}{3} \quad (\text{A.7e})$$

The filter of field products  $(XY)$  and  $(\frac{XY}{Z})$  are defined in equations (8.16) and (8.17) and repeated here

$$\overline{(XY)} = \bar{X}\bar{Y} + \frac{\Delta^2}{12} (\partial_\beta \bar{X}) (\partial_\beta \bar{Y}) + \mathcal{O}(\Delta^4) \quad (\text{A.8a})$$

$$\begin{aligned} \overline{\left(\frac{XY}{Z}\right)} &= \frac{\bar{X}\bar{Y}}{\bar{Z}} + \frac{\Delta^2}{12\bar{Z}} \left[ (\partial_\beta \bar{X}) (\partial_\beta \bar{Y}) \right. \\ &\quad \left. - \frac{(\partial_\beta \bar{Z})}{\bar{Z}} \left( \bar{X} (\partial_\beta \bar{Y}) + \bar{Y} (\partial_\beta \bar{X}) - \frac{\bar{X}\bar{Y} (\partial_\beta \bar{Z})}{\bar{Z}} \right) \right] + \mathcal{O}(\Delta^4) \end{aligned} \quad (\text{A.8b})$$

The filter equations can be directly applied to the previously found equilibrium mo-

ment equations (A.6) and (A.7) to become

$$\begin{aligned} \bar{M}_3^{(0)} = & \frac{\bar{M}_1 \bar{M}_2}{\bar{M}_0} - \bar{B}_x \bar{B}_y - \frac{\Delta^2}{12} (\partial_\beta \bar{B}_x) (\partial_\beta \bar{B}_y) + \frac{\Delta^2}{12 \bar{M}_0} \left[ (\partial_\beta \bar{M}_1) (\partial_\beta \bar{M}_2) \right. \\ & \left. - \frac{(\partial_\beta \bar{M}_0)}{\bar{M}_0} \left( \bar{M}_1 (\partial_\beta \bar{M}_2) + \bar{M}_2 (\partial_\beta \bar{M}_1) - \frac{\bar{M}_1 \bar{M}_2 (\partial_\beta \bar{M}_0)}{\bar{M}_0} \right) \right] \end{aligned} \quad (\text{A.9a})$$

$$\begin{aligned} \bar{M}_4^{(0)} = & \frac{\bar{M}_1^2 - \bar{M}_2^2}{\bar{M}_0} - \bar{B}_x^2 + \bar{B}_y^2 - \frac{\Delta^2}{12} \left[ (\partial_\beta \bar{B}_x)^2 - (\partial_\beta \bar{B}_y)^2 \right] \\ & + \frac{\Delta^2}{12 \bar{M}_0} \left[ (\partial_\beta \bar{M}_1)^2 - (\partial_\beta \bar{M}_2)^2 \right. \\ & \left. - \frac{(\partial_\beta \bar{M}_0)}{\bar{M}_0} \left( 2\bar{M}_1 (\partial_\beta \bar{M}_1) - 2\bar{M}_2 (\partial_\beta \bar{M}_2) - \frac{(\bar{M}_1^2 - \bar{M}_2^2) (\partial_\beta \bar{M}_0)}{\bar{M}_0} \right) \right] \end{aligned} \quad (\text{A.9b})$$

$$\bar{M}_5^{(0)} = -\bar{M}_1 \quad (\text{A.9c})$$

$$\bar{M}_6^{(0)} = -\bar{M}_2 \quad (\text{A.9d})$$

$$\begin{aligned} \bar{M}_7^{(0)} = & -3 \left\{ \frac{\bar{M}_1^2 + \bar{M}_2^2}{\bar{M}_0} + \frac{\Delta^2}{12 \bar{M}_0} \left[ (\partial_\beta \bar{M}_1)^2 + (\partial_\beta \bar{M}_2)^2 \right. \right. \\ & \left. \left. - \frac{(\partial_\beta \bar{M}_0)}{\bar{M}_0} \left( 2\bar{M}_1 (\partial_\beta \bar{M}_1) + 2\bar{M}_2 (\partial_\beta \bar{M}_2) - \frac{(\bar{M}_1^2 + \bar{M}_2^2) (\partial_\beta \bar{M}_0)}{\bar{M}_0} \right) \right] \right\} \end{aligned} \quad (\text{A.9e})$$

$$\begin{aligned} \bar{M}_8^{(0)} = & \frac{5}{3} \bar{M}_0 - 3 \left\{ \frac{\bar{M}_1^2 + \bar{M}_2^2}{\bar{M}_0} + \frac{\Delta^2}{12 \bar{M}_0} \left[ (\partial_\beta \bar{M}_1)^2 + (\partial_\beta \bar{M}_2)^2 \right. \right. \\ & \left. \left. - \frac{(\partial_\beta \bar{M}_0)}{\bar{M}_0} \left( 2\bar{M}_1 (\partial_\beta \bar{M}_1) + 2\bar{M}_2 (\partial_\beta \bar{M}_2) - \frac{(\bar{M}_1^2 + \bar{M}_2^2) (\partial_\beta \bar{M}_0)}{\bar{M}_0} \right) \right] \right\} \end{aligned} \quad (\text{A.9f})$$

$$\bar{N}_{x1}^{(0)} = \bar{N}_{y2}^{(0)} = 0 \quad (\text{A.10a})$$

$$\begin{aligned} \bar{N}_{y1}^{(0)} = & \frac{\bar{M}_1 \bar{B}_y - \bar{M}_2 \bar{B}_x}{\bar{M}_0} + \frac{\Delta^2}{12\bar{M}_0} \left[ (\partial_\beta \bar{M}_1) (\partial_\beta \bar{B}_y) - (\partial_\beta \bar{M}_2) (\partial_\beta \bar{B}_x) \right. \\ & - \frac{(\partial_\beta \bar{M}_0)}{\bar{M}_0} \left( \bar{M}_1 (\partial_\beta \bar{B}_y) + \bar{B}_y (\partial_\beta \bar{M}_1) - \bar{M}_2 (\partial_\beta \bar{B}_x) - \bar{B}_x (\partial_\beta \bar{M}_2) \right) \\ & \left. - \frac{(\bar{M}_1 \bar{B}_y - \bar{M}_2 \bar{B}_x) (\partial_\beta \bar{M}_0)}{\bar{M}_0} \right] \end{aligned} \quad (\text{A.10b})$$

$$\begin{aligned} \bar{N}_{x2}^{(0)} = & \frac{\bar{M}_2 \bar{B}_x - \bar{M}_1 \bar{B}_y}{\bar{M}_0} + \frac{\Delta^2}{12\bar{M}_0} \left[ (\partial_\beta \bar{M}_2) (\partial_\beta \bar{B}_x) - (\partial_\beta \bar{M}_1) (\partial_\beta \bar{B}_y) \right. \\ & - \frac{(\partial_\beta \bar{M}_0)}{\bar{M}_0} \left( \bar{M}_2 (\partial_\beta \bar{B}_x) + \bar{B}_x (\partial_\beta \bar{M}_2) - \bar{M}_1 (\partial_\beta \bar{B}_y) - \bar{B}_y (\partial_\beta \bar{M}_1) \right) \\ & \left. - \frac{(\bar{M}_2 \bar{B}_x - \bar{M}_1 \bar{B}_y) (\partial_\beta \bar{M}_0)}{\bar{M}_0} \right] \end{aligned} \quad (\text{A.10c})$$

$$\bar{N}_{x3}^{(0)} = \bar{N}_{x4}^{(0)} = \frac{\bar{B}_x}{3} \quad (\text{A.10d})$$

$$\bar{N}_{y3}^{(0)} = \bar{N}_{y4}^{(0)} = \frac{\bar{B}_y}{3} \quad (\text{A.10e})$$

Next, determine the lower order time derivative of non-conserved moments by using the chain rule on the non-conserved filtered equilibrium equations (A.6) (A.7).

$$\begin{aligned} \partial_t^{(0)} \bar{M}_i^{(0)} (\bar{M}_1, \bar{M}_2, \bar{M}_3, \bar{B}_x, \bar{B}_y) = \\ \frac{\partial \bar{M}_i^{(0)}}{\partial \bar{M}_0} \partial_t^{(0)} \bar{M}_0 + \frac{\partial \bar{M}_i^{(0)}}{\partial \bar{M}_1} \partial_t^{(0)} \bar{M}_1 + \frac{\partial \bar{M}_i^{(0)}}{\partial \bar{M}_2} \partial_t^{(0)} \bar{M}_2 + \frac{\partial \bar{M}_i^{(0)}}{\partial \bar{B}_x} \partial_t^{(0)} \bar{B}_x + \frac{\partial \bar{M}_i^{(0)}}{\partial \bar{B}_y} \partial_t^{(0)} \bar{B}_y \end{aligned} \quad (\text{A.11a})$$

$$\partial_t^{(0)} \bar{M}_3^{(0)} = \partial_t^{(0)} \left( \frac{\bar{M}_1 \bar{M}_2}{\bar{M}_0} - \bar{B}_x \bar{B}_y + \mathcal{O}(\varepsilon^2) \right) \rightarrow 0 \quad (\text{A.12a})$$

$$\partial_t^{(0)} \bar{M}_4^{(0)} = \partial_t^{(0)} \left( \frac{\bar{M}_1^2 - \bar{M}_2^2}{\bar{M}_0} - \bar{B}_x^2 + \bar{B}_y^2 + \mathcal{O}(\varepsilon^2) \right) \rightarrow 0 \quad (\text{A.12b})$$

$$\partial_t^{(0)} \bar{M}_5^{(0)} = -\partial_t^{(0)} \bar{M}_1 = \partial_x \left( \frac{\bar{M}_0}{3} + \frac{\bar{M}_1^2}{\bar{M}_0} - \frac{\bar{B}_x^2}{2} + \frac{\bar{B}_y^2}{2} \right) + \partial_y \left( \frac{\bar{M}_1 \bar{M}_2}{\bar{M}_0} - \bar{B}_x \bar{B}_y \right) \quad (\text{A.12c})$$

$$\partial_t^{(0)} \bar{M}_6^{(0)} = -\partial_t^{(0)} \bar{M}_2 = \partial_x \left( \frac{\bar{M}_1 \bar{M}_2}{\bar{M}_0} - \bar{B}_x \bar{B}_y \right) + \partial_y \left( \frac{\bar{M}_0}{3} + \frac{\bar{M}_2^2}{\bar{M}_0} + \frac{\bar{B}_x^2}{2} - \frac{\bar{B}_y^2}{2} \right) \quad (\text{A.12d})$$

$$\partial_t^{(0)} \bar{M}_7^{(0)} = -3\partial_t^{(0)} \left( \frac{\bar{M}_1^2 + \bar{M}_2^2}{\bar{M}_0} + \mathcal{O}(\varepsilon^2) \right) \rightarrow 0 \quad (\text{A.12e})$$

$$\partial_t^{(0)} \bar{M}_8^{(0)} = -\frac{1}{3}\partial_t^{(0)} \left( 5\bar{M}_0 - 9\frac{\bar{M}_1^2 + \bar{M}_2^2}{\bar{M}_0} \right) \rightarrow 0 \quad (\text{A.12f})$$

$$\partial_t^{(0)} \bar{N}_{x1}^{(0)} = \partial_t^{(0)} \bar{N}_{y2}^{(0)} = 0 \quad (\text{A.13a})$$

$$\partial_t^{(0)} \bar{N}_{y1}^{(0)} = \partial_t^{(0)} \left( \frac{\bar{M}_1 \bar{B}_y - \bar{M}_2 \bar{B}_x}{\bar{M}_0} + \mathcal{O}(\varepsilon^2) \right) \rightarrow 0 \quad (\text{A.13b})$$

$$\partial_t^{(0)} \bar{N}_{x2}^{(0)} = \partial_t^{(0)} \left( \frac{\bar{M}_2 \bar{B}_x - \bar{M}_1 \bar{B}_y}{\bar{M}_0} + \mathcal{O}(\varepsilon^2) \right) \rightarrow 0 \quad (\text{A.13c})$$

$$\partial_t^{(0)} \bar{N}_{x3}^{(0)} = \partial_t^{(0)} \bar{N}_{x4}^{(0)} = \frac{1}{3}\partial_t^{(0)} \bar{B}_x = -\frac{1}{3}\partial_y \left( \frac{\bar{M}_2 \bar{B}_x - \bar{M}_1 \bar{B}_y}{\bar{M}_0} \right) \quad (\text{A.13d})$$

$$\partial_t^{(0)} \bar{N}_{y3}^{(0)} = \partial_t^{(0)} \bar{N}_{y4}^{(0)} = \frac{1}{3}\partial_t^{(0)} \bar{B}_y = -\frac{1}{3}\partial_x \left( \frac{\bar{M}_1 \bar{B}_y - \bar{M}_2 \bar{B}_x}{\bar{M}_0} \right) \quad (\text{A.13e})$$

The filtered evolution equations at order  $\mathcal{O}(\varepsilon)$  (A.2 and A.4) can be written by transforming the LB evolution equations at  $\mathcal{O}(\varepsilon)$  to a set of moment equations. Filtered Evo-

lution equations at order  $\mathcal{O}(\varepsilon)$ .

$$\partial_t^{(0)} \bar{M}_0 + \partial_x \bar{M}_1^{(0)} + \partial_y \bar{M}_2^{(0)} = 0 \quad (\text{A.14a})$$

$$\partial_t^{(0)} \bar{M}_1 + \partial_x \left( \frac{\bar{M}_0}{3} + \frac{\bar{M}_1^2}{\bar{M}_0} - \frac{\bar{B}_x^2}{2} + \frac{\bar{B}_y^2}{2} \right) + \partial_y \left( \frac{\bar{M}_1 \bar{M}_2}{\bar{M}_0} - \bar{B}_x \bar{B}_y \right) = 0 \quad (\text{A.14b})$$

$$\partial_t^{(0)} \bar{M}_2 + \partial_x \left( \frac{\bar{M}_1 \bar{M}_2}{\bar{M}_0} - \bar{B}_x \bar{B}_y \right) + \partial_y \left( \frac{\bar{M}_0}{3} + \frac{\bar{M}_2^2}{\bar{M}_0} + \frac{\bar{B}_x^2}{2} - \frac{\bar{B}_y^2}{2} \right) = 0 \quad (\text{A.14c})$$

$$\begin{aligned} \partial_t^{(0)} \bar{M}_3^{(0)} + \frac{1}{3} \partial_x \bar{M}_2 + \frac{1}{3} \partial_y \bar{M}_1 = & -s_3 \bar{M}_3^{(1)} + \frac{\Delta^2}{12 \bar{M}_0} \left[ (\partial_\beta \bar{M}_1) (\partial_\beta \bar{M}_2) \right. \\ & \left. - \frac{(\partial_\beta \bar{M}_0)}{\bar{M}_0} \left( \bar{M}_1 (\partial_\beta \bar{M}_2) + \bar{M}_2 (\partial_\beta \bar{M}_1) - \frac{\bar{M}_1 \bar{M}_2 (\partial_\beta \bar{M}_0)}{\bar{M}_0} \right) \right] \end{aligned} \quad (\text{A.15a})$$

$$\begin{aligned} \partial_t^{(0)} \bar{M}_4^{(0)} + \frac{2}{3} \partial_x \bar{M}_1 - \frac{2}{3} \partial_y \bar{M}_2 = & -s_4 \bar{M}_4^{(1)} + \frac{\Delta^2}{12 \bar{M}_0} \left[ (\partial_\beta \bar{M}_1)^2 - (\partial_\beta \bar{M}_2)^2 \right. \\ & \left. - \frac{(\partial_\beta \bar{M}_0)}{\bar{M}_0} \left( 2 \bar{M}_1 (\partial_\beta \bar{M}_1) - 2 \bar{M}_2 (\partial_\beta \bar{M}_2) - \frac{(\bar{M}_1^2 - \bar{M}_2^2) (\partial_\beta \bar{M}_0)}{\bar{M}_0} \right) \right] \\ & - \frac{\Delta^2}{12} \left[ (\partial_\beta \bar{B}_x)^2 - (\partial_\beta \bar{B}_y)^2 \right] \end{aligned} \quad (\text{A.15b})$$

$$\partial_t^{(0)} \bar{M}_5^{(0)} - \partial_x \left( \frac{\bar{M}_0}{3} + \frac{\bar{M}_1^2 - \bar{M}_2^2}{\bar{M}_0} - \bar{B}_x^2 + \bar{B}_y^2 \right) + \partial_y \left( \frac{\bar{M}_1 \bar{M}_2}{\bar{M}_0} - \bar{B}_x \bar{B}_y \right) = -s_5 \bar{M}_5^{(1)} \quad (\text{A.15c})$$

$$\partial_t^{(0)} \bar{M}_6^{(0)} + \partial_x \left( \frac{\bar{M}_1 \bar{M}_2}{\bar{M}_0} - \bar{B}_x \bar{B}_y \right) - \partial_y \left( \frac{\bar{M}_0}{3} + \frac{\bar{M}_2^2 - \bar{M}_1^2}{\bar{M}_0} + \bar{B}_x^2 - \bar{B}_y^2 \right) = -s_6 \bar{M}_6^{(1)} \quad (\text{A.15d})$$

$$\begin{aligned} \partial_t^{(0)} \bar{M}_7^{(0)} - 2 \partial_x \bar{M}_1 - 2 \partial_y \bar{M}_2 = & -s_7 \bar{M}_7^{(1)} - \frac{3 \Delta^2}{12 \bar{M}_0} \left[ (\partial_\beta \bar{M}_1)^2 + (\partial_\beta \bar{M}_2)^2 \right. \\ & \left. - \frac{(\partial_\beta \bar{M}_0)}{\bar{M}_0} \left( 2 \bar{M}_1 (\partial_\beta \bar{M}_1) + 2 \bar{M}_2 (\partial_\beta \bar{M}_2) - \frac{(\bar{M}_1^2 + \bar{M}_2^2) (\partial_\beta \bar{M}_0)}{\bar{M}_0} \right) \right] \end{aligned} \quad (\text{A.15e})$$

$$\begin{aligned} \partial_t^{(0)} \bar{M}_8^{(0)} - \frac{1}{3} \partial_x \bar{M}_1 - \frac{1}{3} \partial_y \bar{M}_2 = & -s_8 \bar{M}_8^{(1)} - \frac{3 \Delta^2}{12 \bar{M}_0} \left[ (\partial_\beta \bar{M}_1)^2 + (\partial_\beta \bar{M}_2)^2 \right. \\ & \left. - \frac{(\partial_\beta \bar{M}_0)}{\bar{M}_0} \left( 2 \bar{M}_1 (\partial_\beta \bar{M}_1) + 2 \bar{M}_2 (\partial_\beta \bar{M}_2) - \frac{(\bar{M}_1^2 + \bar{M}_2^2) (\partial_\beta \bar{M}_0)}{\bar{M}_0} \right) \right] \end{aligned} \quad (\text{A.15f})$$

$$\partial_t^{(0)} \bar{B}_x + \partial_y \left( \frac{\bar{M}_2 \bar{B}_x - \bar{M}_1 \bar{B}_y}{\bar{M}_0} \right) = 0 \quad (\text{A.16a})$$

$$\partial_t^{(0)} \bar{B}_y + \partial_x \left( \frac{\bar{M}_1 \bar{B}_y - \bar{M}_2 \bar{B}_x}{\bar{M}_0} \right) = 0 \quad (\text{A.16b})$$

$$\partial_t^{(0)} \bar{N}_{x1}^{(0)} + \frac{1}{3} \partial_x \bar{B}_x = -s_{N,x1} \bar{N}_{x1}^{(1)} \quad (\text{A.16c})$$

$$\partial_t^{(0)} \bar{N}_{y2}^{(0)} + \frac{1}{3} \partial_y \bar{B}_y = -s_{N,y2} \bar{N}_{y2}^{(1)} \quad (\text{A.16d})$$

$$\begin{aligned} \partial_t^{(0)} \bar{N}_{y1}^{(0)} + \frac{1}{3} \partial_x \bar{B}_y = & -s_{N,y1} \bar{N}_{y1}^{(1)} - \frac{\Delta^2}{12\bar{M}_0} \left[ (\partial_\beta \bar{M}_2) (\partial_\beta \bar{B}_x) - (\partial_\beta \bar{M}_1) (\partial_\beta \bar{B}_y) \right. \\ & - \frac{(\partial_\beta \bar{M}_0)}{\bar{M}_0} \left( \bar{M}_2 (\partial_\beta \bar{B}_x) + \bar{B}_x (\partial_\beta \bar{M}_2) - \bar{M}_1 (\partial_\beta \bar{B}_y) - \bar{B}_y (\partial_\beta \bar{M}_1) \right) \\ & \left. - \frac{(\bar{M}_2 \bar{B}_x - \bar{M}_1 \bar{B}_y) (\partial_\beta \bar{M}_0)}{\bar{M}_0} \right] \end{aligned} \quad (\text{A.16e})$$

$$\begin{aligned} \partial_t^{(0)} \bar{N}_{x2}^{(0)} + \frac{1}{3} \partial_y \bar{B}_x = & -s_{N,x2} \bar{N}_{x2}^{(1)} + \frac{\Delta^2}{12\bar{M}_0} \left[ (\partial_\beta \bar{M}_2) (\partial_\beta \bar{B}_x) - (\partial_\beta \bar{M}_1) (\partial_\beta \bar{B}_y) \right. \\ & - \frac{(\partial_\beta \bar{M}_0)}{\bar{M}_0} \left( \bar{M}_2 (\partial_\beta \bar{B}_x) + \bar{B}_x (\partial_\beta \bar{M}_2) - \bar{M}_1 (\partial_\beta \bar{B}_y) - \bar{B}_y (\partial_\beta \bar{M}_1) \right) \\ & \left. - \frac{(\bar{M}_2 \bar{B}_x - \bar{M}_1 \bar{B}_y) (\partial_\beta \bar{M}_0)}{\bar{M}_0} \right] \end{aligned} \quad (\text{A.16f})$$

$$\partial_t^{(0)} \bar{N}_{x3}^{(0)} = -s_{N,x3} \bar{N}_{x3}^{(1)} \quad (\text{A.16g})$$

$$\partial_t^{(0)} \bar{N}_{y4}^{(0)} = -s_{N,y3} \bar{N}_{y4}^{(1)} \quad (\text{A.16h})$$

$$\partial_t^{(0)} \bar{N}_{y3}^{(0)} + \partial_x \left( \frac{\bar{M}_1 \bar{B}_y - \bar{M}_2 \bar{B}_x}{\bar{M}_0} \right) = -s_{N,y3} \bar{N}_{y3}^{(1)} \quad (\text{A.16i})$$

$$\partial_t^{(0)} \bar{N}_{x4}^{(0)} + \partial_y \left( \frac{\bar{M}_2 \bar{B}_x - \bar{M}_1 \bar{B}_y}{\bar{M}_0} \right) = -s_{N,x4} \bar{N}_{x4}^{(1)} \quad (\text{A.16j})$$

Follow the same method for conserved  $\mathcal{O}(\varepsilon^2)$  moment equations (A.3 and A.5) as  $\mathcal{O}(\varepsilon)$



above. Filtered evolution equations at  $\mathcal{O}(\varepsilon^2)$  for conserved moments.

$$\partial_t^{(1)} \bar{M}_0 = 0 \quad (\text{A.17a})$$

$$\partial_t^{(1)} \bar{M}_1 + \partial_x \left[ \frac{1}{2} \left( 1 - \frac{s_4}{2} \right) \bar{M}_4^{(1)} + \frac{1}{30} \left( 1 - \frac{s_7}{2} \right) \bar{M}_7^{(1)} - \frac{1}{5} \left( 1 - \frac{s_8}{2} \right) \bar{M}_8^{(1)} \right] + \partial_y \left[ \left( 1 - \frac{s_3}{2} \right) \bar{M}_3^{(1)} \right] = 0 \quad (\text{A.17b})$$

$$\partial_t^{(1)} \bar{M}_2 + \partial_x \left[ \left( 1 - \frac{s_3}{2} \right) \bar{M}_3^{(1)} \right] + \partial_y \left[ -\frac{1}{2} \left( 1 - \frac{s_4}{2} \right) \bar{M}_4^{(1)} + \frac{1}{30} \left( 1 - \frac{s_7}{2} \right) \bar{M}_7^{(1)} - \frac{1}{5} \left( 1 - \frac{s_8}{2} \right) \bar{M}_8^{(1)} \right] = 0 \quad (\text{A.17c})$$

$$\partial_t^{(1)} \bar{B}_x + \partial_x \left[ \left( 1 - \frac{s_{N,x1}}{2} \right) \bar{N}_{x1}^{(1)} \right] + \partial_y \left[ \left( 1 - \frac{s_{N,x2}}{2} \right) \bar{N}_{x2}^{(1)} \right] = 0 \quad (\text{A.17d})$$

$$\partial_t^{(1)} \bar{B}_y + \partial_x \left[ \left( 1 - \frac{s_{N,y1}}{2} \right) \bar{N}_{y1}^{(1)} \right] + \partial_y \left[ \left( 1 - \frac{s_{N,y2}}{2} \right) \bar{N}_{y2}^{(1)} \right] = 0 \quad (\text{A.17e})$$

The full equations for conserved moments (combining all respective moment equations for  $\mathcal{O}(\varepsilon)$  and  $\mathcal{O}(\varepsilon^2)$ ).

$$\partial_t \bar{M}_0 + \partial_x \bar{M}_1 + \partial_y \bar{M}_2 = 0 \quad (\text{A.18a})$$

$$\begin{aligned} \partial_t \bar{M}_1 + \partial_x \left[ \frac{\bar{M}_0}{3} + \frac{\bar{M}_1^2}{\bar{M}_0} - \frac{\bar{B}_x^2}{2} + \frac{\bar{B}_y^2}{2} + \varepsilon \left\{ \frac{1}{2} \left( 1 - \frac{s_4}{2} \right) \bar{M}_4^{(1)} + \frac{1}{30} \left( 1 - \frac{s_7}{2} \right) \bar{M}_7^{(1)} - \frac{1}{5} \left( 1 - \frac{s_8}{2} \right) \bar{M}_8^{(1)} \right\} \right] \\ + \partial_y \left[ \frac{\bar{M}_1 \bar{M}_2}{\bar{M}_0} - \bar{B}_x \bar{B}_y + \varepsilon \left\{ \left( 1 - \frac{s_3}{2} \right) \bar{M}_3^{(1)} \right\} \right] = 0 \end{aligned} \quad (\text{A.18b})$$

$$\begin{aligned} \partial_t \bar{M}_2 + \partial_y \left[ \frac{\bar{M}_0}{3} + \frac{\bar{M}_2^2}{\bar{M}_0} + \frac{\bar{B}_x^2}{2} - \frac{\bar{B}_y^2}{2} + \varepsilon \left\{ -\frac{1}{2} \left( 1 - \frac{s_4}{2} \right) \bar{M}_4^{(1)} + \frac{1}{30} \left( 1 - \frac{s_7}{2} \right) \bar{M}_7^{(1)} - \frac{1}{5} \left( 1 - \frac{s_8}{2} \right) \bar{M}_8^{(1)} \right\} \right] \\ + \partial_x \left[ \frac{\bar{M}_1 \bar{M}_2}{\bar{M}_0} - \bar{B}_x \bar{B}_y + \varepsilon \left\{ \left( 1 - \frac{s_3}{2} \right) \bar{M}_3^{(1)} \right\} \right] = 0 \end{aligned} \quad (\text{A.18c})$$

$$\partial_t \bar{B}_x + \partial_x \left[ \varepsilon \left( 1 - \frac{s_{N,x1}}{2} \right) \bar{N}_{x1}^{(1)} \right] + \partial_y \left[ \frac{\bar{M}_2 \bar{B}_x - \bar{M}_1 \bar{B}_y}{\bar{M}_0} + \varepsilon \left( 1 - \frac{s_{N,x2}}{2} \right) \bar{N}_{x2}^{(1)} \right] = 0 \quad (\text{A.18d})$$

$$\partial_t \bar{B}_y + \partial_x \left[ \frac{\bar{M}_1 \bar{B}_y - \bar{M}_2 \bar{B}_x}{\bar{M}_0} + \varepsilon \left( 1 - \frac{s_{N,y1}}{2} \right) \bar{N}_{y1}^{(1)} \right] + \partial_y \left[ \varepsilon \left( 1 - \frac{s_{N,y2}}{2} \right) \bar{N}_{y2}^{(1)} \right] = 0 \quad (\text{A.18e})$$

Now, find the perturbed moments by directly solving the lowest order moment equations (A.15 and A.16) for the perturbed moments. Perturbed moments solved to  $\mathcal{O}(\text{Ma}^2)$  from  $\mathcal{O}(\varepsilon)$  equations are

$$\begin{aligned} \bar{M}_3^{(1)} = & -\frac{1}{3s_3} \left\{ \partial_x \bar{M}_2 + \partial_y \bar{M}_1 \right\} + \frac{\Delta^2}{12\bar{M}_0} \left[ (\partial_\beta \bar{M}_1) (\partial_\beta \bar{M}_2) \right. \\ & \left. - \frac{(\partial_\beta \bar{M}_0)}{\bar{M}_0} \left( \bar{M}_1 (\partial_\beta \bar{M}_2) + \bar{M}_2 (\partial_\beta \bar{M}_1) - \frac{\bar{M}_1 \bar{M}_2 (\partial_\beta \bar{M}_0)}{\bar{M}_0} \right) \right] \end{aligned} \quad (\text{A.19a})$$

$$\begin{aligned} & -\frac{\Delta^2}{12} (\partial_\beta \bar{B}_x) (\partial_\beta \bar{B}_y) \\ \bar{M}_4^{(1)} = & -\frac{2}{3s_4} \left\{ \partial_x \bar{M}_1 - \partial_y \bar{M}_2 \right\} + \frac{\Delta^2}{12\bar{M}_0} \left[ (\partial_\beta \bar{M}_1)^2 - (\partial_\beta \bar{M}_2)^2 \right. \\ & \left. - \frac{(\partial_\beta \bar{M}_0)}{\bar{M}_0} \left( 2\bar{M}_1 (\partial_\beta \bar{M}_1) - 2\bar{M}_2 (\partial_\beta \bar{M}_2) - \frac{(\bar{M}_1^2 - \bar{M}_2^2) (\partial_\beta \bar{M}_0)}{\bar{M}_0} \right) \right] \end{aligned} \quad (\text{A.19b})$$

$$- \frac{\Delta^2}{12} \left[ (\partial_\beta \bar{B}_x)^2 - (\partial_\beta \bar{B}_y)^2 \right]$$

$$\bar{M}_5^{(1)} = \frac{1}{s_5} \partial_t^{(0)} \bar{M}_1 + \frac{1}{3s_5} \partial_x \bar{M}_0 = 0 \quad (\text{A.19c})$$

$$\bar{M}_6^{(1)} = \frac{1}{s_6} \partial_t^{(0)} \bar{M}_2 + \frac{1}{3s_6} \partial_y \bar{M}_0 = 0 \quad (\text{A.19d})$$

$$\begin{aligned} \bar{M}_7^{(1)} = & \frac{2}{s_7} \left\{ \partial_x \bar{M}_1 + \partial_y \bar{M}_2 \right\} - \frac{3\Delta^2}{12\bar{M}_0} \left[ (\partial_\beta \bar{M}_1)^2 + (\partial_\beta \bar{M}_2)^2 \right. \\ & \left. - \frac{(\partial_\beta \bar{M}_0)}{\bar{M}_0} \left( 2\bar{M}_1 (\partial_\beta \bar{M}_1) + 2\bar{M}_2 (\partial_\beta \bar{M}_2) - \frac{(\bar{M}_1^2 + \bar{M}_2^2) (\partial_\beta \bar{M}_0)}{\bar{M}_0} \right) \right] \end{aligned} \quad (\text{A.19e})$$

$$\begin{aligned} \bar{M}_8^{(1)} = & \frac{1}{3s_8} \left\{ \partial_x \bar{M}_1 + \partial_y \bar{M}_2 \right\} - \frac{5}{3s_8} \partial_t^{(0)} \bar{M}_0 - \frac{3\Delta^2}{12\bar{M}_0} \left[ (\partial_\beta \bar{M}_1)^2 + (\partial_\beta \bar{M}_2)^2 \right. \\ & \left. - \frac{(\partial_\beta \bar{M}_0)}{\bar{M}_0} \left( 2\bar{M}_1 (\partial_\beta \bar{M}_1) + 2\bar{M}_2 (\partial_\beta \bar{M}_2) - \frac{(\bar{M}_1^2 + \bar{M}_2^2) (\partial_\beta \bar{M}_0)}{\bar{M}_0} \right) \right] \end{aligned} \quad (\text{A.19f})$$

$$= \frac{2}{s_8} \left\{ \partial_x \bar{M}_1 + \partial_y \bar{M}_2 \right\} - \frac{3\Delta^2}{12\bar{M}_0} \left[ (\partial_\beta \bar{M}_1)^2 + (\partial_\beta \bar{M}_2)^2 \right. \\ \left. - \frac{(\partial_\beta \bar{M}_0)}{\bar{M}_0} \left( 2\bar{M}_1 (\partial_\beta \bar{M}_1) + 2\bar{M}_2 (\partial_\beta \bar{M}_2) - \frac{(\bar{M}_1^2 + \bar{M}_2^2) (\partial_\beta \bar{M}_0)}{\bar{M}_0} \right) \right]$$

$$\bar{N}_{x1}^{(1)} = -\frac{1}{3s_{N,x1}}\partial_x\bar{B}_x \quad (\text{A.20a})$$

$$\bar{N}_{y2}^{(1)} = -\frac{1}{3s_{N,y2}}\partial_y\bar{B}_y \quad (\text{A.20b})$$

$$\begin{aligned} \bar{N}_{y1}^{(1)} = & -\frac{1}{3s_{N,y1}}\partial_x\bar{B}_y - \frac{\Delta^2}{12\bar{M}_0} \left[ (\partial_\beta\bar{M}_2)(\partial_\beta\bar{B}_x) - (\partial_\beta\bar{M}_1)(\partial_\beta\bar{B}_y) \right. \\ & - \frac{(\partial_\beta\bar{M}_0)}{\bar{M}_0} \left( \bar{M}_2(\partial_\beta\bar{B}_x) + \bar{B}_x(\partial_\beta\bar{M}_2) - \bar{M}_1(\partial_\beta\bar{B}_y) - \bar{B}_y(\partial_\beta\bar{M}_1) \right) \\ & \left. - \frac{(\bar{M}_2\bar{B}_x - \bar{M}_1\bar{B}_y)(\partial_\beta\bar{M}_0)}{\bar{M}_0} \right] \end{aligned} \quad (\text{A.20c})$$

$$\begin{aligned} \bar{N}_{x2}^{(1)} = & -\frac{1}{3s_{N,x2}}\partial_y\bar{B}_x + \frac{\Delta^2}{12\bar{M}_0} \left[ (\partial_\beta\bar{M}_2)(\partial_\beta\bar{B}_x) - (\partial_\beta\bar{M}_1)(\partial_\beta\bar{B}_y) \right. \\ & - \frac{(\partial_\beta\bar{M}_0)}{\bar{M}_0} \left( \bar{M}_2(\partial_\beta\bar{B}_x) + \bar{B}_x(\partial_\beta\bar{M}_2) - \bar{M}_1(\partial_\beta\bar{B}_y) - \bar{B}_y(\partial_\beta\bar{M}_1) \right) \\ & \left. - \frac{(\bar{M}_2\bar{B}_x - \bar{M}_1\bar{B}_y)(\partial_\beta\bar{M}_0)}{\bar{M}_0} \right] \end{aligned} \quad (\text{A.20d})$$

$$\bar{N}_{x3}^{(1)} = = -\frac{1}{3s_{N,x3}}\partial_t^{(0)}\bar{B}_x = -\frac{1}{3s_{N,x3}}\partial_y \left( \frac{\bar{M}_2\bar{B}_x - \bar{M}_1\bar{B}_y}{\bar{M}_0} \right) \quad (\text{A.20e})$$

$$\bar{N}_{x4}^{(1)} = = -\frac{1}{3s_{N,x4}}\partial_t^{(0)}\bar{B}_x = -\frac{1}{3s_{N,x4}}\partial_y \left( \frac{\bar{M}_2\bar{B}_x - \bar{M}_1\bar{B}_y}{\bar{M}_0} \right) \quad (\text{A.20f})$$

$$\bar{N}_{y3}^{(1)} = = -\frac{1}{3s_{N,y3}}\partial_t^{(0)}\bar{B}_y = -\frac{1}{3s_{N,y3}}\partial_x \left( \frac{\bar{M}_1\bar{B}_y - \bar{M}_2\bar{B}_x}{\bar{M}_0} \right) \quad (\text{A.20g})$$

$$\bar{N}_{y4}^{(1)} = = -\frac{1}{3s_{N,y4}}\partial_t^{(0)}\bar{B}_y = -\frac{1}{3s_{N,y4}}\partial_x \left( \frac{\bar{M}_1\bar{B}_y - \bar{M}_2\bar{B}_x}{\bar{M}_0} \right) \quad (\text{A.20h})$$

The final MHD equations are found by inserting the perturbed moment values (A.19



$$\begin{aligned}
& \partial_t \bar{B}_x + \partial_x \left[ \varepsilon \left( 1 - \frac{s_{N,x1}}{2} \right) \left\{ -\frac{1}{3s_{N,x1}} \partial_x \bar{B}_x \right\} \right] + \partial_y \left[ \frac{\bar{M}_2 \bar{B}_x - \bar{M}_1 \bar{B}_y}{\bar{M}_0} \right. \\
& + \varepsilon \left( 1 - \frac{s_{N,x2}}{2} \right) \left\{ -\frac{1}{3s_{N,x2}} \partial_y \bar{B}_x + \frac{\Delta^2}{12\bar{M}_0} \left[ (\partial_\beta \bar{M}_2) (\partial_\beta \bar{B}_x) - (\partial_\beta \bar{M}_1) (\partial_\beta \bar{B}_y) \right. \right. \\
& - \frac{(\partial_\beta \bar{M}_0)}{\bar{M}_0} \left( \bar{M}_2 (\partial_\beta \bar{B}_x) + \bar{B}_x (\partial_\beta \bar{M}_2) - \bar{M}_1 (\partial_\beta \bar{B}_y) - \bar{B}_y (\partial_\beta \bar{M}_1) \right. \\
& \left. \left. \left. - \frac{(\bar{M}_2 \bar{B}_x - \bar{M}_1 \bar{B}_y) (\partial_\beta \bar{M}_0)}{\bar{M}_0} \right) \right] \right\} \left. \right] = 0
\end{aligned} \tag{A.22a}$$

$$\begin{aligned}
& \partial_t \bar{B}_y + \partial_x \left[ \frac{\bar{M}_1 \bar{B}_y - \bar{M}_2 \bar{B}_x}{\bar{M}_0} + \varepsilon \left( 1 - \frac{s_{N,y1}}{2} \right) \left\{ -\frac{1}{3s_{N,y1}} \partial_x \bar{B}_y - \frac{\Delta^2}{12\bar{M}_0} \left[ (\partial_\beta \bar{M}_2) (\partial_\beta \bar{B}_x) - (\partial_\beta \bar{M}_1) (\partial_\beta \bar{B}_y) \right. \right. \right. \\
& - \frac{(\partial_\beta \bar{M}_0)}{\bar{M}_0} \left( \bar{M}_2 (\partial_\beta \bar{B}_x) + \bar{B}_x (\partial_\beta \bar{M}_2) - \bar{M}_1 (\partial_\beta \bar{B}_y) - \bar{B}_y (\partial_\beta \bar{M}_1) \right. \\
& \left. \left. \left. - \frac{(\bar{M}_2 \bar{B}_x - \bar{M}_1 \bar{B}_y) (\partial_\beta \bar{M}_0)}{\bar{M}_0} \right) \right] \right\} \left. \right] + \partial_y \left[ \varepsilon \left( 1 - \frac{s_{N,y2}}{2} \right) \left\{ -\frac{1}{3s_{N,y2}} \partial_y \bar{B}_y \right\} \right] = 0
\end{aligned} \tag{A.22b}$$

In simplifying the MHD equations above, they become

$$\partial_t \rho + \nabla \cdot \bar{\rho} \bar{\mathbf{u}} = 0 \tag{A.23a}$$

$$\begin{aligned}
\partial_t (\bar{\rho} \bar{\mathbf{u}}) + \nabla \cdot \left( \frac{\bar{\rho} \bar{\rho} \bar{\mathbf{u}}}{\bar{\rho}} \right) &= -\nabla \bar{p} + \nabla \cdot (\bar{\mathbf{B}} \bar{\mathbf{B}}) - \frac{1}{2} \nabla (\bar{\mathbf{B}} \cdot \bar{\mathbf{B}}) + \left( \xi + \frac{1}{3} \nu \right) \nabla (\nabla \cdot \bar{\rho} \bar{\mathbf{u}}) + \nu \nabla^2 \bar{\rho} \bar{\mathbf{u}} \\
&- \nabla \cdot \left\{ \frac{6\nu}{6\nu+1} \frac{\Delta^2}{12\bar{\rho}} \left[ (\partial_\beta (\bar{\rho} \bar{\mathbf{u}})) (\partial_\beta (\bar{\rho} \bar{\mathbf{u}})) - \frac{\partial_\beta \bar{p}}{\bar{p}} \left( \bar{\rho} \bar{\mathbf{u}} (\partial_\beta (\bar{\rho} \bar{\mathbf{u}})) + (\partial_\beta (\bar{\rho} \bar{\mathbf{u}})) \bar{\rho} \bar{\mathbf{u}} - \bar{\rho} \bar{\mathbf{u}} \bar{\rho} \frac{\partial_\beta \bar{p}}{\bar{p}} \right) \right] \right\} \\
&- \nabla \cdot \left\{ \left( \frac{s_4}{4} + \frac{s_7}{20} - \frac{3s_8}{10} \right) \frac{\Delta^2}{12\bar{\rho}} \left[ (\partial_\beta (\bar{\rho} \bar{\mathbf{u}})) \cdot (\partial_\beta (\bar{\rho} \bar{\mathbf{u}})) - \frac{\partial_\beta \bar{p}}{\bar{p}} \left( 2\bar{\rho} \bar{\mathbf{u}} \cdot (\partial_\beta (\bar{\rho} \bar{\mathbf{u}})) - \bar{\rho} \bar{\mathbf{u}} \cdot \bar{\rho} \frac{\partial_\beta \bar{p}}{\bar{p}} \right) \right] \right\} \\
&- \frac{6\nu}{6\nu+1} \frac{\Delta^2}{12} \left\{ \frac{1}{2} \nabla [(\partial_\beta \bar{\mathbf{B}}) \cdot (\partial_\beta \bar{\mathbf{B}})] - \nabla \cdot [(\partial_\beta \bar{\mathbf{B}}) (\partial_\beta \bar{\mathbf{B}})] \right\}
\end{aligned} \tag{A.23b}$$

$$\begin{aligned}
\partial_t \bar{\mathbf{B}} &= \nabla \times \left( \frac{\bar{\rho} \bar{\mathbf{u}} \times \bar{\mathbf{B}}}{\bar{\rho}} \right) + \eta \nabla^2 \bar{\mathbf{B}} + \nabla \times \left[ \frac{\Delta^2}{12\bar{\rho}} \frac{6\eta}{6\eta+1} \{ (\partial_\beta (\bar{\rho} \bar{\mathbf{u}})) \times (\partial_\beta \bar{\mathbf{B}}) \right. \\
& \left. - \frac{\partial_\beta \bar{p}}{\bar{p}} \left( (\bar{\rho} \bar{\mathbf{u}}) \times (\partial_\beta \bar{\mathbf{B}}) + (\partial_\beta (\bar{\rho} \bar{\mathbf{u}})) \times \bar{\mathbf{B}} - \frac{(\partial_\beta \bar{p})}{\bar{p}} (\bar{\rho} \bar{\mathbf{u}}) \times \bar{\mathbf{B}} \right) \right]
\end{aligned} \tag{A.23c}$$

# APPENDIX B

## Local Spatial Derivatives

Calculating spatial derivatives typically requires information from neighboring nodes. In lattice Boltzmann, it is possible to calculate the spatial derivative of a conserved quantity locally using perturbed moments. Perturbed moments are necessarily determined midway through Chapman-Enskog (A.19 and A.20). The fluid and magnetic perturbed moments without the LES filters from Appendix A are respectively

$$M_3^{(1)} = -\frac{1}{3s_3} \{\partial_x M_2 + \partial_y M_1\} \quad (\text{B.1a})$$

$$M_4^{(1)} = -\frac{2}{3s_4} \{\partial_x M_1 - \partial_y M_2\} \quad (\text{B.1b})$$

$$M_5^{(1)} = \frac{1}{s_5} \partial_t^{(0)} M_1 + \frac{1}{3s_5} \partial_x M_0 = 0 \quad (\text{B.1c})$$

$$M_6^{(1)} = \frac{1}{s_6} \partial_t^{(0)} M_2 + \frac{1}{3s_6} \partial_y M_0 = 0 \quad (\text{B.1d})$$

$$M_7^{(1)} = \frac{2}{s_7} \{\partial_x M_1 + \partial_y M_2\} \quad (\text{B.1e})$$

$$M_8^{(1)} = \frac{1}{3s_8} \{\partial_x M_1 + \partial_y M_2\} - \frac{5}{3s_8} \partial_t^{(0)} M_0 = \frac{2}{s_8} \{\partial_x M_1 + \partial_y M_2\} \quad (\text{B.1f})$$

$$N_{x1}^{(1)} = -\frac{1}{3s_{N,x1}}\partial_x B_x \quad (\text{B.2a})$$

$$N_{y2}^{(1)} = -\frac{1}{3s_{N,y2}}\partial_y B_y \quad (\text{B.2b})$$

$$N_{y1}^{(1)} = -\frac{1}{3s_{N,y1}}\partial_x B_y \quad (\text{B.2c})$$

$$N_{x2}^{(1)} = -\frac{1}{3s_{N,x2}}\partial_y B_x \quad (\text{B.2d})$$

$$N_{x3}^{(1)} = = -\frac{1}{3s_{N,x3}}\partial_t^{(0)} B_x = -\frac{1}{3s_{N,x3}}\partial_y \left( \frac{M_2 B_x - M_1 B_y}{M_0} \right) \quad (\text{B.2e})$$

$$N_{x4}^{(1)} = = -\frac{1}{3s_{N,x4}}\partial_t^{(0)} B_x = -\frac{1}{3s_{N,x4}}\partial_y \left( \frac{M_2 B_x - M_1 B_y}{M_0} \right) \quad (\text{B.2f})$$

$$N_{y3}^{(1)} = = -\frac{1}{3s_{N,y3}}\partial_t^{(0)} B_y = -\frac{1}{3s_{N,y3}}\partial_x \left( \frac{M_1 B_y - M_2 B_x}{M_0} \right) \quad (\text{B.2g})$$

$$N_{y4}^{(1)} = = -\frac{1}{3s_{N,y4}}\partial_t^{(0)} B_y = -\frac{1}{3s_{N,y4}}\partial_x \left( \frac{M_1 B_y - M_2 B_x}{M_0} \right) \quad (\text{B.2h})$$

These perturbed moment equations can be solved directly for a strictly local set of equations describing each spatial derivative. One set of solutions from these equations is

found to be

$$\partial_x B_x = -3s_{N,x1}N_{x1}^{(1)} \quad (\text{B.3a})$$

$$\partial_y B_y = -3s_{N,y2}N_{y2}^{(1)} \quad (\text{B.3b})$$

$$\partial_x B_y = -3s_{N,y1}N_{y1}^{(1)} \quad (\text{B.3c})$$

$$\partial_y B_x = -3s_{N,x2}N_{x2}^{(1)} \quad (\text{B.3d})$$

$$\partial_x M_2 + \partial_y M_1 = -3s_4 M_3^{(1)} \quad (\text{B.3e})$$

$$\begin{aligned} \partial_x M_1 = & - \left[ \frac{1}{2} \left( 1 - \frac{s_4}{2} \right) M_4^{(1)} + \frac{1}{30} \left( 1 - \frac{s_7}{2} \right) M_7^{(1)} - \frac{1}{5} \left( 1 - \frac{s_8}{2} \right) M_8^{(1)} \right] \\ & - \left( \frac{2}{3}\nu - \xi \right) \left( -\frac{3}{2}s_4 M_4^{(1)} \right) / 2\nu \end{aligned} \quad (\text{B.3f})$$

$$\begin{aligned} \partial_y M_2 = & - \left[ -\frac{1}{2} \left( 1 - \frac{s_4}{2} \right) M_4^{(1)} + \frac{1}{30} \left( 1 - \frac{s_7}{2} \right) M_7^{(1)} - \frac{1}{5} \left( 1 - \frac{s_8}{2} \right) M_8^{(1)} \right] \\ & - \left( \frac{2}{3}\nu - \xi \right) \left( -\frac{3}{2}s_4 M_4^{(1)} \right) / 2\nu \end{aligned} \quad (\text{B.3g})$$

$$N_{x3}^{(1)} = = -\frac{1}{3s_{N,x3}} \partial_t^{(0)} B_x = -\frac{1}{3s_{N,x3}} \partial_y \left( \frac{M_2 B_x - M_1 B_y}{M_0} \right) \quad (\text{B.3h})$$

$$N_{x4}^{(1)} = = -\frac{1}{3s_{N,x4}} \partial_t^{(0)} B_x = -\frac{1}{3s_{N,x4}} \partial_y \left( \frac{M_2 B_x - M_1 B_y}{M_0} \right) \quad (\text{B.3i})$$

$$N_{y3}^{(1)} = = -\frac{1}{3s_{N,y3}} \partial_t^{(0)} B_y = -\frac{1}{3s_{N,y3}} \partial_x \left( \frac{M_1 B_y - M_2 B_x}{M_0} \right) \quad (\text{B.3j})$$

$$N_{y4}^{(1)} = = -\frac{1}{3s_{N,y4}} \partial_t^{(0)} B_y = -\frac{1}{3s_{N,y4}} \partial_x \left( \frac{M_1 B_y - M_2 B_x}{M_0} \right) \quad (\text{B.3k})$$

where  $M_0 = \rho$ ,  $M_1 = \rho u_x$ , and  $M_2 = \rho u_y$ .

In determining the simulation value of a perturbed moment, it can be simply calculated as the difference of a moment from its equilibrium

$$M_i^{(1)} = M_i - M_i^{(0)}. \quad (\text{B.4})$$



# APPENDIX C

## Entropic Derivation for LB

This appendix derives the solution for  $\gamma^*$  found in section 6.2.

The relative entropy of a distribution of particles with discrete positions and momenta, such as in lattice Boltzmann, is defined as

$$S = - \sum_i f_i \ln \frac{f_i}{W_i} \quad , \quad (\text{C.1})$$

where  $f_i$  is a distribution of the fluid at some lattice site with velocity  $i$ , and  $W_i$  is a normalized vector of lattice weights ( $\sum_i W_i = 1$ ).

Entropy is naturally a concave function. We know this because the derivative of  $-u \log u$  is the strictly decreasing function  $-(1 + \log u)$  on  $u \in [0, 1]$ . A sum of concave functions remains concave and so we can say that (C.1) is concave since  $f_i$  is a positive definite distribution defined as  $f_i \in [0, 1]$ .

We begin by substituting the postcollisional state

$$f_i \quad \Rightarrow \quad f'_i[\gamma] = f_i - \beta(2\Delta s_i + \gamma\Delta h_i) \quad (\text{C.2})$$

into the relative entropy equation (C.1) to produce a new postcollision entropy equation which is explicitly a function of  $\gamma$ ;

$$S[\gamma] = - \sum_i (f_i - \beta(2\Delta s_i + \gamma\Delta h_i)) \ln \left( \frac{f_i - \beta(2\Delta s_i + \gamma\Delta h_i)}{W_i} \right) , \quad (\text{C.3})$$

with  $\beta$  related to the original relaxation rate and the fluid viscosity as  $\beta = \frac{1}{2\tau} = \frac{1}{6\nu+1}$ ,  $\Delta s_i = s_i - s_i^{\text{eq}}$ , and  $\Delta h_i = h_i - h_i^{\text{eq}}$ .

Using the property,  $f_i = k_i + s_i + h_i$ , we find that  $f_i - f_i^{\text{eq}} = \Delta s_i + \Delta h_i$  and the postcollision entropy equation (C.3) can be modified to

$$S[\gamma] = - \sum_i (f_i - \beta(2\Delta s_i + \gamma\Delta h_i)) \ln \left( \frac{f_i^{\text{eq}} + (1 - 2\beta)\Delta s_i + (1 - \gamma\beta)\Delta h_i}{W_i} \right) . \quad (\text{C.4})$$

To lowest order in  $\mathbf{u}$ ,  $f_i^{\text{eq}}$  is linear with respect to  $W_i$ . It can be shown that

$$f_i^{\text{eq}} = \rho W_i (1 + \mathcal{O}(\mathbf{u})) . \quad (\text{C.5})$$

Expanding this equation about  $\mathbf{u} = 0$  and  $\rho = 1$ ,  $f_i^{\text{eq}} \simeq W_i$ . So  $W_i$  in (C.4) can be replaced by  $f_i^{\text{eq}}$  to become

$$S[\gamma] = - \sum_i (f_i - \beta(2\Delta s_i + \gamma\Delta h_i)) \ln \left( 1 + \frac{(1 - 2\beta)\Delta s_i + (1 - \gamma\beta)\Delta h_i}{f_i^{\text{eq}}} \right) . \quad (\text{C.6})$$

Since entropy is naturally a concave function, it can be maximized by setting it's derivative to zero.

$$\frac{\partial S[\gamma]}{\partial \gamma} = 0 = \sum_i \beta \Delta h_i + \sum_i \beta \Delta h_i \ln \left( 1 + \frac{(1 - 2\beta)\Delta s_i + (1 - \gamma\beta)\Delta h_i}{f_i^{\text{eq}}} \right) \quad (\text{C.7})$$

This equation can be simplified to the critical point defining maximum entropy if we look

at how the post-collisional scalar distribution,  $f'_i$ , changes with respect to  $\gamma$ . It is evident that the conserved moments are unchanged during a collision which allows us to specify the constraint

$$\sum_i f'_i = \sum_i f_i = \rho . \quad (\text{C.8})$$

We can now remove the  $\sum_i \Delta h_i$  term from (C.7) by substituting the derivative of (C.8) with respect to  $\gamma$ , which appears as

$$\frac{\partial}{\partial \gamma} \sum_i f'_i = \sum_i \frac{\partial}{\partial \gamma} (f_i - \beta (2\Delta s_i + \gamma \Delta h_i)) = \sum_i \beta \Delta h_i = 0 . \quad (\text{C.9})$$

The critical point defining maximum entropy is thus shown to be

$$\frac{\partial S[\gamma]}{\partial \gamma} = 0 = \sum_i \Delta h_i \ln \left( 1 + \frac{(1 - 2\beta) \Delta s_i + (1 - \gamma\beta) \Delta h_i}{f_i^{\text{eq}}} \right) . \quad (\text{C.10})$$

From the critical point, determining a solution for  $\gamma$  is relatively straight-forward. We begin the solution by expanding the equation about  $\frac{\Delta s_i}{f_i^{\text{eq}}}$  and  $\frac{\Delta h_i}{f_i^{\text{eq}}}$  to lowest order so we can remove the troublesome  $(\ln)$  term. This results in

$$0 = \sum_i (\Delta h_i - \gamma\beta \Delta h_i) \frac{\Delta h_i}{f_i^{\text{eq}}} + \sum_i (\Delta h_i - 2\beta \Delta h_i) \frac{\Delta s_i}{f_i^{\text{eq}}} . \quad (\text{C.11})$$

Now, a terminology is introduced to simplify the summed terms where

$$\langle X|Y \rangle = \sum_i \frac{X_i Y_i}{f_i^{\text{eq}}} \quad (\text{C.12})$$

and (C.11) becomes

$$0 = (1 - \gamma\beta) \langle \Delta h | \Delta h \rangle + (1 - 2\beta) \langle \Delta s | \Delta h \rangle . \quad (\text{C.13})$$

Dividing  $\langle \Delta h | \Delta h \rangle$  and solving for  $\gamma$  we get the final solution.

$$\gamma^* = \frac{1}{\beta} + \left( \frac{1}{\beta} - 2 \right) \frac{\langle \Delta s | \Delta h \rangle}{\langle \Delta h | \Delta h \rangle} . \quad (\text{C.14})$$

## BIBLIOGRAPHY

- [1] F. Chen, A. Xu, G. Zhang, Y. Li, and S. Succi, EPL (Europhysics Letters) **90**, 54003 (2010), URL <http://stacks.iop.org/0295-5075/90/i=5/a=54003>.
- [2] N. Frapolli, S. S. Chikatamarla, and I. V. Karlin, Phys. Rev. Lett. **117**, 010604 (2016), URL <https://link.aps.org/doi/10.1103/PhysRevLett.117.010604>.
- [3] F. Bösch, S. S. Chikatamarla, and I. V. Karlin, Physical Review E **92**, 043309 (2015).
- [4] S. Ansumali, I. V. Karlin, and S. Succi, Physica A: Statistical Mechanics and its Applications **338**, 379 (2004).
- [5] R. L. Liboff, *Introduction to the Theory of Kinetic Equations* (John Wiley & Sons Ltd, 1969), ISBN 0471534129.
- [6] A. I. Macnab, G. Vahala, L. Vahala, J. Carter, M. Soe, and W. Dorland, Physica A: Statistical Mechanics and its Applications **362**, 48 (2006), ISSN 0378-4371, discrete Simulation of Fluid Dynamics, URL <http://www.sciencedirect.com/science/article/pii/S0378437105009519>.
- [7] J. Carter, M. Soe, L. Oliker, Y. Tsuda, G. Vahala, L. Vahala, and A. Macnab, Lawrence Berkeley National Laboratory (2005).
- [8] P. Pavlo, G. Vahala, and L. Vahala, Phys. Rev. Lett. **80**, 3960 (1998), URL <https://link.aps.org/doi/10.1103/PhysRevLett.80.3960>.

- [9] X. He and L.-S. Luo, Phys. Rev. E **56**, 6811 (1997), URL <https://link.aps.org/doi/10.1103/PhysRevE.56.6811>.
- [10] M. Bouzidi, D. d’Humières, P. Lallemand, and L.-S. Luo, Journal of Computational Physics **172**, 704 (2001).
- [11] P. Lallemand and L.-S. Luo, Physical Review E **61**, 6546 (2000).
- [12] R. O. Dendy, *Plasma physics: an introductory course* (Cambridge University Press, 1995).
- [13] P. J. Dellar, Journal of Computational Physics **179**, 95 (2002).
- [14] S. Pope, *Turbulent Flows* (Cambridge University Press, 2000), ISBN 9780521598866, URL <https://books.google.com/books?id=HZsTw9SMx-0C>.
- [15] S. Chandrasekhar, *Hydrodynamic and Hydrodynamic stability* (OUP, 1961).
- [16] S. Succi, *The lattice Boltzmann equation: for fluid dynamics and beyond* (Oxford university press, 2001).
- [17] C. Flint, G. Vahala, L. Vahala, and M. Soe, Computers & Mathematics with Applications **72**, 394 (2016).
- [18] P. J. Dellar, Journal of Statistical Mechanics: Theory and Experiment **2009**, P06003 (2009).
- [19] M. Pattison, K. Premnath, N. Morley, and M. Abdou, Fusion Engineering and Design **83**, 557 (2008).
- [20] P. J. Dellar, Computers & Fluids **46**, 201 (2011), ISSN 0045-7930, 10th ICFD Conference Series on Numerical Methods for Fluid Dynamics (ICFD 2010), URL <http://www.sciencedirect.com/science/article/pii/S0045793010003518>.

- [21] I. Karlin, F. Bösch, and S. Chikatamarla, *Physical Review E* **90**, 031302 (2014).
- [22] Q. Chen, A. Otto, and L. Lee, *Journal of Geophysical Research: Space Physics* **102**, 151 (1997).
- [23] D. Biskamp and H. Welter, *Physics of Fluids B* **1**, 1964 (1989), URL <http://scitation.aip.org/content/aip/journal/pofb/1/10/10.1063/1.859060>.
- [24] F. Bösch, S. S. Chikatamarla, and I. Karlin, *ESAIM: Proc.* **52**, 1 (2015), URL <https://doi.org/10.1051/proc/201552001>.
- [25] H. Lu, C. J. Rutland, and L. M. Smith, *Journal of Turbulence* **8**, N37 (2007).
- [26] S. Chen, J. Tölke, and M. Krafczyk, *Physical Review E* **80**, 026702 (2009).
- [27] M. Krafczyk, J. Tölke, and L.-S. Luo, *International Journal of Modern Physics B* **17**, 33 (2003).
- [28] O. Agullo, W.-C. Müller, B. Knaepen, and D. Carati, *Physics of Plasmas* **8**, 3502 (2001).
- [29] W.-C. Müller and D. Carati, *Physics of Plasmas* **9**, 824 (2002).
- [30] S. Hou, J. Sterling, S. Chen, and G. Doolen, *Pattern Formation and Lattice Gas Automata* **6**, 149 (1996).
- [31] K. N. Premnath, M. J. Pattison, and S. Banerjee, *Physica A: Statistical Mechanics and its Applications* **388**, 2640 (2009).
- [32] H. Chen, S. Kandasamy, S. Orszag, R. Shock, S. Succi, and V. Yakhot, *Science* **301**, 633 (2003).
- [33] A. Yoshizawa, *Physics of Fluids* **30**, 1089 (1987).

- [34] T. Passot, H. Politano, A. Pouquet, and P. Sulem, *Theoretical and Computational Fluid Dynamics* **2**, 47 (1990).
- [35] Y. Zhou and G. Vahala, *Journal of Plasma Physics* **45**, 239 (1991).
- [36] M. L. Theobald, P. A. Fox, and S. Sofia, *Physics of Plasmas* **1**, 3016 (1994).
- [37] R. A. Clark, J. H. Ferziger, and W. C. Reynolds, *Journal of Fluid Mechanics* **91**, 116 (1979).
- [38] B. Vreman, B. Geurts, and H. Kuerten, *Journal of Fluid Mechanics* **339**, 357 (1997).
- [39] H. Kobayashi and Y. Shimomura, *Physics of Fluids* **15**, L29 (2003).
- [40] H. Chen, S. Succi, and S. Orszag, *Physical Review E* **59**, R2527 (1999).
- [41] S. Succi, I. V. Karlin, H. Chen, and S. Orszag, *Physica A: Statistical Mechanics and its Applications* **280**, 92 (2000).
- [42] S. Succi, O. Filippova, H. Chen, and S. Orszag, *Journal of Statistical physics* **107**, 261 (2002).
- [43] H. Yu, S. S. Girimaji, and L. S. Luo, *Journal of Computational Physics* **209**, 599 (2005).
- [44] C. Flint and G. Vahala, *Radiation Effects and Defects in Solids* **172**, 12 (2017).
- [45] P. J. Dellar, *Physical Review E* **64**, 031203 (2001).
- [46] P. J. Dellar, *Journal of Computational Physics* **190**, 351 (2003).
- [47] P. J. Dellar, *Journal of Computational Physics* **237**, 115 (2013).
- [48] P. J. Dellar, *Journal of Computational Physics* **259**, 270 (2014).



- [49] G. Vahala, B. Keating, M. Soe, J. Yepez, L. Vahala, J. Carter, and S. Ziegeler, Commun. Comput. Phys. **4**, 624 (2008).

## VITA

### Christopher Flint

Christopher Flint, originally from Orlando, Florida, began his early years in education shifting from school to school with no aspirations of obtaining a higher education. After witnessing the role of higher education in the lives of family members, Christopher changed his mind and decided to go to college. He graduated from Charlottesville High School in 2005 and entered James Madison University in the fall of the same year. Christopher originally majored in computer science, but later chose to add physics as a double major after falling in love with the challenges presented by the subject. Christopher completed his bachelors degree in May 2010 and entered the physics PhD program at William and Mary in August 2011. In May 2013, he began research on new lattice Boltzmann techniques with Professor George Vahala. That summer he also married the love of his life, Morgan, and three years later fathered their beautiful daughter Aliyah. After graduating from his current program, Christopher hopes to begin working in a field which marries his two passions of physics and computers.